David Pfeifer, BSc

Ultra-Bright Red Emitting Perylene Indicator Dyes for Optical Chemosensors

MASTERARBEIT

zur Erlangung des akademischen Grades

Diplom-Ingenieur

Masterstudium Technische Chemie

eingereicht an der

Technischen Universität Graz

Betreuer
Univ.-Prof. Dipl.-Chem. Dr.rer.nat. Ingo Klimant
Ass.Prof. Kand. Sergey Borisov

Institut für Analytische Chemie und Lebensmittelchemie
Technische Universität Graz

Graz, September 2015

Abstract

In this thesis, new luminescent indicator dyes for optical pH sensing were developed. The obtained high pK_a value supplementary enables optical carbon dioxide monitoring in different dynamic ranges. The presented high fluorescent perylene bisimide dyes were modified by laterally extension of the perylene core with phenylimidazol groups starting with commercially available Lumogen Orange. For sensor applications the dyes were physically entrapped into polyurethane-based hydrogels. The perception that the protonated form has a different absorbance than the deprotonated form enables colorimetric measurements as well as ratiometric fluorescence determination.

Due to outstanding photostability, high brightness (molar absorption coefficients up to 80 000 $[L \cdot mol^{-1} \cdot cm^{-1}]$ and quantum yields of ~ 0.9), no observed leaching out of the sensor matrix and the covered wavelength ranges (580-650 nm in absorption, 590-660 nm in emission for protonated forms) emphasise a promising class of new indicator dyes.

Additionally to calibration measurements for pH and carbon dioxide, proof of concepts for carbon dioxide determination under high pressures and in drinks were achieved. Further modification of the dye at the protonation site enables optical water sensing with a FRET-based concept in a swellable polymer environment without pH cross sensitivity.

Kurzfassung

Im Rahmen dieser Arbeit konnten neue fluoreszierende pH sensitive Farbstoffe für optische Sensoren synthetisiert werden. Die erhaltenen hohen pK_a Werte der Indikatoren ermöglichten auch optische Detektion von Kohlendioxid in unterschiedlichen dynamischen Bereichen. Die präsentierten lumineszierenden Farbstoffe wurden ausgehend von kommerziell erhältlichem Fluoreszenz Orange durch laterale Ringerweiterung modifiziert. Als Sensormaterial wurde ein Polyurethan basiertes Hydrogel verwendet, worin die Farbstoffe physikalisch eingebettet wurden. Die Tatsache, dass sich die protonierte Form von der deprotonierten Form des Moleküls in der Lager der Absorptionsbanden unterscheiden, ermöglicht Messungen basierend auf colorimetrischen, sowie auf ratiometrischen Methoden.

Ausgezeichnete Photostabilität, hohe Helligkeitswerte (molare Absorptionskoeffizienten bis zu 80 000 $[L \cdot mol^{-1} \cdot cm^{-1}]$ und Quantenausbeuten von ~ 0.9), kein beobachtetes Leaching aus der Sensormatrix, sowie der abgedeckte Wellenlängenbereich (580-650 nm für Absorption, 590-660 nm für Emission der protonierten Form) machen die Farbstoffe zu einer viel versprechenden neuen pH Indikatorklasse.

Zusätzlich zu pH- und Kohlendioxid Kalibrationen, konnten Proof of Concepts für CO_2 Messungen unter erhöhten Drücken, sowie für Getränkemessungen durchgeführt werden. Des Weiteren wurde ein Wassersensor basierend auf FRET und der Quellung der verwendeten Polymermatrix entwickelt. Durch Alkylierung der Protonierungsstelle verlor der Farbstoff seine pH Sensitivität, welche bei der Anwendung im Falle des Wassersensors störend gewesen wäre.

Statutory Declaration

I declare that I have authored this thesis independently, that I have not used other than the declared sources / resources, and that I have explicitly marked all material which has been quoted either literally or by content from the used sources.

2. September, 2015

Date Signature

Danksagung

Mein erster Dank gilt Professor Ingo Klimant, der diese Arbeit erst ermöglicht und finanziert hat, mir mit neuen Ideen und Anregungen stets eine große Unterstützung war und mir mit der Anstellung als Stud. Mitarbeiter einige Jahre vor Beginn dieser Arbeit die Tür zu dieser tollen Arbeitsgruppe geöffnet hat.
Danke Sergey, für deine großartige Unterstützung bei jeglichen Problemen im und rund um das Labor. Danke für deinen unaufhaltsamen Tatendrang und das Streben nach neuen Erkenntnissen. Die zahlreichen Diskussionen und Gespräche im Sozialraum waren eine Quelle für neue Wege und Überlegungen. Egal an welchem Wochentag, du hattest immer ein offenes Ohr und die Geduld auch schnell was auszuprobieren.
Danke an das NMR-Team und das MS-Team für die Hilfe bei der Aufnahme und Interpretation der Spektren.
Danke an die Arbeitsgruppe für die gemeinsamen Stunden, in denen wir vor scheinbar unüberwindbaren (IT-) Problemen gestanden sind, das eine oder andere Mal einfach Sachen gesucht, zusammen geräumt, auseinander gebaut oder auf etwas gewartet haben. Danke Simon, für die Unterstützung während deines Praktikumsmonats in Graz. Ihr seid auch außerhalb des Chemiegebäudes ein Teil meines Lebens geworden und nicht einfach nur Kollegen.

Danke sagen möchte ich auch meinen Studienkollegen, die mich vom ersten Studientag als Jahrgangskollegen oder als Tutoren begleitet haben. An dieser Stelle sind die Burschen und Mädls speziell aus dem 08er Jahrgang zu erwähnen, die auch außerhalb des Studiums zu tollen Freunden geworden sind.
Speziell möchte ich mich bei "meinem" Partybüro bedanken. Tobi, es war so lehrreich, geistreich aber auch extrem reich an Unterhaltung, was wir gemeinsam unternommen haben. Berni, ich weiß nicht, was damals im Oktober 2009 den Ausschlag für deine großartige Unterstützung gegeben hat, aber dafür möchte ich dir danken.
Danke an meine Schulfreunde, ihr habt mir auch oft wieder gezeigt, wie die Welt außerhalb des Chemiegebäudes so aussieht.

Der abschließende Dank gilt meiner Familie, meinen Eltern, ihr habt mich finanziell und in allen Entscheidungen immer unterstützt, bei Chrissi, ohne dich hätte ich in den vergangenen Jahren wohl nur die Hälfte erlebt und du gibst mir die Kraft für neue Abenteuer, sowie bei meinen Brüdern, ihr führt mir den Wert der Familie täglich vor Augen.

Contents

1 Introduction

pH determination is an issue of main interest for many applications belonging to biotechnological processes, marine science, diagnostics and many other fields. The most commonly used method for pH measurements is the well-established electrochemical one, using a pH glass electrode. Developments of fluorescent indicator dyes for optical pH sensors feature better sensitivity within their dynamic range and can be combined with fibre optics. Compared to the electrochemical method, optical sensors are easier to miniaturise and robust against electrochemical interferences.

Determination of pH with a chromophoric indicator dye depends on a reversible binding of the analyte (H^+) to the receptor (dye). The (de)protonation influences the spectral properties of the indicator dye, which can be detected by absorption or emission. Therefore three sensing mechanisms are distinguished: photoinduced electron transfer (PET), photoinduced proton transfer (PPT) or intramolecular charge transfer (ICT), that neither show PET nor PPT.

The aim of this work was the development of an optical pH sensor. The preparation and characterisation of new ultra-bright perylene bisimide dyes which undergo intramolecular charge transfer (ICT) was the first part of the thesis. The second part consisted of the immobilisation of the dye into a polymer matrix and achievements either in calibration or proof of concepts.

Perylene dyes are known for their high fluorescence brightness, good photostability and their good versatility in consideration of synthetic modifications. Hence, perylene bisimides (PBIs) appear to be promising candidates for optical sensor applications, due to their good compatibility with immobilisation matrices.

Most of the pH samples of mayor importance are located at pH values below 9. Dyes with pK_a values fitting for measurements above 9, may also be suitable for optical carbon dioxide sensing, which is based on the determination pH changes. For this concept, the basic (anionic) form of a pH sensitive dye is entrapped in a polymer matrix as a ion pair with a quaternary ammonium cation. During the reaction with carbon dioxide the protonation of the dye can be measured.

2 Theoretical Background

2.1 Luminescence

This chapter is based on reference [1, 2]. Other references will be cited independently. Luminescence in general means the emission of photons as a reason of relaxation of an excited state. Primary an electron is going to be excited from its ground state to an electronically higher excited level. The electron is not able to stay at the excited state and falls back to the lower ground state loosing energy in form of electromagnetic radiation. Luminescence emission is separated in two types called phosphorescence, if the de-excitation process is spin-forbidden, and fluorescence, if the relaxation is spin-allowed. A multitude of luminescent compounds has been explored, including organic, inorganic and organometallic compounds. There are several modes for the excitation of the electronic state. For this work the most important one will be the photoluminescence, which includes fluorescence, delayed fluorescence and phosphorescence, where excitation of a electron is caused by absorption of photons. The electron returns back to the energetically lower ground state and emits energy in form of photons.

2.1.1 Absorption

If a molecule in its most stable energetically state with the lowest energy (ground state) absorbs light in form of photons with energy from the UV-Vis region, an electron rises up to an higher excited unoccupied energy level. The highest occupied molecular orbital (HOMO) and the lowest unoccupied molecular orbital (LUMO) are the most important types of orbitals for absorption processes. The energy of the photon has to be as high as the energy gap between ground state and the excited state.
If absorption in the UV-Vis region occurs the excitation most likely happens to an excited π orbital π^* from the ground state of a π or n (π or non-bonding) orbitals. Excitations from a σ to σ^* need higher energy, respectively shorter wavelengths, which is not that important for spectroscopic uses. The greater the conjugated π-electron system of a molecule, the lower energy

for $\pi \rightarrow \pi^*$ transition is required. The mathematically description for absorption efficiency at a certain wavelength is given by the Lambert Beer law 2.1.

$$A = log\,(\frac{I_0}{I}) = \epsilon \cdot c \cdot d \tag{2.1}$$

A	...	absorption
I_0	...	intensity of light entering the sample
I	...	intensity of light getting through the sample
ϵ	...	molar absorption coefficient
c	...	concentration of the sample [mol /l]
d	...	optical path length of the sample [cm]

2.1.2 Visualisation of Electronic States

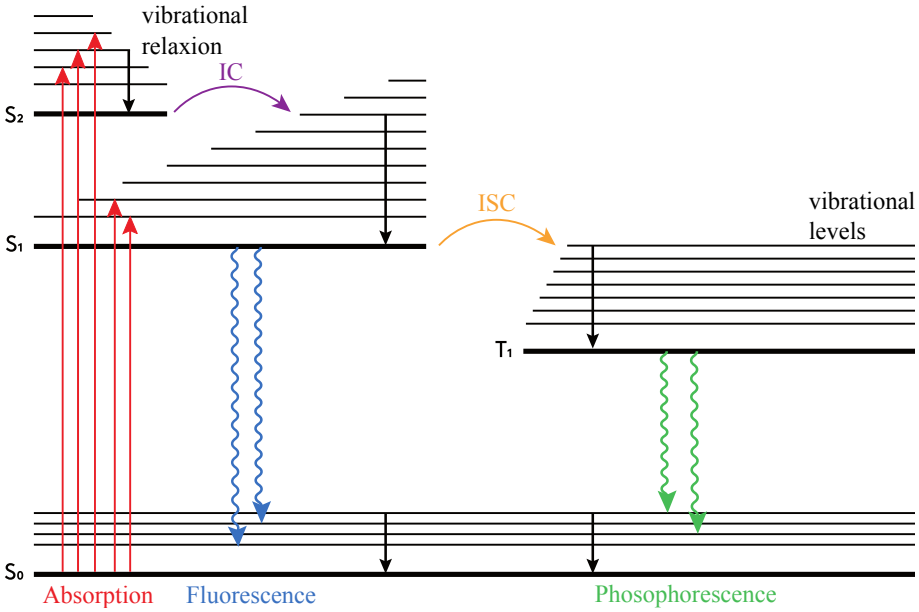

Figure 2.1: Jablonski diagram with electronic transitions

The most common way to visualise luminescence processes with its different energy levels and the (de)-excitation is the Jablonski-Diagram shown in figure 2.1. The spin multiplicity is arranged horizontally and on the vertical axis energy is plotted. S_0 is the ground state with the lowest energy. S_1, S_2 are excited singlet states, with the same spin multiplicity as in the ground state respectively. T_1 is the excited triplet state, but with changed spin comparing to S_0. Usually electronic transitions are just allowed without spin changes during an excitation process, resulting in quantum mechanically forbidden transitions between singlet and triplet

states. However, singlet-triplet de-excitation processes may occur in special cases, as can be seen in section 2.1.4, 2.1.5.
If absorption takes place an electron is enhanced to an vibrational level of the excited state, there vibrational relaxation occurs to the energetically lowest excited state and is followed by de-excitation processes back to ground state S_0.

2.1.3 Franck-Condon principle

According to the Born-Oppenheimer approximation, the movements of electrons are much faster than movements of the nuclei. An excitation of an electron up to an excited molecular orbital takes about 10^{-15} seconds, compared to the time range for molecular vibrations ($10^{-10} - 10^{-12}$ seconds), it is very fast. This leads to the fact, that the nuclei in a molecule does not change the positions while an electronic transition takes place. This means that the transition occurs when the atoms are equidistant to each other, in the ground state as well as in excited states.

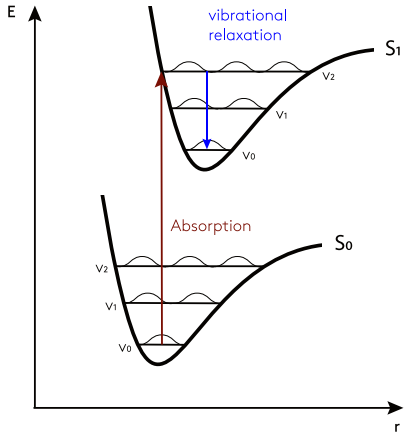

Figure 2.2: Franck-Condon-principle

2.1.4 Non-Radiative De-excitation

Internal Conversion (IC)

The non-radiative de-excitation process called Internal Conversion takes place after excitation and before emission of photons. The transition between two excited states is only possible, when the same spin multiplicity is given. Molecules may be excited to different high excited

states (S_1, S_2) and then Internal Conversion is able to convert the energy of molecules in high excited states (e.g. S_2) to the lowest excited state (S_1). Internal Conversion between the lowest excited level S_1 and the ground state S_0 might be possible, but due to the larger energy gap less efficient. Usually Internal Conversion appears in a time scale of $10^{-13} - 10^{-11}$ seconds and is not as fast as absorption processes.

Intersystem Crossing (ISC)

Intersystem Crossing explains a transition between the excited singlet state to the triplet state, which have different spin multiplicities but equal vibrational levels. The change of the spin, is quantum-mechanically forbidden, but spin-orbit coupling may be strong enough to make ISC possible. The presence of heavy atoms like Br or Pb increases the spin-orbit coupling and following the ISC possibility increases. The time scale of Intersystem Crossing is $10^{-9} - 10^{-7}$ seconds which is compatible with other deactivation processes. If once ISC occurred, T_1 lifetimes can be in the range of $10^{-6} - 1$ seconds.

2.1.5 Radiative De-excitation

Fluorescence

If a relaxation of an electron from S_1 to S_0 occurs and photons are emitted, the process is called fluorescence. The emission spectrum of such a phenomena compared to the absorption spectrum is shifted to longer wavelengths (lower energy). Nevertheless 0-0 transition is usually the same for absorption and fluorescence. The bathochromic shift is caused by the loss of energy in the excited state due to vibrational relaxation. The band gap of the absorption maximum and fluorescence maximum which appears in the difference of the wavelengths is named Stokes shift. However, mostly absorption and fluorescence spectra partly overlap at room temperature. Fluorescence as well as absorption is based on the Frank-Condon principle, what leads to the fact that de-excitation takes place from the lowest excited level to a higher vibrational level of the ground state. The energy differences of vibrational levels in excited as well as in the ground state are usually similar accordingly the emission spectrum is a reflection of the absorption spectrum.
The absorption and emission of photons take about 10^{-15} s. Nevertheless, an excited molecule stays for a certain amount of time ($10^{-11} - 10^{-7}$ seconds) in the excited S_1 state before undergoing relaxation (e.g. emission of photons, Intersystem Crossing, ...), which is described as excited-state lifetime.

Phosphorescence

Radiative deactivation processes, from the excited triplet state to the ground state ($T_1 \rightarrow S_0$), where photons are emitted is called phosphorescence. The process is as ISC spin forbidden, but can be observed with previous Intersystem Crossing. The time rate of phosphorescence is as slow as $10^{-6} - 1$ seconds and thus non-radiative relaxation like reversed ISC or vibrational relaxation is favoured. At low temperatures or in rigid media the lifetime of the triplet state may be long enough to observe phosphorescence phenomena up to seconds or longer. Because of the lower energy level the triplet state T_1 has, compared with the S_1 state, the phosphorescence spectrum is shifted to longer wavelengths (lower energy) than the fluorescence spectrum.

Delayed Fluorescence

If an Intersystem Crossing process takes place from $S_1 \rightarrow T_1$ followed by a reversed Intersystem Crossing back from $T_1 \rightarrow S_1$ because the energy gap between singlet and triplet state is small enough. Furthermore, delayed fluorescence, radiative de-excitation from S_1 to the ground state S_0 can occur. The emission spectrum is the same as the fluorescence spectrum but the luminescence lifetime is longer because the molecule stays at the triplet state before going back to S_1. The whole process is thermally activated and occurs preferred at higher temperatures.

2.1.6 Quantum yield

Both quantum yield and lifetime are main characteristics with high importance. The return of a quantity of excited molecules paired with emission of fluorescence photons back to the ground state S_0 is the fluorescence quantum yield ϕ_F.

$$\phi_F = \frac{emitted\ photons}{absorbed\ photons} = \frac{\tau_S}{\tau_r} = \frac{k_r}{k_r + k_{nr}} = k_r \cdot \tau_S \tag{2.2}$$

τ_S ... lifetime of excited state
τ_r ... radiative lifetime
k_r ... radiative rate constant
k_{nr} ... non-radiative rate constant

As can be seen in equation 2.2, it is defined as ratio of the number of emitted photons during the fluorescence process to the number of absorbed photons by excitation. ϕ_F can be close to unity if the rate of radiative decay k_r is much higher than the non-radiative decay rate k_{nr}.

2.1.7 Lifetime

If a molecule is excited to state S_1, it stays there for a certain amount of time, until fluorescence emission or non-radiative de-excitation occur. The average time the molecule stays in the excited state S_1 prior to the de-excitation to the ground state is defined as excited state S_1 lifetime:

$$\tau = \frac{1}{k_r^S + k_{nr}^S} \tag{2.3}$$

The de-excitation procedures are generally first order kinetic processes.

$$[A] = [A]_0 \cdot e^{\frac{-t}{\tau}} \tag{2.4}$$

Lifetimes of excited singlet states S_1 are usually in a range from $10^{-11} - 10^{-7}$ seconds, whereas the triplet lifetimes T_1 are in a range from $10^{-6} - 1$ seconds.
As a result of the relation of non-radiative processes to thermal agitation (collisions of molecules, intramolecular vibrations, ...) increase of temperature mostly leads to a decrease of the fluorescence quantum yield and lifetime.

2.1.8 Quenching

All de-excitation processes mentioned before, are of intramolecular origin. In contrast, "quenching" describes the reaction or interaction between an excited luminophore (M*) and a quencher molecule (Q), which causes de-excitation of (M*). Such intermolecular process may be proton transfer, electron transfer, energy transfer, complex formation or collisions with heavy atoms.

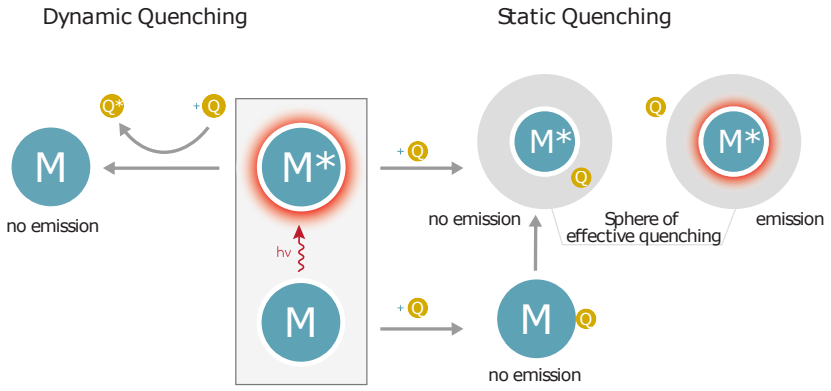

Figure 2.3: Different quenching mechanisms

Dynamic Quenching

Molecule and quencher are interacting, while the molecule is in the excited state. The de-excitation process is called *dynamic quenching*, if a collision of Q with M* occur and energy is

transferred in a non-radiative process to Q. It can be observed more often, if the excited state takes a longer time. The luminophore lifetime is reduced in presence of a quencher. Furthermore a self-quenching can occur, if Q and M are the same molecules. For visualization of the dynamic quenching the Stern-Volmer plot is used.

Static Quenching

If M and Q are forming a non-fluorescent complex MQ, static quenching happens. The MQ complex can be formed in the ground state as well as in the excited state of M, if Q is located in the sphere of effective quenching, in a small distance to M*. Both models cause a decrement of the luminophore concentration and consequently lower fluorescence intensity. However, the lifetime of M out of the complex is not effected.

2.1.9 Förster Resonance Energy Transfer - FRET

This section is based on reference [3]. Other references will be cited independently. The Förster mechanism is a special case of a non-radiative photoinduced energy transfer process. Energy can be transferred from an excited molecule D (donor) to another molecule A (acceptor) in its ground state.

$$D^* + A \rightarrow D + A^*$$

The non-radiative excitation energy transfer can occur if several conditions are given:

D and A are close to each other (0.5 - 10 nm) - A Coulombic interaction between D* and A take place electrodynamically, consisting of long-range dipole-dipole interactions

Emission spectrum of D overlaps with absorption spectrum of A, due to several vibronic transitions of D have nearly the same energy as the corresponding transitions of A, such transitions are coupled, e.g. in resonance.

The quantum yield of D is high.

The molar absorption coefficient of A is high.

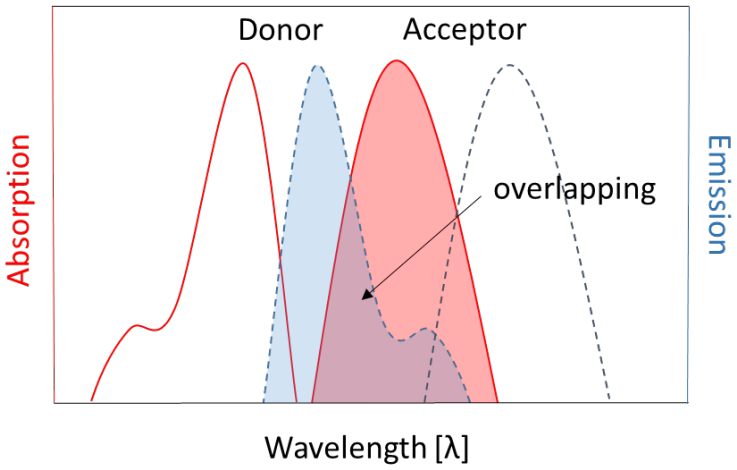

Figure 2.4: Schematic principle of spectral overlapping of donor and acceptor

For FRET it is not required that the acceptor show fluorescence. It should only be possible that the energy is transferred from the donor to the acceptor. This kind of quenching process was successfully applied for fluorescence-based carbon dioxide sensors [4, 5]. Nevertheless, if A is a fluorophore, emission is characteristic for its fluorescence spectrum even D was excited, this emission is called *sensitized emission*.

2.2 Optical Chemical Sensor (Optodes)

This section is based on reference [6–8]. All other references will be cited independently. Sensors have become an essential part of our everyday life. Determination of certain parameters of the environment in quality and quantities is the goal of sensors. Chemical sensors are enabled to detect specified analyts (of chemical or biochemical origin) and convert the received information into a measurable electronic signal.

An optical sensor in general consists of an analyte specific receptor, a transducer and a detecting device, which transforms the gained information into processable data. The recognition element is responsible for the specific interaction to the analyte. Receptors can be of synthetic origin or biological compounds, such as anti-bodies or enzymes, due the sensors are divided into two types: *chemosensors* and *biosensors* [9]. The transducer is the element, which shows different optical properties belonging to the recognition of an analyte or not. That significant differences can be detected and supply data for the output signal.

The field of optical *chemosensors* with indicator dyes as receptor/transducer provide a broad range of analyte specific applications suitable for O_2, CO_2, NH_3, pH, ionic species and temperature determination, as they are related to optical phenomena, such as absorption, luminescence or refractivity [10].
One of the main developments of the last years are the multicomponent analysis combined with the miniaturisation of sensors as well as sensor devices consist of fibre optics. The improvements in this research area make them cost-effective, smaller, easier to handle, robust and finally essential and of main interest for industrial as well as for environmental applications.

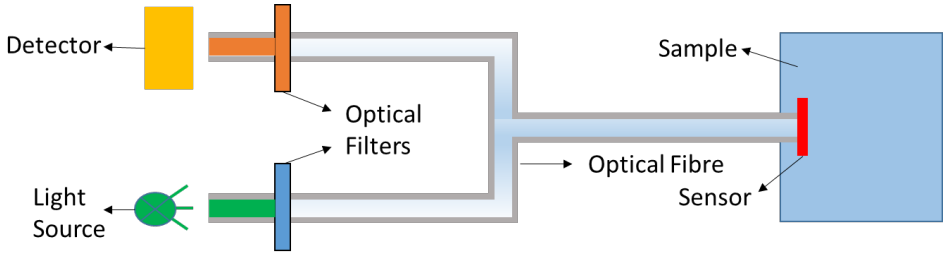

Figure 2.5: Schematic principle of a fibre optic sensors

2.2.1 Optical pH Sensors

Most common in the field of pH measurements is the well-developed electrochemical method using a glass electrode. An alternative is an optical pH sensor, which is easier to miniaturise and is robust against electromagnetical interferences. Fluorescence based indicator dyes show a much better sensitivity within their dynamic range and can be combined with fibre optics [11]. The definition of pH value is correlated with the activity of H^+. The relation of H^+ concentration and their activity is given in Henderson-Hasselbalch equation:

$$pH = pK_a \; + \; log\frac{[B^-]}{[HB]} + log\frac{f_{B^-}}{f_{HB}} \; - \; log\, a_{H_2O} \tag{2.5}$$

$[B^-]\,[HB]$	...	concentrations of basic form B^- and acidic form HB [mol /l]
f_{B^-}, f_{HB}	...	activity coefficients os basic form B^- and acidic form HB
a_{H_2O}	...	activity of water

High sensitivity is limited to the range pH $= pK_a \pm 1.5$. According to equation 2.5 ionic strength has an influence on the activity coefficients, which causes cross-sensitivity. This is a drawback of pH determination with indicator dyes because actually concentrations of H^+ are measured, not the activity. The pK_a value only refers to measurements in water. However, the apparent acidity constant K'_a is determined under modified conditions (presence of organic solvents,

immobilisation layer). The relation to pK_a is shown in equation 2.6:

$$pK_a = pK'_a + log\frac{f_{B^-}}{f_{HB}} \tag{2.6}$$

pK'_a ... apparent pK_a value

Determination of pH with a chromophoric indicator dye depends on a reversible binding of the analyte (H^+) to the receptor (dye). The (de)protonation influences the spectral properties of the indicator dye, which can be detected by absorption or emission. For practical applications the pK_a, pK'_a respectively, should fit the pH range that will be measured. Indicator dyes with pK_a values of 6 - 8.5 will fit for biotechnological (pH $\sim$ 6.5) [12], physiological (pH 7.4) or marine (pH 7.5 - 8.5) [13] applications. Nevertheless, dyes with lower pK_a values might be suitable for ammonia sensing, or dyes with higher values are promising candidates for CO_2 determination (2.2.2). pK_a values can be modified by introducing electron-donating or electron-withdrawing groups into the indicator dye [14, 15].

Immobilisation of the indicator dye into a hydrophilic matrix is necessary to obtain a pH sensor since such matrices are permeable for protons. Entrapment can be achieved physically or by covalent coupling. Therefore additional molecule modifications are required. On the one hand, immobilisation via covalent coupling may prevent leaching effects or aggregation issues. On the other hand physical entrapment is much easier to perform. pK_a properties of the indicator dye can be strongly influenced by the immobilisation environment.
Depending on the sensing mechanism, the dye may undergo upon excitation, three types of classes are distinguished: photoinduced electron transfer (PET), photoinduced proton transfer (PPT) or intramolecular charge transfer (ICT), that neither show PET nor PPT.

Class A: PET-based pH Indicators (Photoinduced Electron Transfer)

Usually the fluorescence quantum yield of the basic species of a PET indicator dye is low, because of intramolecular quenching by electron transfer. Due to protonation (suppression of electron transfer) the fluorescence intensity enhance at low pH values. The spectral shapes of excitation and emission do not depend of pH. A common modification for introducing a PET-group into indicator dyes is achieved by attaching a amine moiety to the dye. Subsequently the fluorescence quenching is based on the photoinduced electron transfer of the amine group to the chromophoric system of the dye. However, protonation of the amine causes an enhancement

of fluorescence intensity (fig. 2.6). Aigner et al. investigated the introduction of phenoxide PET groups, which enable higher flexibility than amine groups, because they are able to quench fluorophores at basic pH which are not quenched by the commonly used amines [16]. Numerous examples could be found in literature, some of them based on different fluorophores (fig. 2.7): for example perylene [17], anthracene [18] and rhodamine [19].

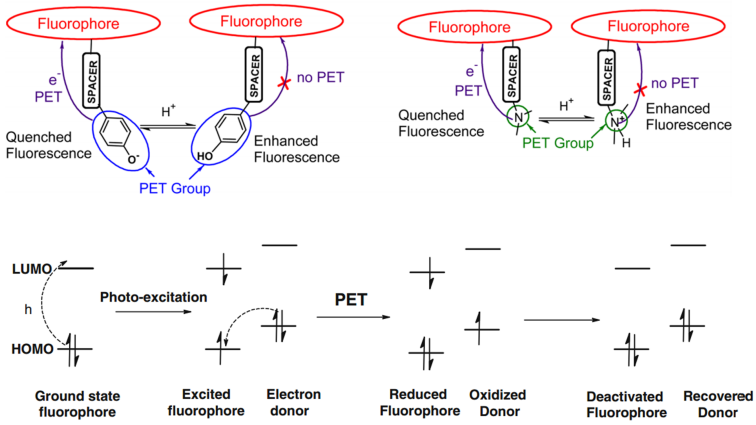

Figure 2.6: Schematic demonstration of the PET mechanism. Above: the principles of quenching by a phenolic PET group and a amino PET group [20]. Below: Molecular orbital illustration of a PET process [21].

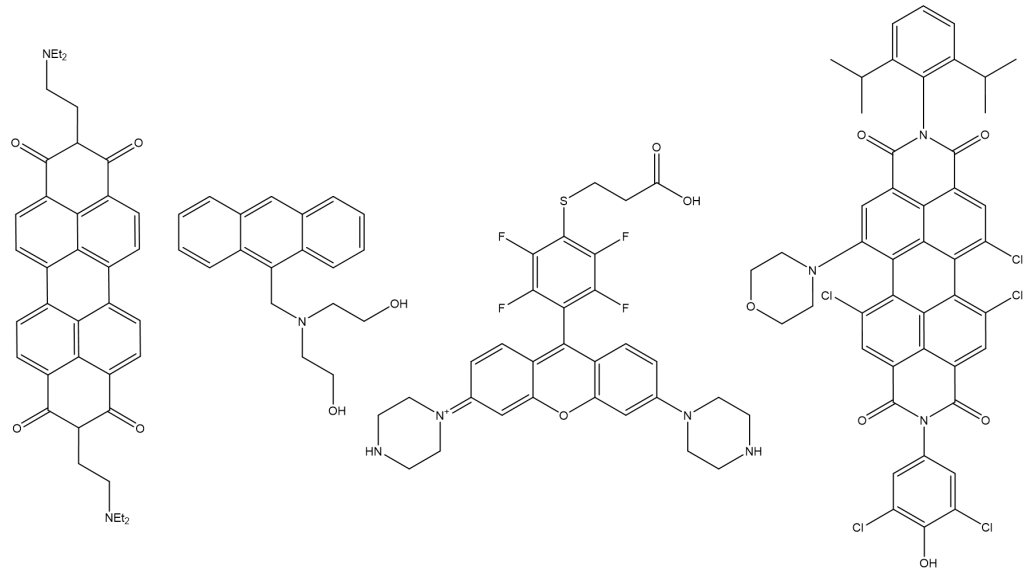

Figure 2.7: Structures of perylene, anthracene, rhodamine and perylene bisimide derivates bearing PET groups.

Class B: PPT-based pH Indicators (Photoinduced Proton Transfer)

In the case of PPT, the excited state of the fluorophore shows higher acidity (lower pK_a) than the molecule in its ground state. Consequently, deprotonation takes place immediately and only the emission of one form can be observed. The excitation spectra of such indicator dyes show pH dependency, in contrast to unchanged emission spectra. Commonly used fluorophores are HPTS [22] and 7-hydroxy-4-methylcoumarin [23], which were developed for intracellular applications.

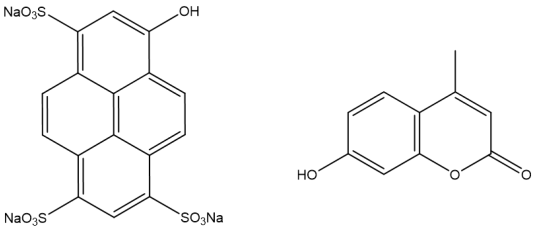

Figure 2.8: Structures of HPTS and 7-hydroxy-4-methylcoumarin, that are able to undergo PPT

Class C: ICT-based pH Indicators (Intramolecular Charge Transfer)

In this case, an indicator dye shows pH dependency and different spectral properties of acidic/basic (protonated/deprotonated) form can be observed. Corresponding pK_a curves of absorption and emission spectra should be similar. Under basic conditions the signal intensity (both absorption and emission) of the deprotonated form decreases with a concomitant increase of the signal intensity (both absorption and emission) of the protonated form. Well known examples are fluorescein dyes [24], SNAFL and SNARF [25].

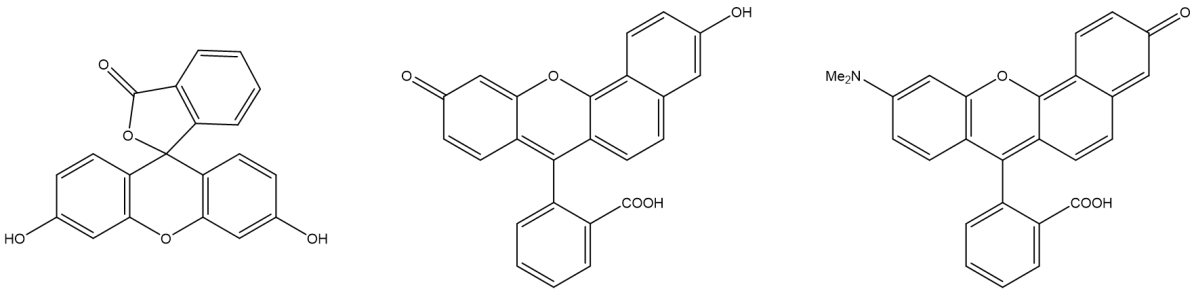

Figure 2.9: Structures of fluorescein, SNAFL-1 and SNARF-2

2.2.2 Optical Carbon Dioxide Sensors

Carbon dioxide is omnipresent in media, society and an often discussed issue concerning climate protection, because the CO_2 emissions increase continuously. Therefore, CO_2 is one of the analyts of extraordinary interest. Since the late 1950´s the *Severinghaus electrode* was the most common used measurement devices for carbon dioxide determination in solution [26]. The application consist of a pH glass electrode, located in a buffer (usually sodium bicarbonate buffer) chamber, which is separated from the sample with a hydrophobic gas-permeable and a ion-inpermeable membrane. CO_2 can diffuse through the sample, reacts with the buffer (shown in the reaction eq.) and the protons change the pH of the buffer solution.

$$CO_2 + H_2O \leftrightarrow H_2CO_3 \leftrightarrow HCO_3^- + H^+$$

The electrode shows excellent sensitivity, but suffers of electromagnetic interferences and has a long response time. Applications, wherein the *Severinghaus* concept are used for optical sensors due to pH sensitive fluorescent layers, which are soaked with bicarbonate buffer were reported [27–29].

Mills et al [30, 31] developed the *dry sensors* or *plastic type sensors*. For this concept, the basic (anionic) form of a pH indicator dye is entrapped in a polymer matrix as a ion pair with a quaternary ammonium cation - usually tetraoctylammonium (TOA^+). The reaction with carbon dioxide is shown.

$$TOA^+Ind^- + CO_2 + H_2O \rightarrow HInd + TOA^+HCO_3^-$$

The polymer matrix should be rather hydrophobic, permeable for CO_2 and inpermeable for ions and should have a low water uptake capability. Commonly used polymers are ethyl cellulose matrices [32, 33]. HPTS is an established pH indicator dye used for CO_2 measurements [4]. A few examples of numerous applications for optical carbon dioxide determination are for marine interests [34], clinical uses [35] and for modified atmospheric food packaging applications [36].

2.2.3 Physical Entrapment into Polymer Matrices

Hydrogels

Hydrogels are in general water-insoluble polymers. The hydrophilic patterns of the structure make them swellable with water to an uptake of as much as 70-90% of their own volume. Cross-linking prevents them from being soluble in water. Synthetic hydrogels based on polyvinyl alcohol, polyurethanes and poly(meth)acrylamides are commercial available. For bioscience applications hydrogels were frequently used to host and release drugs. Furthermore agarose

and poly(acrylamide)-based hydrogels were useful components in electrophoresis [37]. The use of hydrogel as hydrophilic immobilisation matrices of fluorescence pH sensors was investigated in the past [11, 38].

Poly(styrene-block-vinylpyrrolidone) (PS/PVP) Particles

Hydrophobic polystyrene and hydrophilic polyvinylpyrrolidone are the two building blocks of the block copolymer forming a hydrophobic core and a hydrophilic shell particle. Luminescent indicator dyes can be embedded into both domains, depending on the solvent used for staining. If EtOH/H_2O (70:30 v/v) is used, the shell is swollen and indicator dyes with more hydrophilic character can be embedded there, once the organic solvent is evaporated. On the other hand, if THF/H_2O (50:50 v/v) is used as solvent, the lipophilic core swells and indicator dyes are able to diffuse into it. Temperature, oxygen and lipophilic pH indicator dyes should be stained in the core, whereas ion and pH indicators should be immobilised into the shell of the PS/PVP particles [39]. A variety of indicator dye incorporations have been established [40–42].

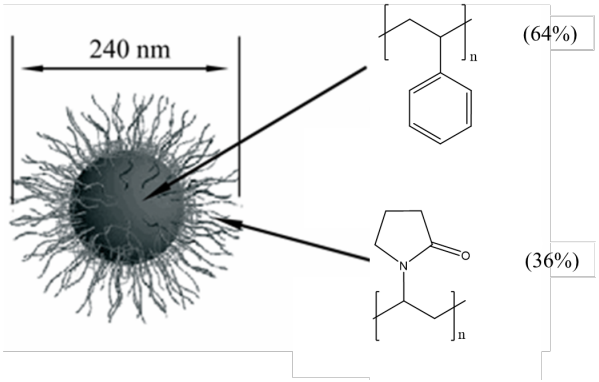

Figure 2.10: Schematic model of polystyrene and polyvinylpyrrolidone patterns of PS/PVP particle

Eudragit RL 100 Particles

The RL 100 bulk polymer is commercial available and consists of poly(methylacrylate) bearing a certain amount of positively charged quaternary ammonium groups ($\sim 10\%$). Nanoparticles can be prepared by dissolving the polymer and an organic solvent such as THF and a subsequently precipitation with water. The nano beads have a size average of 30 nm in solution [43]. Incorporation of the fluorescent dye has to be accomplished physically during the precipitation process [44]. The charge of the particles may have an influence on the cross sensitivity to the ionic strength in pH sensors. Due to the biocompatibility of the material several applications were reported [45–47].

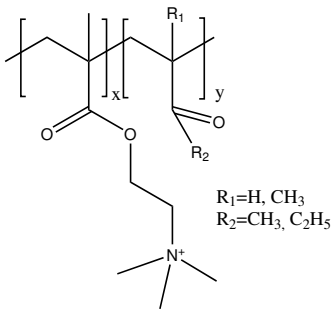

Figure 2.11: Structur of RL 100 particles with $\sim 10\%$ positively charged quaternary ammonium groups

2.3 Perylene Dyes

The perylene structure was developed in the early 20$^{\text{th}}$ century. Following the chromophoric system was well established and resulted in a great variety of perylene modifications. The class of perylene bisimide (PBI) dyes are one of the most reported modifications. They are known for their extraordinary spectral properties such as high molar absorption coefficients of 30 000 - 90 000 $\text{mol}\,\text{L}^{-1}\text{cm}^{-1}$ [48, 49] and quantum yields close to 1 [50]. Furthermore, derivates with outstanding photostability properties were reported [51].

Representatively normalized absorption and emission spectra of commercially available Lumogen Orange are shown in figure 2.12. This PBI dye with bulky aryl groups attached in imide-position was chosen as starting material in the practical part of this thesis.

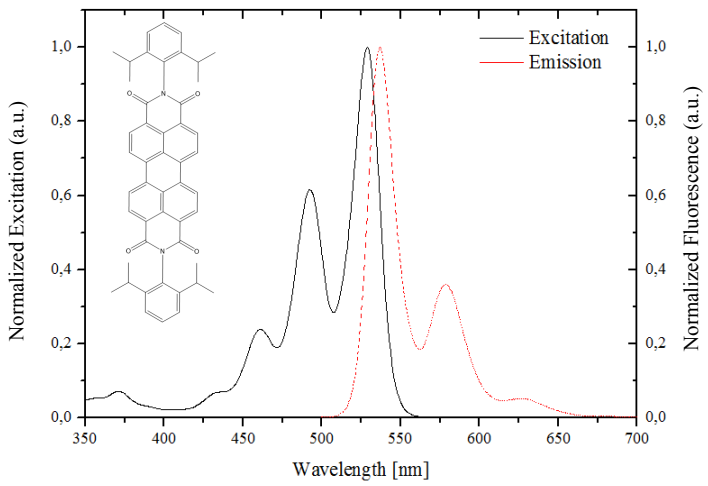

Figure 2.12: Excitation and emission spectra of commercially available Lumogen Orange

According to their spectral properties, some perylene dyes are also convenient standards for quantum yield measurements. In contrast to other commonly used standards such as quinine sulfate, this perylene dyes show quantum yields of 1, are tunable refering their solubility in water and organic solvents and they do not need special storage conditions. This facts offer a simplification for common usage [52].

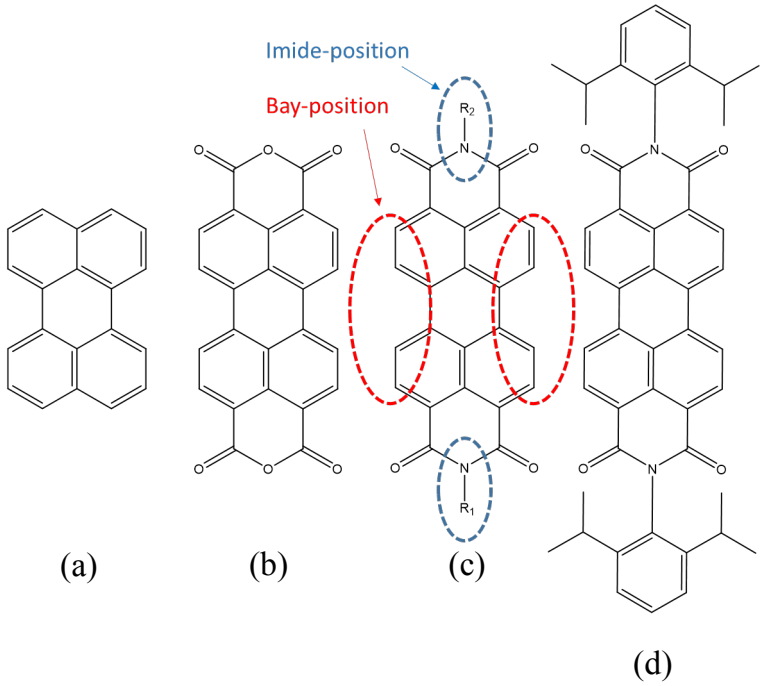

Figure 2.13: Overview of some perylene structures: (a) perylene core, (b) PTCDA, perylene-3,4,9,10-tetracarboxylic bisanhydride (often used as starting material) (c) perylene bisimide, (d) commercial available Lumogen Orange

Moreover, perylene bisimides show good versatility in consideration of synthetic modifications [53–56]. Aigner et al. introduced PET groups for applications in optical pH sensors [20, 21, 57]. Additionally to often used amines the introduction of phenoxide PET groups, which enable higher flexibility than amine groups, because they are able to quench fluorophores at basic pH which are not quenched by the commonly used amines, were reported [16]. Due to the great variety of dyes and their features applications in OLEDs [58], liquid crystal displays [59], fluorescent solar collectors [50] and photovoltaic cells [60] were reported.

Perylene bisimde dyes are often used in light emitting devices, because they possess high (photo)chemical and thermal stability, high brightness and brilliant colours. However, they have drawbacks, which reduce their utility in such applications. On one hand, many perylene derivates have low solubility, which lead to hindered preparation of thin films and concomitant to higher production costs.

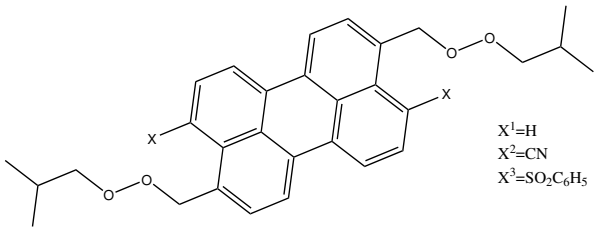

Figure 2.14: Structure of perylene derivate used for fluorescent collectors [50]

On the other hand, they suffer from interactions in the solid-state chromophore, such as migration, aggregation or crystallisation, which may cause a decrease of emission efficiency.

A smart way to overcome both of this problems simultaneously was reported by Qu et al. [61]. The formation of a pentaphenylene shield by using dendrones, in bay-position of the perylene core, which covers the chromophore (fig 2.15). This kind of modification results in high solubility and layer preparation properties as well as in high red-orange luminescence with reduced fluorophore interactions.

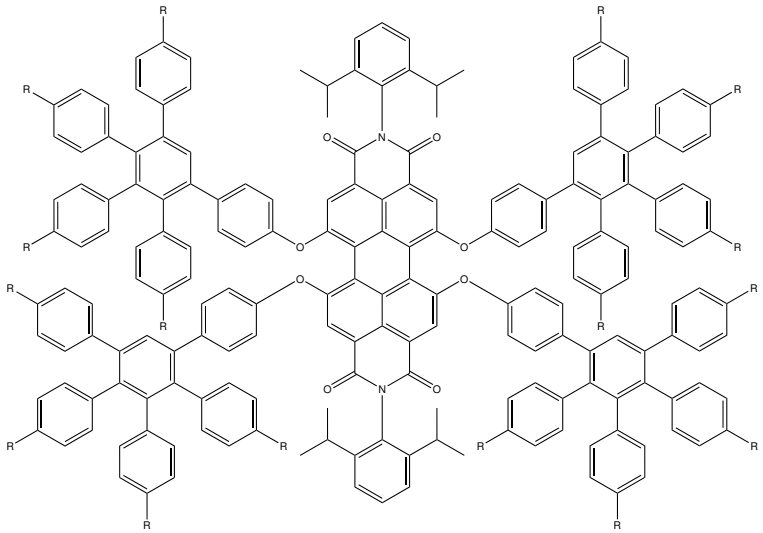

Figure 2.15: Structure of perylene core bearing pentaphenylene dendrones first generation for organic light emitting diode, R = alkyl chain [61]

A small overview of perylene structures is shown in figure 2.13. The structure shown in figure 2.16 present a nice sample how perylene modification can be achieved. In this case for the use in dye-sensitized solar cells, which are of interest due to their efficiency in conversion of solar energy to electricity at low cost [62].

Asymmetrical functionalisation in the imide-position of perylene bisimides can be achieved as well as introducing of an analyte sensitive group, e.g. for pH. A further synthetical modification

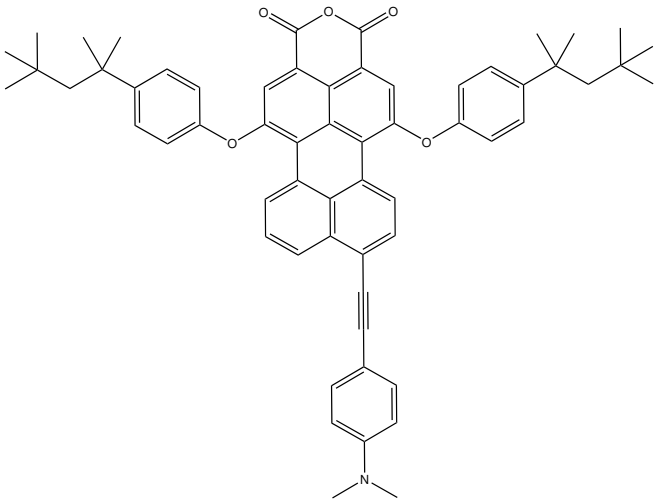

Figure 2.16: Structure of perylene derivate used in dye-sensitized solar cells

of the perylene structure is the interaction between two or three identical chromophores by linking them in imide-position. The distance of the chromophore-chromophore separation is reduced to a single bond of N-N. The low solubility of the bi-chromophoric system can be increased by introduction of solubilizing groups such as aryl substituents bearing *tert*-butyl groups linked to the terminal nitrogen atom (fig 2.17). The main improvement of such systems is the increase of the molar absorption coefficient from $\sim 80\,000\,\mathrm{mol\,L^{-1}cm^{-1}}$ for the single chromophore over $\sim 240\,000\,\mathrm{mol\,L^{-1}cm^{-1}}$ for the di-chromophore to $\sim 420\,000\,\mathrm{mol\,L^{-1}cm^{-1}}$ for the tri-chromophoric system, which can be explained by exciton interactions [63]. Furthermore, substitution in the bay-position influences the localisation of the spectra.

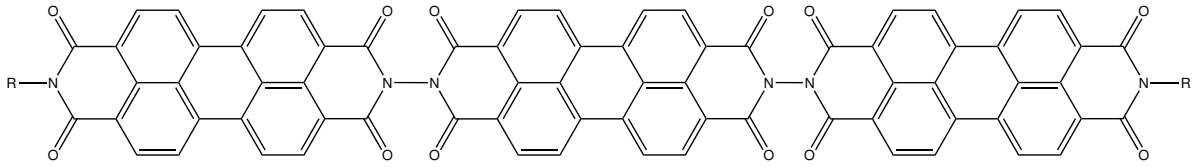

Figure 2.17: Schematic structure of three perylene bisimide molecules linked in imide-position to a tri-chromophore

Another field of applications where perylene derivates are used, are polymer light-emitting diodes (PLEDs). Those electroluminescent conjugated polymers have compared with inorganic and organic light emitting devices advantages in lower production costs, high flexibility and many opportunities of tuning the optical and electrical properties by varying the polymer structure. One integration strategy for perylene dyes, is the covalent coupling to the polymer chain. There are three binding sites for the perylene core attaching the polyfluorene chain for

tuning the emission colour, first as comonomer in the main chain, second as endcapping groups at the termini or third as pendant side groups (fig 2.18). Such polymers may fit individually to act efficiently as emitter for full colour displays covering the whole visible spectra [64].

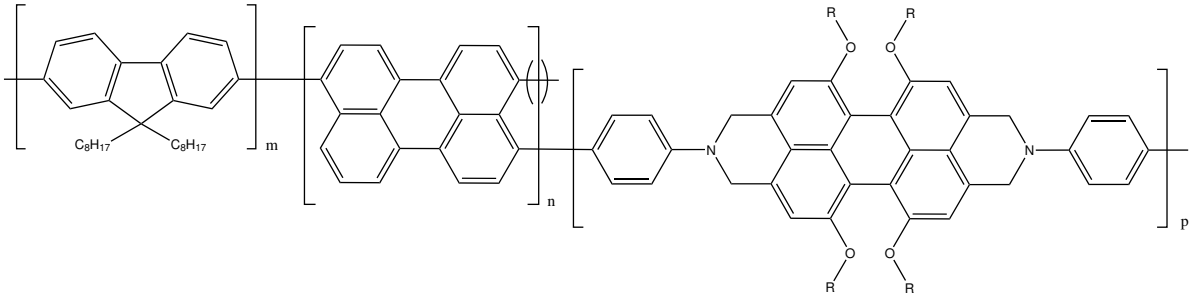

Figure 2.18: Structure of integrated perylene dye into polyfluorene backbone for tuning of emission colour properties

All this features make PBIs to promising candidates for further modifications, e.g. for pH sensitive indicator dyes. Langhals et al. [65] presented laterally extensions of the perylene core, causing a tunable bathochromic shift of the absorption spectral properties. Furthermore, introducing of a pH sensitive group and functionalities, which influence the spectral properties, open the door for the synthesis of a new class of pH sensitive perylene bisimide dyes.

3 Experimental

3.1 Materials and Methods

3.1.1 Photophysical Dye Characterisation

Absorption Spectra

Absorption spectra were recorded on a Varian Cary 50 UV-Vis spectraphotometer by Varian, Palo Alto, United States (www.agilent.com), between 800 nm and 350 nm using fast scan rate with baseline correction with an adequate blank sample. Precision cuvettes Hellma 100-OS 10 mm and 104-OS 10 mm were used.

Emission and Excitation Spectra

Emission and excitation spectra were recorded on a FluoroLog 3 Spectrofluorometer from Horiba Scientific Jobin Yvon (www.horiba.com) and corrected for detector response. Precision cuvettes Hellma 101-OS mm were used.

Quantum Yields

Determination of fluorescence quantum yields Φ_F were performed in THF using commercially available Lumogen Red (www.kremer-pigmente.com) or phtalocyanine as references [66, 67]. Lumogen Red was used for determination of Φ_F of Per-(PhIm), Per-(ClPhIm), Per-(Cl_2PhIm) and Per-(ClPhIm)-tBuPh. Phtalocyanine was used for quantum yield measurements of Per-$(PhIm)_2$.

Photostability

The photostability setup consisted of a high power green LED with 12x OSRAM Oslon SSL 80 and a cooling block (Wavelength: 528 nm, Voltage: 9.10 V, Photon flux: 15600 μmol s^{-1} m^{-2}, www.led-tech.de). Dye solutions in water-free toluene with an absorption maximum of 0.8 were

prepared. The cuvette was placed in focus of the LED setup and the absorption was measured every 15-30 minutes from 350 - 850 nm.

Single Photon Counting

Single Photon Counting lifetime measurements were performed on a FluoroLog 3 Spectrofluorometer from Horiba Scientific Jobin Yvon with a DeltaHub module. Data analysis was carried out with DAS6 software (www.horiba.com) using a mono-exponential fit. For determination of the fluorescence lifetimes, a certain amount of the dye was dissolved in THF to get a maximal absorption at λ_{exc} of 0.2. As excitation light source two Nano-LEDs (435 nm, 635 nm) were used to fit the spectral properties of the PBIs.

3.1.2 Chemical Dye Characterisation

Mass Spectrometry

Mass spectroscopy was performed on Micromass TofSpec 2E Time-of-Flight Mass Spectrometer by Ing. Karin Bartl at the Institute for Chemistry and Technology of Materials, Graz University of Technology.

NMR Spectroscopy

NMR spectra were recorded on a 300 MHz Bruker Instrument (www.bruker.com) using $CDCl_3$ or $DMSO-d^6$ as solvent. Data analysis was carried out with MestReNova software (www.mestrelab.com).

3.1.3 Sensor Properties

Buffer

pH value of different buffer solutions was adjusted with a pH meter (Education Line, Mettler Toledo, www.mt.com) using a glass electrode (InLab Routine Pro, Mettler Toledo, www.mt.com). The pH meter was calibrated at 25 °C with standard buffer solutions of pH 4.01, pH 7.01 and pH 10.01 (Hanna Instruments, www.hannainst.com). The ionic strength (150 mmol) of the buffers was regulated with sodium chloride as background electrolyte.

Calibration of pH Sensor Dyes in Solution

0.1 mg of indicator dye was dissolved in 0.75 ml THF, which was mixed with 0.5 ml EtOH, 0.5 ml buffer solution (20 mM) and 0.75 ml 450 mM NaCl solution, to get a constant ionic strength of 150 mM, to a total volume of 2.5 ml. Absorption spectra were recorded.

Calibration of pH Sensor Foils

The sensor foil was fixed in a glass cuvette, which was filled with 2 ml buffer solution (20 mM) and 1 ml of 450 mM NaCl solution to get a constant ionic strength of 150 mM. Absorption spectra and emission spectra were recorded.

Calibration of pH Sensitive Nanoparticles

An emission cuvette was filled with buffer (20 mM), NaCl solution and a certain amount of nano beads to a total volume of 2.5 ml. Ionic strength was adjusted to 150 mM with NaCl solution. Emission spectra were recorded.

Calibration of Carbon Dioxide Sensor Foils

The sensor foil was fixed in a flow through cell linked to a gas mixer. Gas calibration mixtures were produced with a gas mixing device from MKS (www.mksinst.com), controlled by LabView software. All gas mixtures were humidified to about 85 % relative humidity with silica gel and addition of saturated potassium chloride solution, directly before entering the flow cell. Temperature was controlled with a cryostat Thermostat Thermo Haake K10. Absorption and emission spectra were recorded.

Carbon Dioxide Measurements in Drinks

Sensor response curves were recorded with a two-phase lock-in amplifier (SR830, www.thinksrs.com) equipped with a green LED (λ_{Ex} 535 nm), a band pass filter at the excitation side (535 nm$\pm$ 12.5 nm, Edmund optics, www.edmundoptics.com) and a long pass filter RG 610 (Schott, www.schott.com) before the PMT tube (H5701-02, Hamamatsu, www.hamamatsu.com). 1500 Hz modulation frequency was used. Several samples were tested: pure water, water bubbled with CO_2, mineral water (Römerquelle mild), beer (Puntigamer) and Coca-Cola.

Leaching out of a Matrix

For the absorption-based measurements the 4 different PBIs were embedded into hydrogel D4 using THF as solvent to produce 75 μm thin wet films on a PET support. After evaporation of the solvent at RT the foils were fixed in a house made flow-through-cell. A constant flow of buffer solution through the cell was adjusted with a peristaltic pump equipped with a flexible tube from ismatec (www.ismatec.com; purple/black, ID: 2.29 mm) and absorption spectra were recorded regularly over 24 hours. Two buffer solutions were used (pH 6.57, pH 12.5) to determine both protonated/deprotonated species of the dye. Ionic strength was fixed at 150 mM with NaCl solution.

Size of Nano beads

Size of the beads was determined with a particle analyser Zetasizer Nano ZS (malvern-instruments, www.malvern.com).

3.2 Synthesis

3.2.1 Per-(PhIm)

2,11-Bis(2,6-diisopropyl-benzyl)-5-phenylimidazolo[4',5':3,4]anthra[2,1,9-def:6,5,10-d'e'f']diisochinolin-1,3,10,12(2H,11H)-tetraon

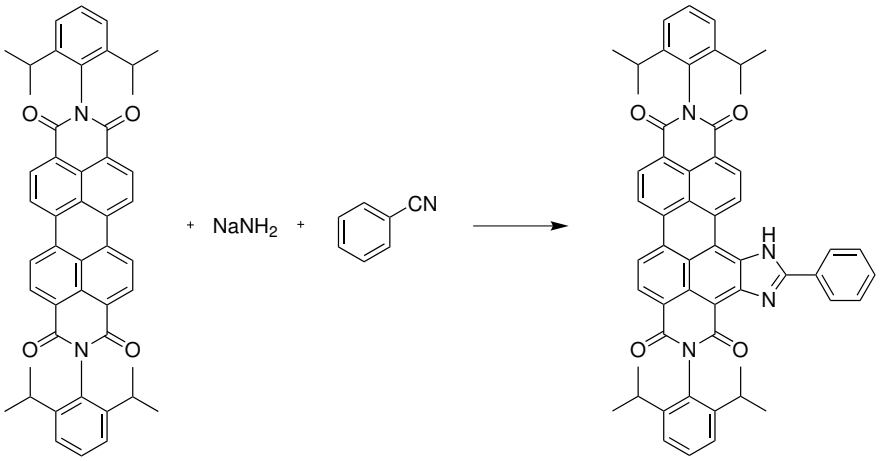

Figure 3.1: Reaction scheme for Per-(PhIm)

Lumogen Orange (400 mg, 0.563 mmol) and $NaNH_2$ (95 %, 440 mg, 11.3 mmol) were dispersed in anhydrous benzonitrile (50 ml) under inert atmosphere of N_2 and heated to 165 °C. The colour changed from orange to green and afterwards to dark blue. Compressed-air was bubbled through the reaction mixture for 30 minutes. The reaction was allowed to cool to RT, a 1:1 mixture of 1 M aqueous HCl/dichloromethane (V/V) (200 ml) was added. The organic phase was washed three times with 1 M aqueous HCl (100 ml) and dried over Na_2SO_4. Dichloromethane was evaporated and the benzonitrile was removed *in fine vacuo*. The purple crude product was purified by column chromatography using silica gel (35-70 μm) as stationary and cyclohexane/ethylacetate 93+7 as mobile phase to yield mono-phenylimidazolsubstituded perylene bisimide Per-(PhIm) (220 mg, 47 %).

^{1}H NMR (300 MHz, Chloroform-d) δ 11.58 (s, 1H), 11.01 (d, J = 8.2 Hz, 1H), 8.98 (d, J = 8.2 Hz, 1H), 8.91-8.78 (m, 4H), 8.34 (dd, J = 6.6, 3.0 Hz, 2H), 7.70-7.62 (m, 3H), 7.53 (dt, J = 13.1, 7.9 Hz, 2H), 7.39 (dd, J = 12.6, 7.7 Hz, 4H), 2.82 (h, J = 6.9 Hz, 4H), 1.21 (dd, J = 6.9, 4.6 Hz, 24H)

MALDI-TOF-MS m/z: $[M]^+$ calc for $C_{55}H_{46}N_4O_4$: 826.352; found: 826.458

λ_{Abs}: 589 nm, 543 nm

ε: 82 000, 45 000 $[L \cdot mol^{-1} \cdot cm^{-1}]$

3.2.2 Per-(PhIm)$_2$

2,10-Bis(2,6-diisopropyl-benzyl)-8,12-dihydro-5-phenylimidazolo[4,5-h]15-phenylimidazolo[4',5':3,4]isochino[6',5',4':10,5,6]anthra[2,1,9-def]isochinolin-1,3,9,11(2H,10H)-tetraon

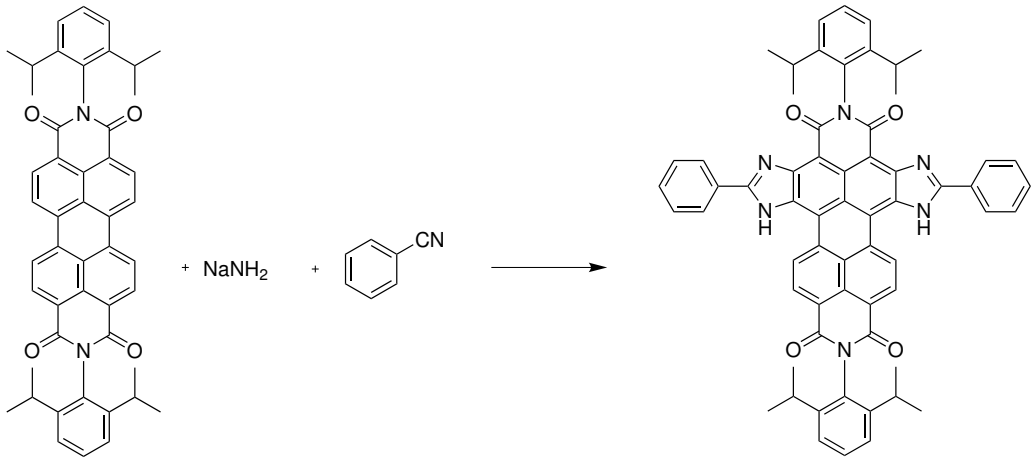

Figure 3.2: Reaction scheme for Per-(PhIm)$_2$

Lumogen Orange (120 mg, 0.169 mmol) and $NaNH_2$ (99 %, 118 mg, 3.02 mmol) were dispersed in anhydrous benzonitrile (15 ml) under inert atmosphere of N_2 and heated to 165 °C. The colour changed from orange to green and afterwards to dark blue. Compressed-air was bubbled through the reaction mixture for 30 minutes. The reaction was allowed to cool to RT, a 1:1 mixture of 1 M aqueous HCl/dichloromethane (V/V) (200 ml) was added and the organic phase was washed three times with 1 M aqueous HCl (100 ml) and dried over Na_2SO_4. Dichloromethane was evaporated and the benzonitrile was removed *in fine vacuo*. The purple crude product was separated by column chromatography using silica gel (35-70 μm) as stationary and cyclohexane/ethylacetate 93+7 as mobile phase to get the side product Per-(PhIm) and cyclohexane/ethylacetate 7+1 to elute the regio isomers of double-phenylimidazolsubstituted perylene bisimide Per-(PhIm)$_2$ (35 mg, 22 %).
MALDI-TOF-MS m/z: $[M]^+$ calc for $C_{62}H_{50}N_6O_4$: 942.389; found: 942.485
λ_{Abs}: 639 nm, 586 nm
ε: 69 000, 29 000 $[L \cdot mol^{-1} \cdot cm^{-1}]$

3.2.3 Per-(PhIm)$_3$

Perylene bisimide substituted with 3 phenylimidazol groups

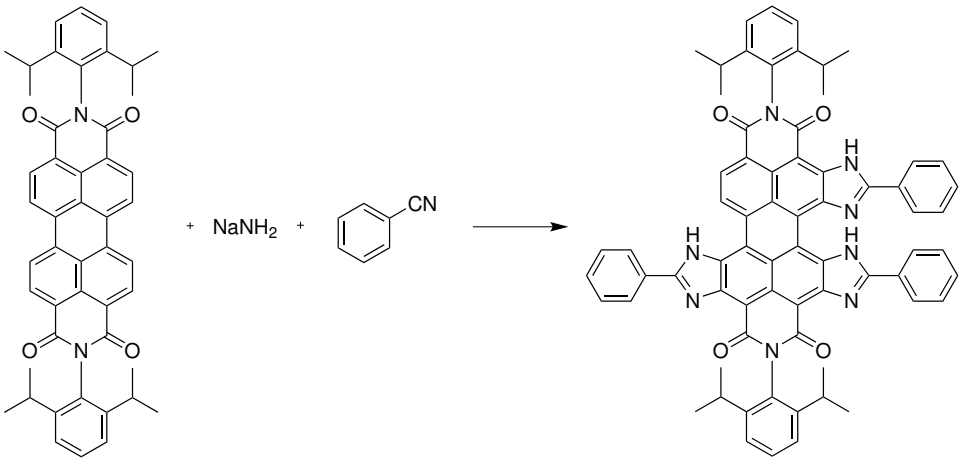

Figure 3.3: Reaction scheme for Per-(PhIm)$_3$

Lumogen Orange (400 mg, 0.563 mmol) and $NaNH_2$ (99 %, 460 mg, 11.79 mmol) were dispersed in anhydrous benzonitrile (50 ml) under inert atmosphere of N_2 and heated to 165 °C. The colour changed from orange to green and afterwards to dark blue. Compressed-air was bubbled through the reaction mixture for 30 minutes. The reaction was allowed to cool to RT, a 1:1 mixture of 1 M aqueous HCl/dichloromethane (V/V) (200 ml) was added and the organic phase was washed three times with 1 M aqueous HCl (100 ml) and dried over Na_2SO_4. Dichloromethane was evaporated and the benzonitrile was removed *in fine vacuo*. The purple crude product was separated by column chromatography using silica gel (35-70 μm) as stationary and cyclohexane/ethylacetate as mobile phase to mono-, regio isomers of double- and tri-phenylimidazolsubstituted perylene bisimide Per-(PhIm)$_3$ (30 mg, 5 %) .
MALDI-TOF-MS m/z: $[MH]^+$ calc for $C_{69}H_{54}N_8O_4$: 1059.4346; found: 1059.4185
λ_{Abs} (I_{rel}): 693 nm (1.00), 634 nm (0.50)

3.2.4 Per-(ClPhIm)

2,11-Bis(2,6-diisopropylphenyl)-5-(4-chlorophenyl)-imidazolo[4',5':3,4]anthra[2,1,9-def:6,5,10-d'e'f']diisochinolin-1,3,10,12(2H,11H)-tetraon

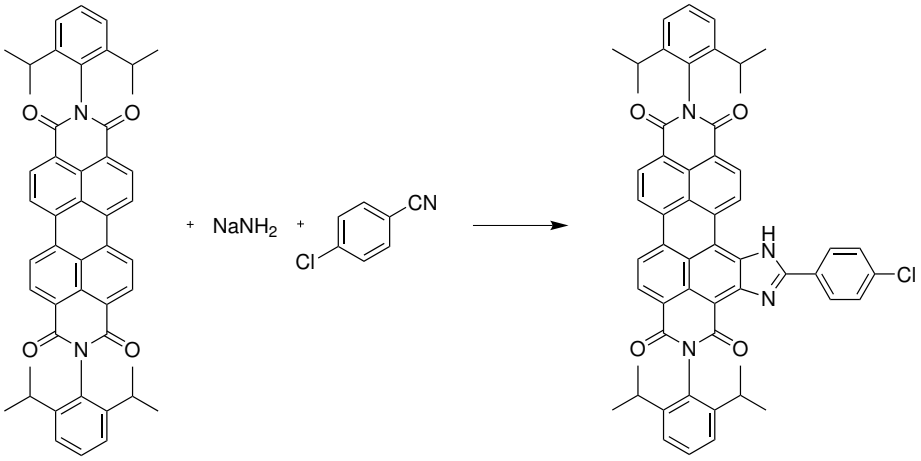

Figure 3.4: Reaction scheme for Per-(ClPhIm)

Lumogen Orange (105 mg, 0.148 mmol), $NaNH_2$ (95 %, 160 mg, 4.10 mmol) were quickly homogenised in a mortar and 4-chlorobenzonitrile (7.16 g) was added. The powder was transfered into a Schlenk flask and heated to 150 °C under inert atmosphere of N_2. The colour changed from orange to purple/dark red. At 160 °C compressed-air was bubbled through the reaction mixture and it was stirred for 3 hours under reflux conditions. The reaction was allowed to cool to RT, a 1:1 mixture of 1 M aqueous HCl/dichloromethane (V/V) (150 ml) was added and the organic phase was washed three times with 1 M aqueous HCl (50 ml) (colour changed from green to purple because of acidic conditions) and dried over Na_2SO_4. Dichloromethane was evaporated and remaining 4-chlorobenzonitrile was removed *in fine vacuo*. The crude product was purified by column chromatography using silica gel (35-70 μm) as stationary and cyclohexane/ethylacetate 94+6 as mobile phase to yield Per-(ClPhIm) (47 mg, 37 %).
^{1}H NMR (300 MHz, Chloroform-d) δ 11.56 (s, 1H), 10.96 (d, J = 8.2 Hz, 1H), 8.97 (d, J = 8.2 Hz, 1H), 8.93-8.76 (m, 4H), 8.31-8.23 (m, 2H), 7.67-7.61 (m, 2H), 7.53 (dt, J = 12.6, 8.0 Hz, 2H), 7.39 (dd, J = 12.1, 7.7 Hz, 4H), 2.81 (m, 4H), 1.23-1.08 (m, 24H)
MALDI-TOF-MS m/z: $[M]^+$ calc for $C_{55}H_{45}ClN_4O_4$: 860.313; found: 860.348
λ_{Abs}: 589 nm, 544 nm
ε: 64 000, 34 000 $[L \cdot mol^{-1} \cdot cm^{-1}]$

3.2.5 Per-(Cl_2PhIm)

2,11-Bis(2,6-diisopropylphenyl)-5-(2,6-dichlorophenyl)-imidazolo[4',5':3,4]anthra[2,1,9-def:6,5,10-d'e'f']diisochinolin-1,3,10,12(2H,11H)-tetraon

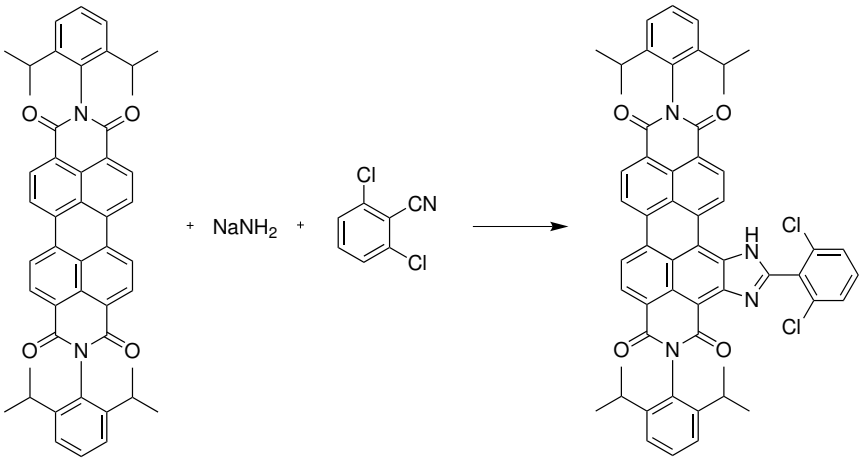

Figure 3.5: Reaction scheme for Per-(Cl_2PhIm)

Lumogen Orange (120 mg, 0.169 mmol), $NaNH_2$ (99 %, 500 mg, 12.82 mmol) were quickly homogenised in a mortar and 2,6-dichlorobenzonitrile (7.05 g)was added. The powder was transfered into a Schlenk flask and heated to 160 °C under inert atmosphere of N_2. The colour changed from orange to purple/dark red. At 170 °C compressed-air was bubbled through the reaction mixture and it was stirred for 1 hour under reflux conditions. The reaction was allowed to cool to RT, a 1:1 mixture of 1 M aqueous HCl/dichloromethane (V/V) (150 ml) was added and the organic phase was washed three times with 1 M aqueous HCl (50 ml) (colour changed from green to purple because of acidic conditions) and dried over Na_2SO_4. Dichloromethane was evaporated and remaining 2,6-dichlorobenzonitrile was removed *in fine vacuo*. The crude product was purified by column chromatography using silica gel (35-70 μm) as stationary and dichloromethane as mobile phase to yield Per-(Cl_2PhIm) (101 mg, 67 %).
^{1}H NMR (300 MHz, Chloroform-d) δ 11.40 (s, 1H), 10.89 (d, J = 8.2 Hz, 1H), 9.00-8.70 (m, 5H), 7.58 (d, J = 7.0 Hz, 2H), 7.54-7.45 (m, 3H), 7.37 (dd, J = 10.3, 7.7 Hz, 4H), 2.81 (m, 4H), 1.19 (m, 24H)
MALDI-TOF-MS m/z: $[M]^+$ calc for $C_{55}H_{44}Cl_2N_4O_4$: 894.2740; found: 894.2684
λ_{Abs}: 579 nm, 534 nm
ε: 42 000, 23 000 $[L \cdot mol^{-1} \cdot cm^{-1}]$

3.2.6 Per-(ClPhIm)-*t*-ButylPh

2,11-Bis(2,6-diisopropylphenyl)-5-((4-(tert-butyl)benzyl)-4-chlorophenyl)-imidazolo[4',5':3,4]anthra[2,1,9-def:6,5,10-d'e'f']diisochinolin-1,3,10,12(2H,11H)-tetraon

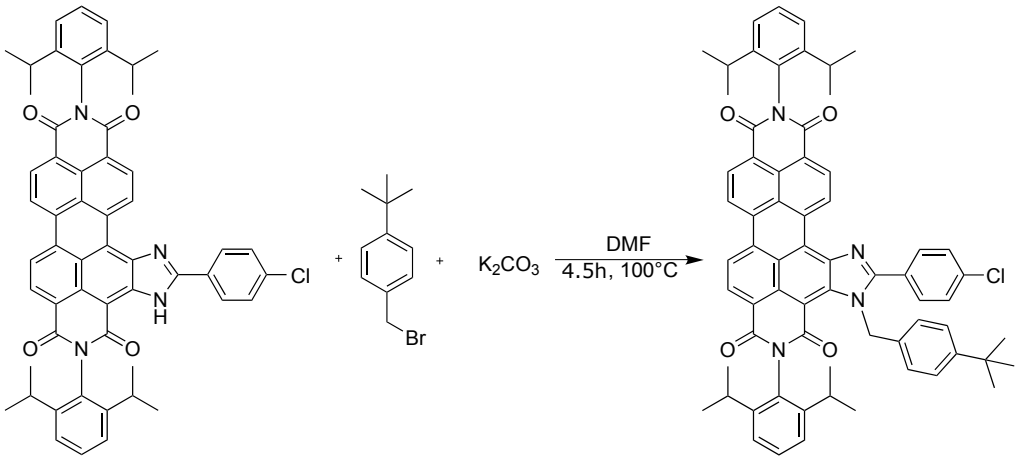

Figure 3.6: Reaction scheme for Per-(ClPhIm)-*t*-ButylPh

Per-(ClPhIm) (20 mg, 0.024 mmol) was dissolved in N,N-dimethylformamide (2 ml) and heated to 100 °C. Potassium carbonate (30 mg, 0.217 mmol) was added and the colour changed from red to dark purple/dark blue. *Tert*-butylbenzylbromide (80 µl, 0.435 mmol) was added dropwise and the colour changed repeatedly to red/purple. After stirring for 4.5 hours at 100 °C the reaction mixture was allowed to cool down to RT and was quenched with 1 M aqueous HCl (4 ml). The dark purple precipitate was filtered, washed with water and dried *in vacuo*. The crude product was purified by column chromatography using silica gel (35-70 μm) as stationary and cyclohexane/dichloromethane 1+2 as mobile phase to yield Per-(ClPhIm)-*t*-ButylPh (14 mg, 58 %).

^{1}H NMR (300 MHz, Chloroform-d) δ 10.93 (d, J = 8.2 Hz, 1H), 8.90 (d, J = 8.0 Hz, 2H), 8.82 (d, J = 1.9 Hz, 3H), 7.92-7.79 (m, 2H), 7.63-7.54 (m, 2H), 7.51 (m, 2H), 7.36 (d, J = 7.7 Hz, 4H), 7.05 (d, J = 8.2 Hz, 2H), 6.43 (d, J = 8.1 Hz, 2H), 6.24 (s, 2H), 2.79 (m, 2H), 2.64 (m, 2H), 1.23-1.04 (m, 33H)

MALDI-TOF-MS m/z: $[M_2H]^+$ calc for $C_{66}H_{59}ClN_4O_4$: 1008.4381; found: 1008.4943

λ_{Abs}: 583 nm, 539 nm

ε: 62 000, 32 000 $[L \cdot mol^{-1} \cdot cm^{-1}]$

3.2.7 Per-(PhIm)-N(EtHex)$_2$

Chlorosulfonation and substitution with di-(2-ethylhexyl)amine

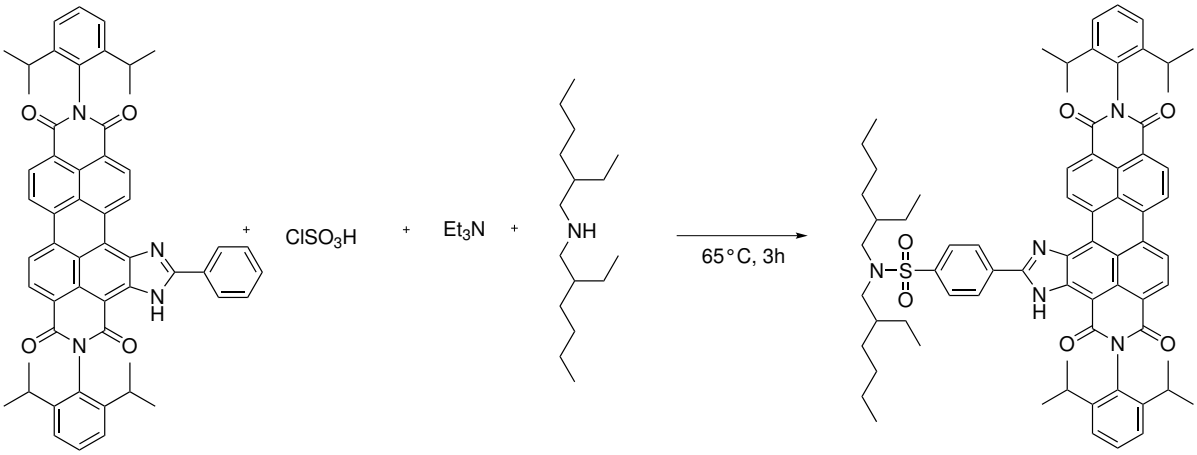

Figure 3.7: Reaction scheme for chlorosulfonation and substitution with di-(2-ethylhexyl)amine

Per-(PhIm) (40 mg, 0.048 mmol) was dissolved and heated to 65 °C in chlorosulfonic acid (0.5 ml) for 3 hours (blue colour). The reaction mixture was cooled to RT and afterwards quenched, while adding dropwise on ice. The dark blue precipitate was filtered and washed with cold water. The filtered precipitate was dissolved in anhydrous N,N-dimethylformamide (6 ml) and dried over Na_2SO_4. Triethylamine (66.5 μl, 0.48 mmol), di-(2-ethylhexyl)amine (82.5 μl, 0.273 mmol) were added. After stirring over night at RT, the product was extracted with 0.1 M aqueous HCl/dichloromethane 1:1 (50 ml) and the organic phase was dried over Na_2SO_4. The organic solvent was evaporated in vacuo. The purple product was purified by column chromatography with silica gel (35-70 μm) as stationary and dichloromethane/MeOH 95+5 as mobile phase to yield Per-(PhIm)-N(EtHex)$_2$ (13 mg, 24 %).
MALDI-TOF-MS m/z: $[M]^+$ calc for $C_{71}H_{78}N_5O_6S$: 1128.57; found: 1128.59

3.2.8 TOATPB

Tetraoctylammonium-tetraphenylborate

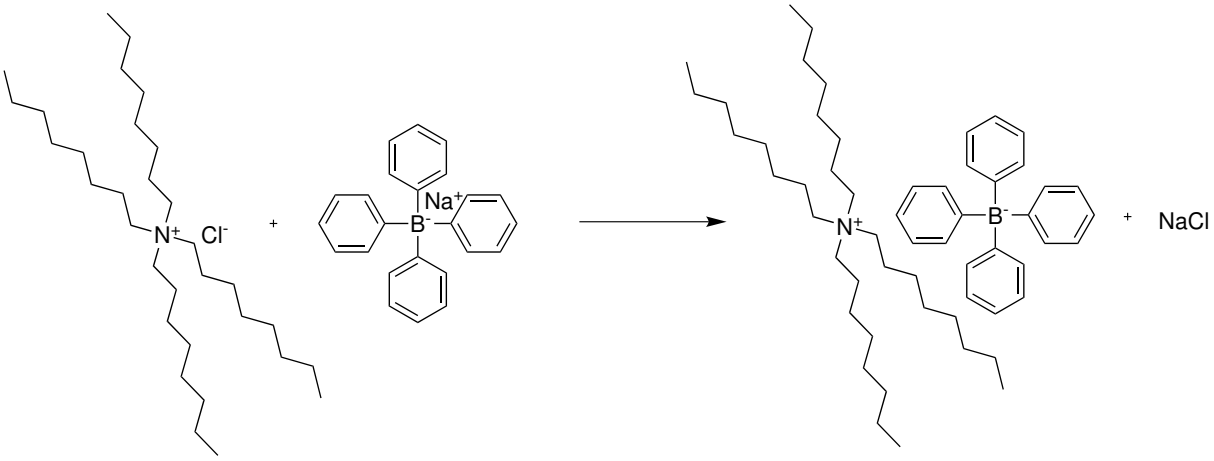

Figure 3.8: Reaction scheme for TOATPB

The reaction was conducted according to literature [68]. Tetraoctylammonium chloride (440 mg, 0.88 mmol) and sodium tetraphenylborate (150 mg, 0.44 mmol) were dissolved in THF (1 ml) and stirred for 10 minutes at RT, followed by a filtration over silica gel (35-70 μm) with THF. The solvent was removed *in vacuo* and a white needle-solid was obtained. The product was filtered for a second time over silica gel with dichloromethane. dichloromethane was evaporated and the product was dissolved in a small amount of dichloromethane and precipitated in cyclohexane, filtered and dried *in vacuo* to yield TOATPB (533 mg, 72 %) as white needles.
^{1}H NMR (300 MHz, DMSO-d6) δ 7.18 (dt, J = 10.1, 3.4 Hz, 8H), 6.92 (t, J = 7.3 Hz, 8H), 6.78 (t, J = 7.2 Hz, 4H), 3.14 (dd, J = 11.2, 5.6 Hz, 8H), 1.56 (q, J = 8.0, 6.8 Hz, 8H), 1.37-1.17 (m, 40H), 0.93-0.81 (m, 12H)
MALDI-TOF-MS m/z: $[M]^+$ calc for $C_{32}H_{68}N^+$: 466.5352; found: 466.5726

3.3 Physical Entrapment into Polymer Matrices

3.3.1 Preparation of Sensor Layers

Stock-Solutions

The stock-solutions of the dyes were prepared by weighing Per-(PhIm), Per-$(PhIm)_2$, Per-(ClPhIm), Per-(Cl_2PhIm), Per-(ClPhIm-tBuPh) and 3-(6-butylbenzothiazol-2-yl)-7-(dibutylamino)-coumarin in vials. The dyes were dissolved in THF to obtain $2\,mg\,ml^{-1}$ solutions. Polymer and plasticizer stock-solutions were prepared by weighing hydrogel D4 and D7 and tetraethyleneglycol (TEG) in 20 ml vials. THF was added and under vigorous stirring polymer and plasticizer were dissolved to obtain solutions of 10 % w/w polymer in solvent and respectively 20 % w/w TEG in solvent. The list of stock-solution is shown in table 3.1:

Table 3.1: Preparation of stock-solutions

Stock-solution	Compound	Solvent		Concentration	
	[mg]	[ml]	[mg]	[mg · ml^{-1}]	[% w/w]
Per-(PhIm)	4	2		2	
Per-$(PhIm)_2$	4	2		2	
Per-(ClPhIm)	4	2		2	
Per-(Cl_2PhIm)	4	2		2	
Per-(ClPhIm)-*t*-ButylPh	2	1		2	
Coumarin	6	3		2	
Polymer D4	100		900		10
Polymer D7	100		900		10
Plasticizer TEG	200		800		20

General Procedure

For the "cocktail" preparation, dye and polymer given in tables 3.2 were mixed and homogenised under vigorous stirring. 400 μl cocktail solution were put onto a PET support and quickly knife-coated in order to obtain a sensor foil with defined thickness. Solvent was evaporated at RT.

pH Sensitive Foils

Dye and polymer stock-solutions were pipetted in a 3 ml vial and homogenised under vigorous stirring. The cocktail was knife coated onto a PET support (polyethyleneterephtalate). Layer-thickness depended on the field of use (absorption spectra, emission spectra) and are given in table 3.2 for wet films before the solvent was evaporated.

Table 3.2: Composition of pH sensitive layers

Cocktail	Dye [mg]	Hydrogel D4 [mg]	Abs. Layer [μm]	Em. Layer [μm]
Per-(PhIm)	1	100	75	25
Per-$(PhIm)_2$	1	100	75	25
Per-(ClPhIm)	1	100	75	25
Per-(Cl_2PhIm)	1	100	25	12.5

Carbon Dioxide Sensitive Foils

The cocktail solution containing 0.25 mg dye, 100 mg hydrogel D7 and 100 mg TEG (stock-solutions can be seen in tab. 3.1) was homogenised under vigorous stirring. The mixture was purged with carbon dioxide. Afterwards 10 μl of TOA-OH solution (20 % w/w solution in MeOH) were added, homogenised and knife coated onto a PET support with a layer-thickness of 75 μm + 70 μm (wet films). Before the solvent was totally evaporated a 47 μm thick hydrophobic Teflon membrane was fixed onto the sensor foil.

H_2O/Humidity Sensitve Foils

The cocktail solution containing 0.25 mg Per-(ClPhIm)-*t*-ButylPh, 1.00 mg 3-(6-butylbenzothiazol-2-yl)-7-(dibutylamino)-coumarin, 50 mg hydrogel D4 and 25 mg TiO_2 P170 was homegenised under vigorous stirring. For preparation of the cocktails stock-solutions (tab. 3.1) were used.

3.3.2 Preparation of Sensitive Nanoparticles

PS/PVP Particles with addition of Tetraoctylammoniumchlorid TOACl

Polystyrene-polyvinylpyrrolidone emulsion (131.5 mg, 38 % w/w emulsion in water) was diluted with 10 ml EtOH and 5 ml water under vigorous stirring. 125 μl (0.5 % w/w) Per-(PhIm)-stock-solution (2 mg ml^{-1} in THF) and 45.5 μl TOACl-stock-solution (4 mg ml^{-1} in THF) were dried and dissolved in 2.5 ml EtOH and added dropwise to the PS/PVP-solution under vigorous stirring. EtOH was removed *in vacuo*, the emulsion was concentrated and diluted with water to a total volume of 10 ml.

PS/PVP Particles with addition of Tetraoctylammoniumtetraphenylborate TOATPB

Polystyrene-polyvinylpyrrolidone emulsion (131.5 mg, 38 % w/w emulsion in water) was diluted in 10 ml EtOH and 5 ml water under vigorous stirring. 125 μl (0.5 % w/w) Per-(PhIm)-stock-solution (2 mg ml^{-1} in THF) and 71 μl TOATPB-stock-solution (4 mg ml^{-1} in THF) were dried and dissolved in 2.5 ml EtOH and added dropwise to the PS/PVP-solution under vigorous stirring. EtOH was removed *in vacuo*, the emulsion was concentrated and diluted with water to a total volume of 10 ml.

PS/PVP Particles with addition of Tetraoctylammoniumhydroxide TOAOH

Polystyrene-polyvinylpyrrolidone emulsion (131.5 mg, 38 % w/w emulsion in water) was diluted in 10 ml EtOH and 5 ml water under vigorous stirring. 125 μl (0.5 % w/w) Per-(PhIm)-stock-solution (2 mg ml^{-1} in THF) were pipetted into a vial and the solvent was evaporated. The dye and TOAOH-solution (30 μl, 20 % w/w solution in MeOH) were dissolved in 2.5 ml EtOH and added dropwise to the PS/PVP-solution under vigorous stirring. EtOH was removed *in vacuo*, the emulsion was concentrated and diluted with water to a total volume of 10 ml.

Eudragit RL 100 Particles

Three probes of Eudragrit RL 100 polymer (50.0 mg) were dissolved in 25 ml acetone under vigorous stirring for 10 minutes. To each of them different amounts 62.5, 125 and 250 μl of Per-(PhIm)-stock-solution (2 mg ml^{-1} in THF) were added to get solutions with 0.25, 0.5 and 1 % w/w dye amount. For the synthesis of nanoparticle 100 g of water were added immediately under vigorous stirring. Acetone was removed *in vacuo*, the clear purple solution was concentrated to a total volume of 10 ml.

4 Results and Discussion

4.1 Synthesis

4.1.1 Substitution of Phenyl-Imidazolgroups on Perylene Bisimide (PBI)

Various commercially available perylene dyes can be modified, using benzonitrile and $NaNH_2$. Subsequently it is possible to obtain a variety of dyes due to changed spectral properties. As starting material Lumogen Orange was chosen because of its high solubility in organic solvents, its spectral properties and its commercial availability.

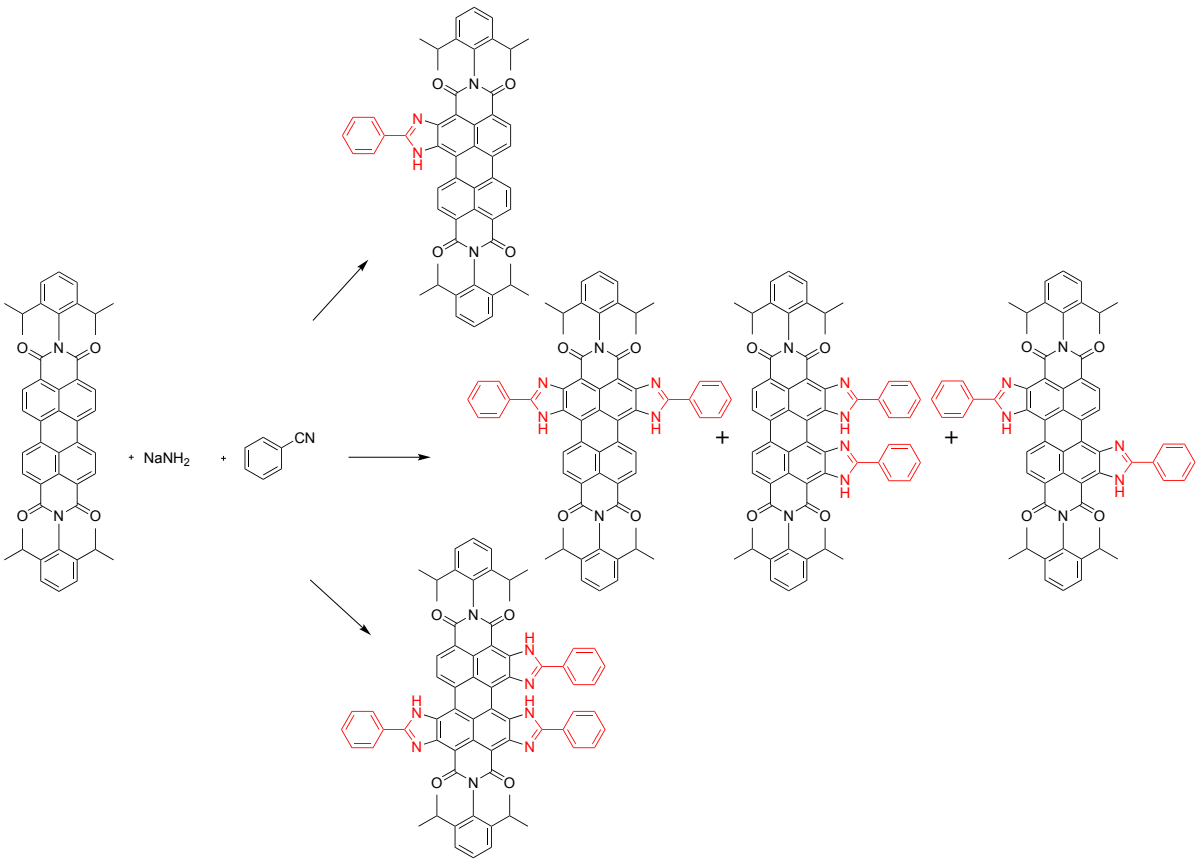

Figure 4.1: Substitution scheme for perylene bisimide at bay-region

The modification of perylene dye at the bay-region of the molecule structure with donor groups which results in a bathochromic shift was investigated by the group of Langhals [69]. The use of a strong nucleophile, basic sodium amide and a dipolar aprotic solvent benzonitrile causes a ring closure and introduce a 2-phenyl-imidazol-group into the perylene structure. This enlargement of the conjugated chromophoric system causes a bathochromic shift of absorption and emission spectra [65]. High reaction temperatures up to 170 °C, the presence of oxygen and the purity of sodium amide are the main requirements for the reaction [70]. The reaction mixture has to be held under inert nitrogen atmosphere prior and after the addition of sodium amide, till the reaction temperature is reached to guarantee the reactivity of sodium amide, what accords with the investigations on sodium amide of Winter [71].

For the synthesis of Lumogen Orange with additional phenyl-imidiazolgroups at the bay-region of the molecule (Per-(PhIm), Per-$(PhIm)_2$, Per-$(PhIm)_3$), commercially available Lumogen Orange and 20 equivalents of $NaNH_2$ were dispersed in anhydrous benzonitrile under inert atmosphere to keep the reactivity. The reaction mixture was stirred and heated to 165 °C. When the reaction temperature was reached, dried air was bubbled through the solution. At this point should be mentioned that change of colour of the mixture indicated a reaction and a shift of absorption spectra can be obtained (fig 4.2). At the beginning the synthesis was focused on Per-$(PhIm)_2$, because its emission is located in the NIR region. Neither additional $NaNH_2$ up to 80 equivalents nor longer reaction times led to the desired result. Each experiment yielded a mixture of Per-(PhIm), Per-$(PhIm)_2$, Per-$(PhIm)_3$.

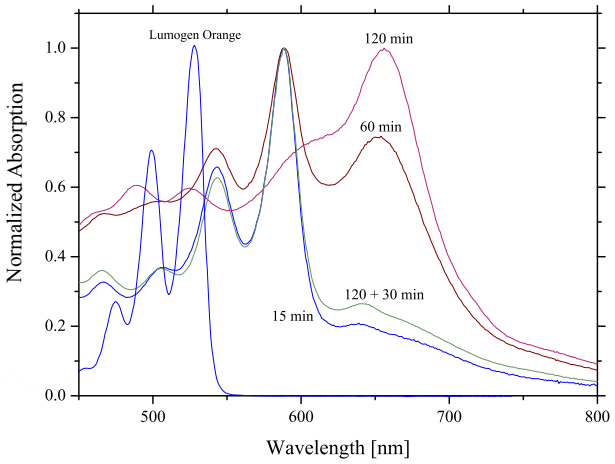

Figure 4.2: Absorption spectra (in DCM) during the reaction of Lumogen Orange with benzonitrile and $NaNH_2$

The main investigation which directed the further work of this thesis can be explained with absorption spectra recorded during the reaction, shown in figure 4.2. The absorption spectrum of

Lumogen Orange, with its maximum at 527 nm is presented and furthermore the spectra of the reaction mixture dissolved in DCM after 15, 60, 120 minutes. The absorption spectrum of the last sample (after 120 min) was recorded and the probe was stored for 30 minutes and repeatedly measured. The first interpretation was that after 15 minutes a mainly mono-substituted product with characteristic absorption band at 589 nm was formed and further $NaNH_2$ was added to the reaction mixture to improve kinetically di-substitution. The spectra after 60 and 120 minutes led to the assumption Per-$(PhIm)_2$ was formed with an increasing expanded absorption band at around 650 nm. However, during the following 30 minutes the colour of the sample changed from blue to pink and the obtained absorption spectrum was nearly identically to the first one, which was taken after 15 minutes.

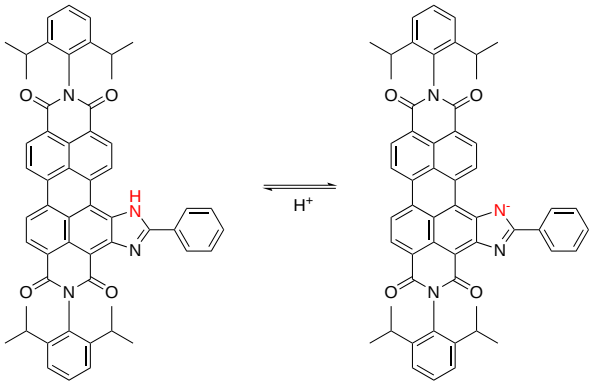

Figure 4.3: Protonation of Per-(PhIm) indicates pH sensitivity

The observed absorption spectra during the reaction (fig. 4.2) indicated a reversible process, not the forming of the expected di-phenylimidazol-substituted product. Rather the influence of the strongly basic properties of sodium amide let to the change of the absorption spectra. The introduced phenylimidazol-substituent can occur in a protonated as well as in a deprotonated state (fig. 4.3). $NaNH_2$ has a bad solubility in dichloromethane and precipitated while cooling. Furthermore, the signal to noise ratio decreased at shorter wavelengths, what might be caused by turbidity of the solution. Indeed the ratio increased when $NaNH_2$ totally precipitated and sank down to the bottom of the flask/cuvette. pH sensitivity of the obtained phenylimidazol substituted perylene bisimide was found.

There are a few phenyl-imidazol substitution possibilities, which are shown in figure 4.1 with mono, di (3 regio isomers) and tri -substitution. Considering literature, it was expected that a higher amount of $NaNH_2$ as well as purer chemicals will lead to di- and tri- substituted products [72]. But during the practical part of this thesis, it was not possible to find the ideal conditions to obtain the preferred products. Nevertheless, 99% pure $NaNH_2$ improves the

reaction equilibrium to yield a mixture of phenyl-imidazol-substituted products. In figure 4.13 (page 50) the bathochromic shifts due to the introduction of phenyl-imidazol groups to the conjugated chromophoric system of Lumogen Orange are shown.

The purification using column chromatography was challenging, because all products have similar polarity. However, the separation of the 3 di-substituted regio isomers, was possible as it can be seen in figure 4.4. The solubility of two of them was worse, which led to the consequence that the isomer with the best solubility was used for further characterisation experiments. Kinzel investigated spectral differences of di-phenyl-imidazol-perylene bisimide isomers in his doctoral thesis [72], which were useful for this work to identify the products. However, different bisimide-substituents were used, but absorption bands with similar shifts were detected.

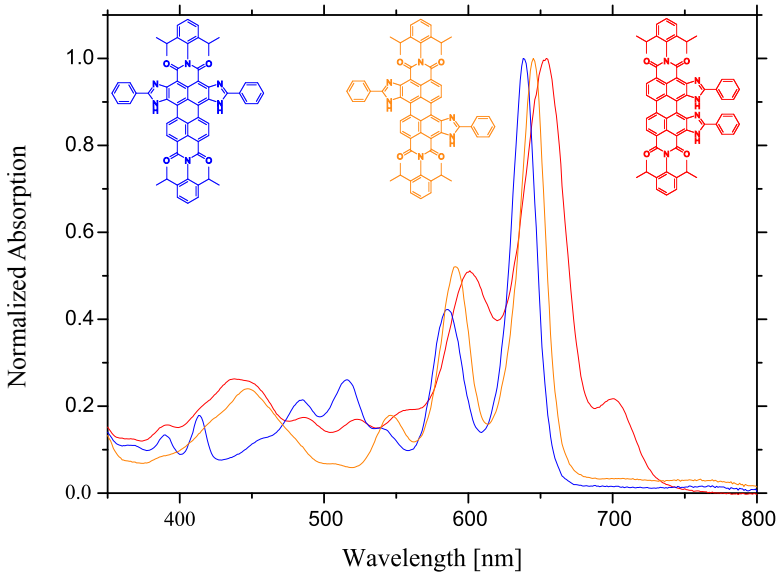

Figure 4.4: Absorption spectra of di-phenylimidazol substitution isomers in DCM

Per-$(PhIm)_3$ could be as well formed in small amounts during the experiments. The polarity is very close to all of the isomers of Per-$(PhIm)_2$ and the solubility was worse, which made the purification challenging. It was not possible to get a ^{1}H NMR spectrum because the yields were too low, but the existence of the species can be proved by mass spectra as well as by absorption and emission spectra.

4.1.2 Substitution of Chloro-Phenyl-Imidazolgroups on Perylene Bisimide

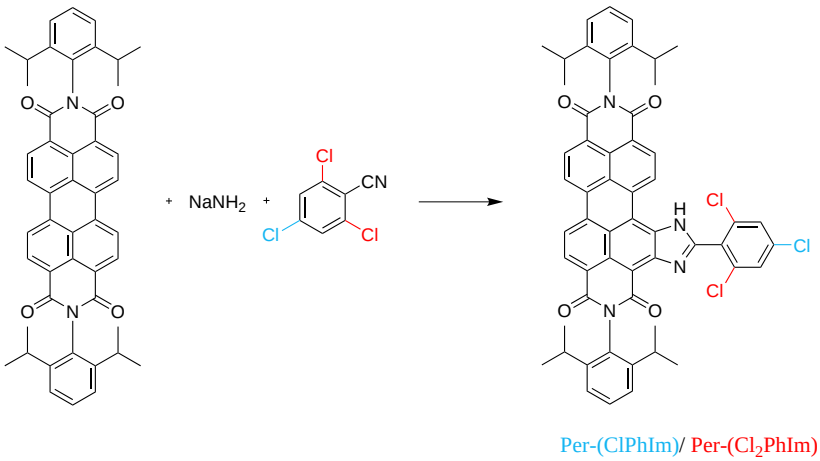

Figure 4.5: Substitution scheme with chlorinated benzonitrile derivates

Investigations of the Per-(PhIm)-derivates related to its pH sensitive properties directed the further work to studies of additional substituents on the PhIm-group. High pK_a values of pH sensitive dyes can be decreased by introduction of electron-withdrawing groups like -Cl or -Br. Schutting et al. showed the influence of halide substitution on the acidity of -OH groups in aza-BODIPY-molecules [15]. Chlorinated benzonitrile-derivates were used to compare mono- and di-chloro substituted phenyl-imidazol groups linked at the bay-region of perylene bisimide (fig. 4.5). In contrast to benzonitrile, which is usually used as liquid solvent and reagent too, the chlorinated derivates 4-chlorobenzonitrile (mp. 90-93 °C), needed for the synthesis of Per-(ClPhIm) as well as 2,6-dichlorobenzonitrile (mp. 140-143 °C), respectively used for the analogue synthesis of Per-(Cl_2PhIm), are still solid, while the reaction mixture is heated. This fact complicated the handling of the whole reactions as well as the purification of the products and the evaporation of solvent under reduced pressure.

Synthesis of Per-(ClPhIm)

The reaction containing Lumogen Orange, 4-chlorobenzonitrile and $NaNH_2$ was carried out under same conditions, as discribed in chapter 4.1.1. The reaction progress was monitored by absorption spectra (fig. 4.6). Purification of Per-(ClPhIm) was performed with column chromatography with cyclohexane/toluene 3+1 as eluent to remove solvent traces. The product was recieved with cyclohexane/ethylacetate 94+6 as mobile phase.

Synthesis of Per-(Cl_2PhIm)

The synthesis of Per-(Cl_2PhIm) with 2,6-dichlorobenzonitrile works analogously to the synthesis of Per-(ClPhIm) respectively with a higher melting point of the benzonitrile derivate. Column chromatography was performed with cyclohexane/toluene mixtures to remove 2,6-dichlorobenzonitrile traces and afterwards with dichloromethane as mobile phase to obtain a deep red coloured product fraction.

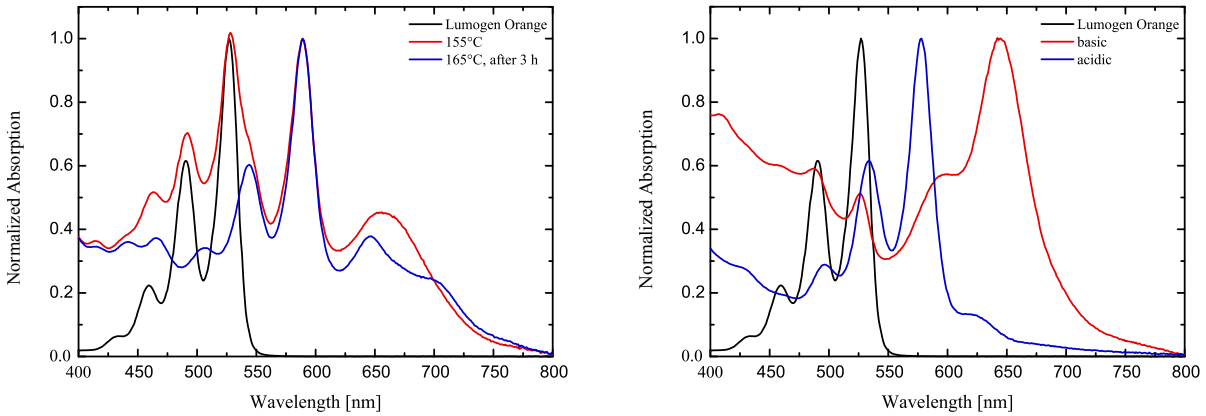

(a) T> 165 °C led to the formation of Per-(ClPhIm)

(b) Basic 2,6-chlorobenzonitrile caused deprotanation of the formed Per-(Cl_2PhIm)

Figure 4.6: Absorption spectra (in DCM) of reaction progress of Per-(ClPhIm) and Per-(Cl_2PhIm)

Absorption spectra in figure 4.6 of the reaction progress of both synthesis show on the one hand the need of temperatures above 165 °C and on the other hand the pH sensitivity of the synthesised dye. The bathochromic shift of the absorption spectra of the deprotonated Per-(Cl_2PhIm) species led to the assumption of a di-(Cl_2PhIm) substitution on the perylene bisimide.

4.1.3 Substitution on Nitrogen of Phenylimidazolgroup of Laterally Extended Perylen Dyes

Different alkyl-substitution reactions on NH-position of the imidazol group were investigated by the group of Langhals [65, 72].

Benzylic positions are preferred for S_N2 mechanism attacks, because the transition state is the electronical stabilised. This leads to an increase of the reaction speed. Primary aliphatic halides react with numerous nucleophilic substances with S_N2 mechanism, but the transition state is not stabilised [73]. To get a better nucleophile the nitrogen of the imidazolgroup is deprotonated with a base. The use of aprotic-dipolar DMF as solvent may increase the S_N2 reactivity of the reaction due to the electronic properties of educts.

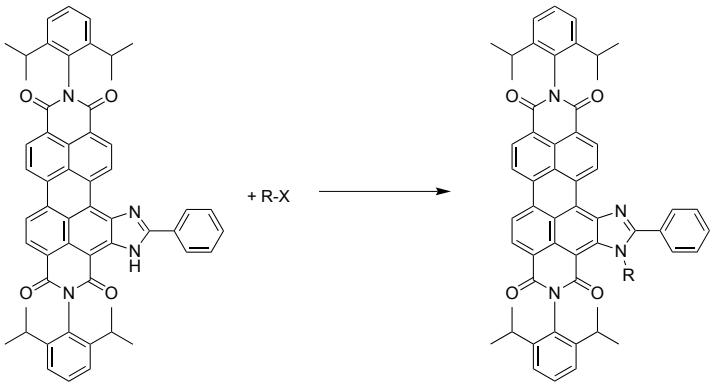

Figure 4.7: General reaction scheme for alkylation of Per-(PhIm)

Unsuccessful Alkyl-Substitution Experiments

Experimental trials were performed with different alkyl halides (4-methoxybenzylbromide, butyliodide, 2-bromoethylmethacrylate, 2-ethylhexylbromide) in toluene under reflux conditions for more than 24 h. For the deprotonation process of the Per-(PhIm)-dye 20 equivalents of solid K_2CO_3 were suspended in toluene and the dye was added and heated to 110 °C. At this point should be mentioned, that the colour of each reaction mixture was blue, what usually indicates the presence of deprotonated species of the dye. Afterwards 30 equivalents alkyl halide were added and stirred for 20-30 h controlled with TLC and absorption spectroscopy. In fact, the taken probes show as well a blue colour directly out of the reaction mixture and when dissolved in dichloromethane. After a few minutes the colour changed to pink, which is the typical colour for the protonated state. This could be explained with the bad solubility of K_2CO_3 in dichloromethane, but as well with the pH sensitivity of the dye and the unsuccessful reaction with alkyl halides.

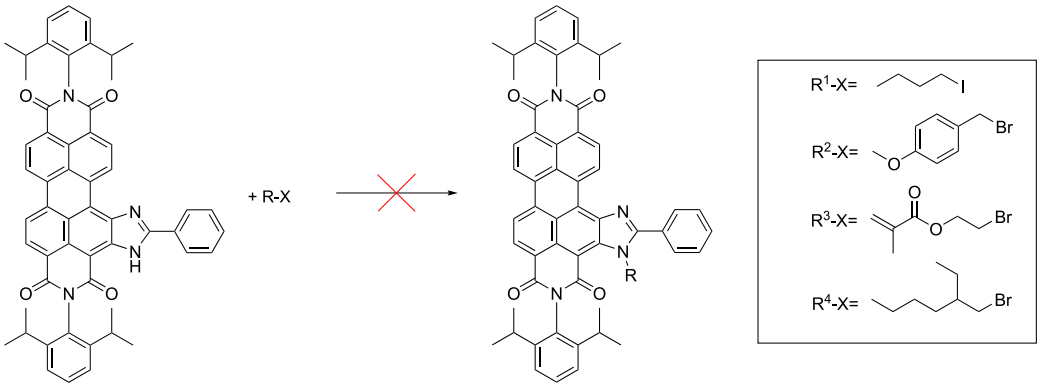

Figure 4.8: Reaction scheme for unsuccessful alkylation of Per-(PhIm) experiments

Substitution with *tert*-Butylbenzylbromide

After the unsuccessful experiments another reactant, *tert*-butylbenzylbromide, was chosen because the bulky *tert*-butyl group may influence the polarity of the molecule more, than the reactants used before. In contrast to former experiments, the reaction with *tert*-butylbenzylbromide resulted in the successful substitution of the pH sensitive group.

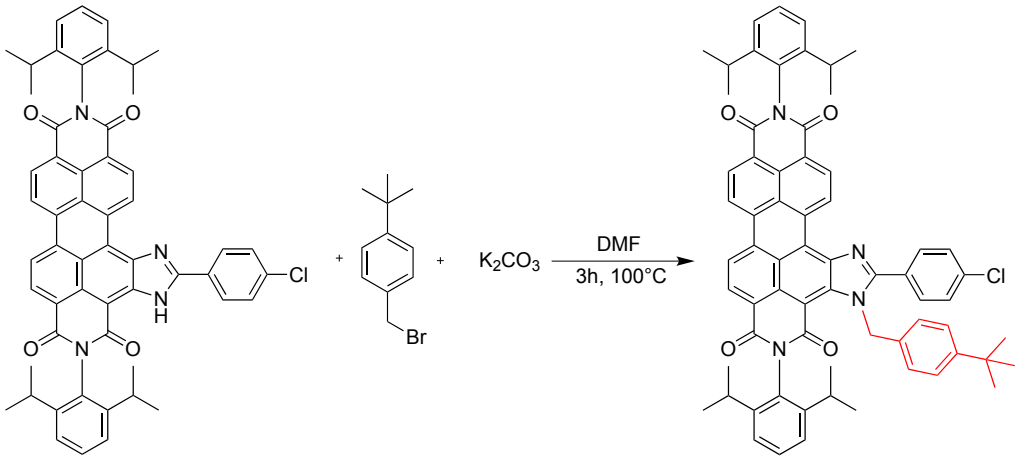

Figure 4.9: Reaction scheme for alkylation of Per-(ClPhIm) with *tert*-butylbenzylbromide

Per-(ClPhIm) was dissolved in DMF and heated to 100 °C, with the addition of the base K_2CO_3 the change of the colour from red to blue was observed. This is caused by the different spectral properties of protonated and deprotonated state of the imidazol-nitrogen. After dropwise addition of *tert*-butylbenzylbromide the colour changed again to redish/purple, which indicates a reaction at deprotonated nitrogen. Figure 4.10 shows absorption spectra. The shift between protonated (589 nm) and depronated (693 nm) form as well as to the product (585 nm) can be

seen. The spectra of the product is similar to the protonated form and exhibits a hypsochromic shift of 4 nm due to the slight electron-withdrawing effect of the benzylic group. The negatively charged nitrogen of the deprotonated state causes the change of the spectral properties. The purification of the product was successfully carried out with column chromatography with cyclohexane/dichloromethane 1+2 as eluent. The dye did not show pH sensitivity. NMR and mass spectra can be seen in appendix figure 9.1.6. The ^{1}H NMR spectrum of the product does not show the singlet signal at 11.56 ppm which can be observed at the educt ^{1}H NMR spectra and indicates the proton at the nitrogen position of imidazol.

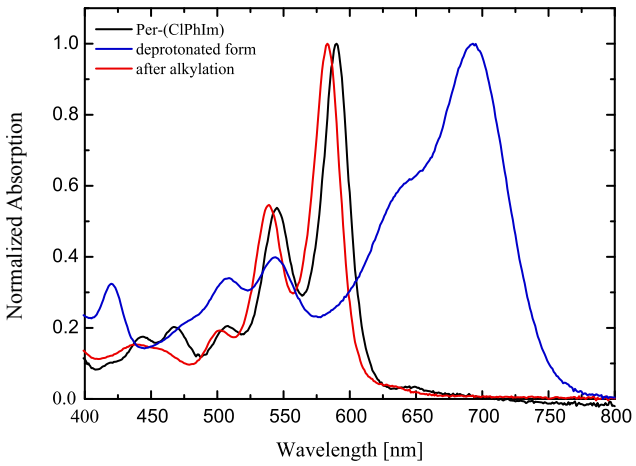

Figure 4.10: Absorption spectra of Per-(ClPhIm) acidic/basic form and Per-(ClPhIm)-*t*-ButylPh

4.1.4 Synthesis of Per-(PhIm)-N(EtHex)$_2$

Investigations on the properties of the pH sensitive probes by modification with sulfonate groups at available phenyl positions of perylene bisimide-dyes as well as diketo-pyrrolo-pyrrole-dyes were published by Aigner and Schutting [5, 20]. The procedure included the use of highly reactive chlorosulfonic acid at temperatures of 65 °C. Subsequently it was followed by a treatment with water to get the charged sulfonate molecule with stabilising TOA^+ cation on one hand. On the other hand a further reaction with bulky di-(2-ethylhexyl)amine in presence of TEA at RT (fig. 4.11) had to be done to get a product with long CH-chains for simplification of characterisation with ^{1}H NMR and mass spectrometry.

After the first reaction step with chlorosulfonic acid at 60 °C stirring for 3 hours, the mixture was allowed to cool to RT and was then quenched, by dropping it onto ice cubes. A deep blue precipitate was obtained. The crude product was filtered and quickly washed with cold water and the remaining purple solid was split up in two fractions. One was dissolved in DMF and

one was dissolved in water, what induced the building of sulfonic acid groups, which could be treated with TOACl subsequently.

The DMF fraction was treated with di-(2-ethylhexyl)amine in presence of TEA over-night. After purification the product fraction, which was soluble in dichloromethane was characterised with mass spectrometry.

The remaining deep blue water-soluble fraction was dissolved in H_2O and extracted with TOACl in dichloromethane solution. The organic phase became pink and protons of sulfonic acid group were replaced by TOA^+ cations. As can be seen in the recorded MALDI-TOF spectra (fig 9.8, page 109) of the fraction, the purification results in a mixture of differently substituted products and TOA^+ contamination.

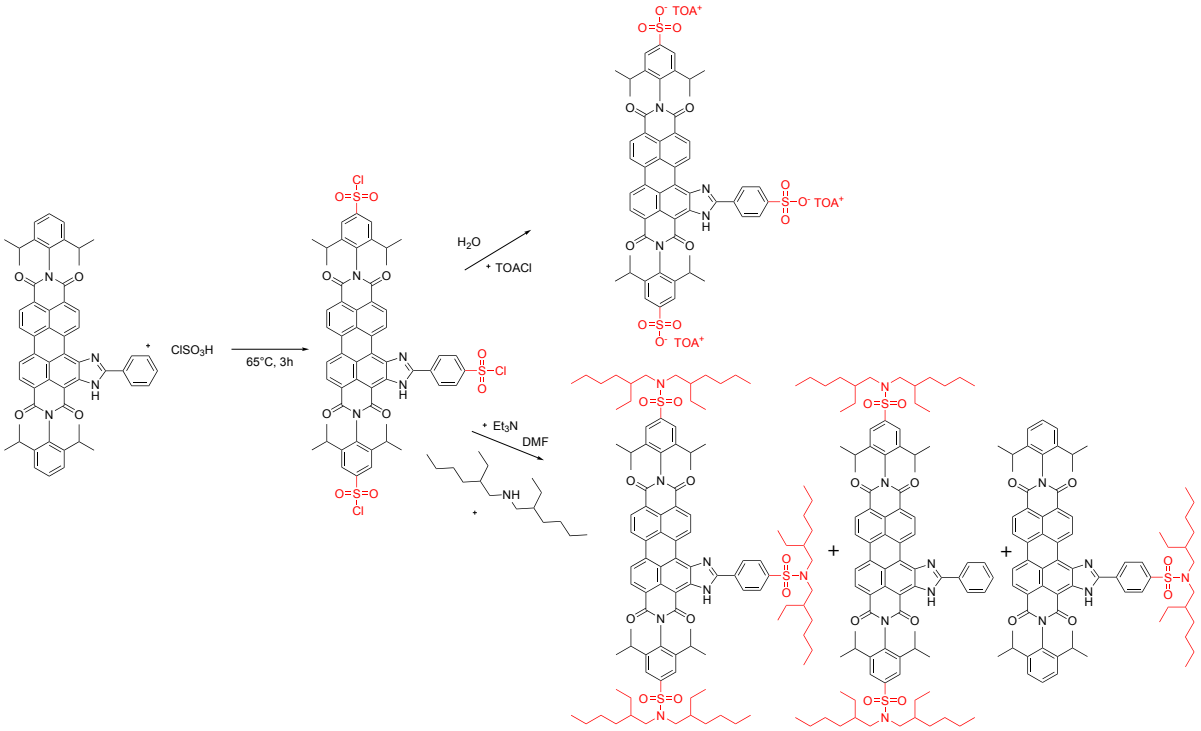

Figure 4.11: Reaction scheme for chlorosulfonation and further treatments

Conclusion

The synthesis of laterally extended PBI by introducing phenylimidazol groups at the bay region of the perylene structure led to a new class of pH sensitive dyes. The pH of the reaction mixtures played an important role on the reaction equilibrium. However, the perception that the basic form of the molecule has a different absorbance than the protonated species opened the door to further investigations in the field of pH sensitive perylene dyes. The synthesis was not time consuming due to an one-step reaction. However, purification of the dye turned out to be the challenging part of the preparation of the new indicator dyes. This is because of the insufficient solubility of the obtained one, two or three phenylimidazol substituted products. Following reactions were performed for investigations in the field of pH, carbon dioxide as well as water/humidity sensing. A further advantage of using perylene bisimide is the availability of various pigments and the low price of educts.

4.2 Dye Characterisation

4.2.1 Absorption and Emission spectra

Absorption and emission spectra were recorded in dichloromethane. Compared to the introduction of one phenylimidazolgroup onto the PBI ($\lambda_{\mathrm{Abs}} = 589\,\mathrm{nm}, \lambda_{\mathrm{Em}} = 599\,\mathrm{nm}$), two or three (PhIm)-groups show spectral differences in form of bathochromic shifts of 50 nm, 104 nm in absorption spectra and 47 nm, 114 nm in emission spectra, respectively according to the enlargement of the chromophoric system, as can be seen in figure 4.13.

However, introduction of chlorinated phenylimidazolgroups instead of (PhIm) leads to small hypsochromic shifts. Per-(ClPhIm) shows no change of the absorption maximum compared with Per-(PhIm). Furthermore for Per$-(\mathrm{Cl_2PhIm})$ hypsochromic shifts of 10 nm in absorption and 9 nm in emission spectra can be observed compared with Per-(PhIm). Due to the alkylation of Per-(ClPhIm) hypsochromic shifts of 6 nm and 4 nm of the Per-(ClPhIm)-*t*-ButylPh spectra can be observed, compared with the educt. All synthesised dyes show Stoke's shifts of 7-11 nm except Per$-(\mathrm{PhIm})_3$, where a larger shift of 20 nm was obtained.

Absorption spectra for calculation of molar absorption coefficients were measured in toluene. Due to insolubility of Per$-(\mathrm{PhIm})_3$ in toluene it was not possible to produce representative results. At this point, it should be mentioned, that the introduction of more than one (PhIm)-group results in a worse solubility of the dye in organic solvents such as dichloromethane, chloroform, toluene e.g..

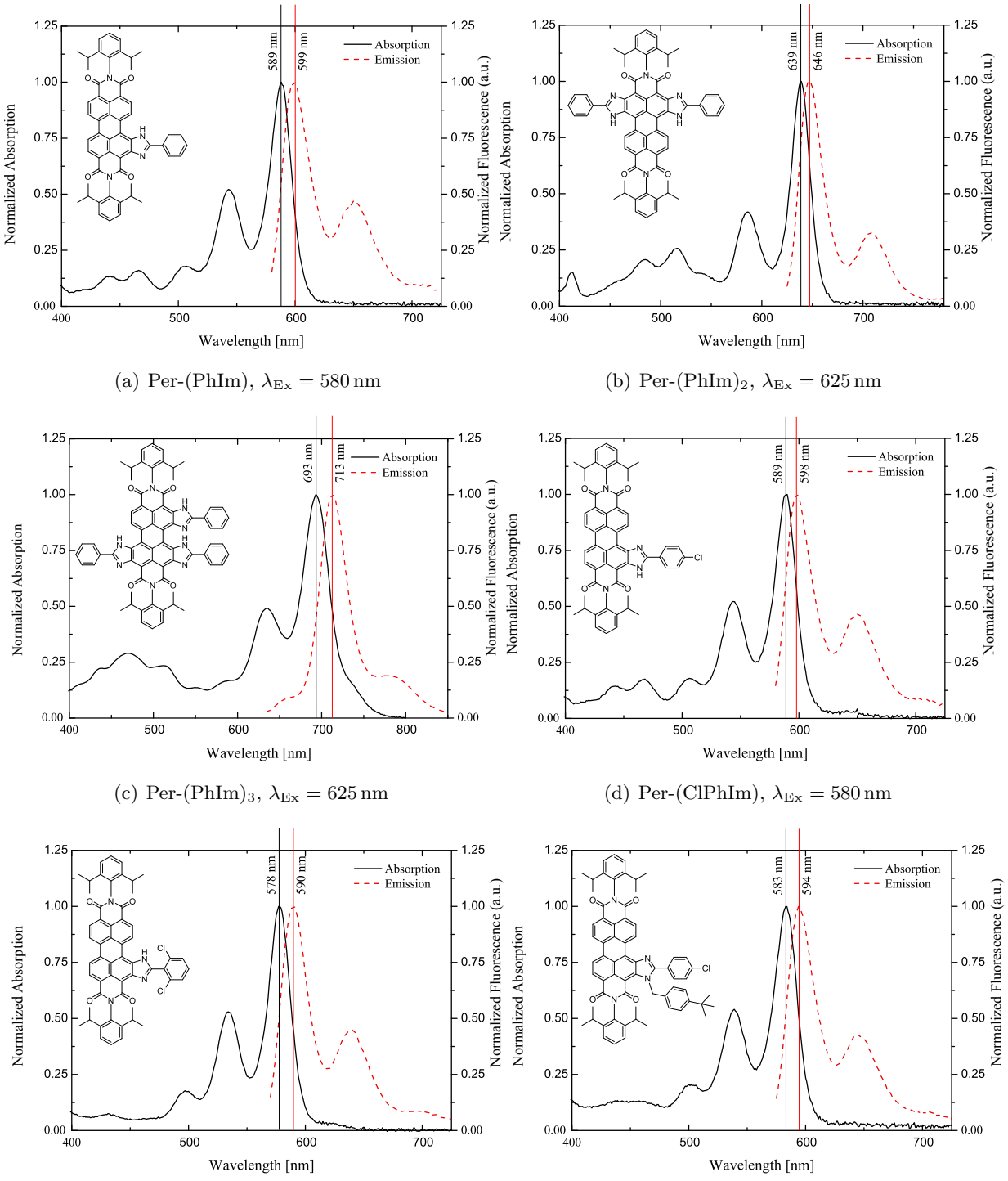

(a) Per-(PhIm), $\lambda_{Ex} = 580\,nm$

(b) Per-$(PhIm)_2$, $\lambda_{Ex} = 625\,nm$

(c) Per-$(PhIm)_3$, $\lambda_{Ex} = 625\,nm$

(d) Per-(ClPhIm), $\lambda_{Ex} = 580\,nm$

(e) Per$-(Cl_2PhIm)$, $\lambda_{Ex} = 570\,nm$

(f) Per-(ClPhIm)-*t*-ButylPh, $\lambda_{Ex} = 575\,nm$

Figure 4.12: Absorption and emission spectra of Per-(PhIm) dyes in DCM

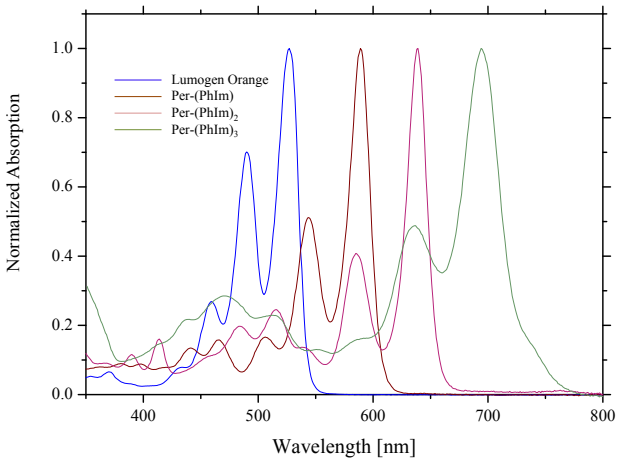

Figure 4.13: Normalized absorption spectra of the new perylenes in DCM

Table 4.1: Photophysical properties of synthesised PBI dyes. ε was determined in toluene and Φ_F in THF; (n.d. not determined)

Dye	λ_{Abs} [nm]	$\varepsilon \cdot 10^{-3}$ $[L \cdot mol^{-1} \cdot cm^{-1}]$	λ_{Em} [nm]	Φ_F
Per-(PhIm)	589, 544	82, 45	597, 647	0.91
Per-$(PhIm)_2$	638, 585	69, 29	646, 706	0.79
Per-$(PhIm)_3$ *	693, 634	n.d.	713	n.d.
Per-(ClPhIm)	590, 544	64, 34	597, 647	0.89
Per-(Cl_2PhIm)	578, 535	42, 23	584, 634	0.95
Per-(ClPhIm)-*t*-ButylPh	584, 539	62, 32	589, 639	0.86

* in DCM

The obtained molar absorption coefficients are in a range 42 000 - 82 000 $L\,mol^{-1}\,cm^{-1}$. Per-(PhIm) has the highest ε. The influence of a second phenylimidazol substituent results in a slight decrease of ε, further substitution with chlorinated phenylimidazol of the perylene core leads to lower molar absorption coefficients.
All dyes show extremely high fluorescence brightness of red emission up to NIR wavelengths $\sim$590-713 nm. In comparison to the educt absorption and emission, wavelengths are increased by laterally enlargement of the chromophoric system.

Comparison of photophysical properties of the new perylene indicator dyes to a few commonly used fluorescent pH indicators, show the high brightness of the PBIs (tab. 4.2). The product of quantum yield and molar absorption coefficient results in excellent brightness.

Table 4.2: Comparison of typical photophysical properties of commonly used bright fluorescent dyes to the new perylene dyes

Dye	λ_{Abs} [nm]	$\varepsilon \cdot 10^{-3}$ $[L \cdot mol^{-1} \cdot cm^{-1}]$	λ_{Em} [nm]	Φ_F	Ref.
Aza-BODIPYs	660-710	~ 80	680-740	~ 0.2	[74]
BODIPYs	500-520	~ 90	510-530	~ 0.9	[75]
Diketo-pyrrolo-pyrrole	500-570	~ 25	520-600	~ 0.8	[5]
Fluoresceins	470-510	~ 100	510-530	~ 0.9	[76]
Rhodamines	540-570	~ 100	560-600	0.7-1.0	[77]
New perylene dyes	580-690	up to 80	590-713	~ 0.9	this work

4.2.2 Lifetimes

Radiative lifetimes are distinguishing properties of luminophores correlated to their absorption behaviour [78]. Various perylene bisimide dyes and their lifetime properties were developed in the past [79].

The observed radiative lifetimes are in a range of 3.8 - 6.5 ns, which is typically for perylene dyes shown in table 4.3. However no general tendency could be determined regarding the different modifications of the perylene core. The decay times are identical for mono-substituted derivates (Per-(PhIm), Per-(ClPhIm) and Per-(Cl_2PhIm)) and do not change upon alkylation. Unexpectedly for Lumogen Orange, Per-(PhIm), Per-$(PhIm)_2$ and Per-$(PhIm)_3$ no tendency was obtained at all. The shortest lifetime was observed for Per-$(PhIm)_3$ and the longest for Per-$(PhIm)_2$. Nevertheless, comparing halogenated dyes and Per-(PhIm), exhibiting differences in absorption coefficients (table 4.1) they show rather similar apparent radiative lifetimes 5.3 - 5.6 ns. The decay curves of the perylene dyes can be seen in appendix (page 110).

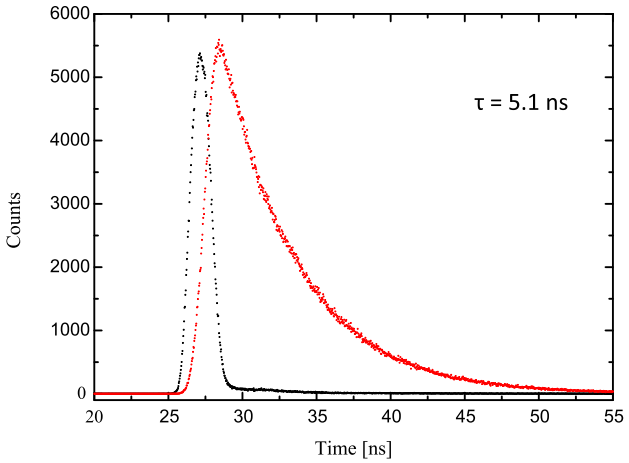

Figure 4.14: Mono-exponential decay curve of Lumogen Orange (red) and prompt measurement (black)

Table 4.3: Measurement parameter and obtained radiative lifetimes of different PBI dyes

Dye	Lifetime [ns]	Nano-LED [nm]	Emission [nm]	Voltage [V]	Bandpass [nm]
Lumogen Orange	5.1	435	550	1200	1
Per-(PhIm)	5.3	435	600	1200	1
Per-$(PhIm)_2$	6.4	635	645	1200	10
Per-$(PhIm)_3$	3.8	635	720	1200	3
Per-(ClPhIm)	5.3	435	600	1200	1
Per-(Cl_2PhIm)	5.3	435	600	1200	2
Per-(ClPhIm)-*t*-ButylPh	5.2	435	600	1200	2

4.2.3 Photostability

Photostability of a dye is of special interest for practical applications not only for optical sensors. E.g. styrian pumpkin seed oil contains fluorescent components, which are destroyed at long term exposure to sunlight, the disappearance of the characteristic greenish colour is used as simple optical quality control criterion [80]. Thus long time measurements and usability with high light densities are cases where photostability has an important influence. Various perylene bisimide dyes were developed with outstanding photostability properties in the past [51]. Interpretation of the data derived from this experiment with 4 synthesised phenylimidazol functionalised perylene bisimide dyes show excellent photostability properties for all of them. The dyes were dissolved in toluene, positioned in focus of high power LED with $\lambda_{Ex} = 525\,nm$

and absorption spectra were recorded each 30 min over 320 min. Neither a strong influence of halogen atoms nor of the second introduced phenylimidazol group observed (fig. 4.15).

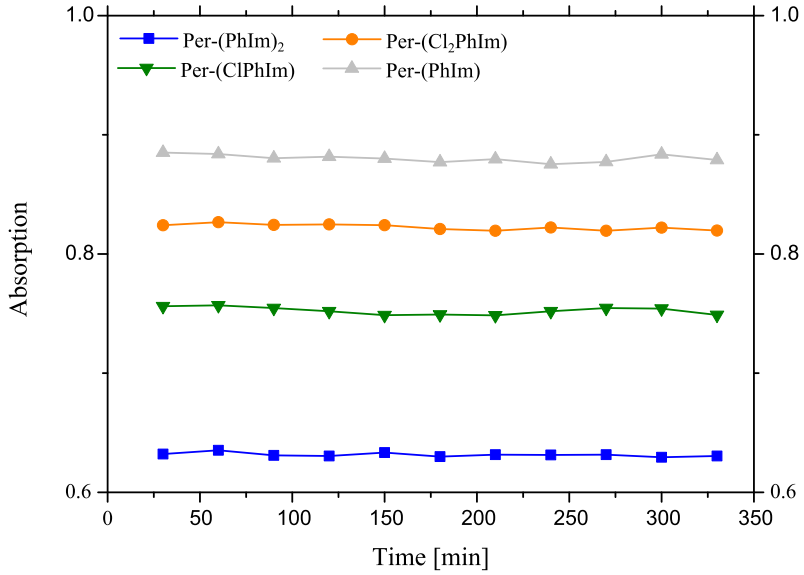

Figure 4.15: Photodegradation profiles for dye solutions in toluene upon irridation with a high power LED (photon flux: 15600 $[\mu\text{mol}\,\text{s}^{-1}\,\text{m}^{-2}]$ at λ_{Ex} 528 nm $\cong$ 353 $\text{mW}\,\text{cm}^{-2}$)

Conclusion

The presented class of perylene bisimide dyes is covering a wavelength range of 580 - 690 nm in absorption and 590-713 nm in emission. High absorption coefficients and high fluorescence quantum yields next to unity enable the use of small dye amounts for various applications. Furthermore, excellent photostability emphasise a promising new pH sensitive dyes, even in the comparison to commonly used indicators. The number of phenylimidazol groups, bearing the perylene core, has a strong influence on the spectral properties (bathochromic shift), which results in high flexibility of the spectral range. Other spectral properties (molar absorption coefficient, quantum yield, lifetimes) are not affected that much.

4.3 Sensor Materials - Applications

4.3.1 pH Sensing with Sensor Layer

For pH sensitive layers, D4, a polyurethane-based hydrogel was used as polymeric matrix, which is able to swell with a water uptake of 50 %. It is a block-copolymer, which consists of hydrophobic and hydrophilic domains [38]. The key factors for the host polymer material should

stabilize the hydrophobic indicator dye and be permeable for water to enable pH measurements [81]. The adhesion properties and the water absorption make the chosen hydrogel a promising polymer matrix. The indicator dyes were physically entrapped into the polymer matrix.

New perylene bisimide dyes embedded in hydrogel show notable changes of their emission as well as colorimetric properties in contact with bases, as can be seen in figure 4.16.

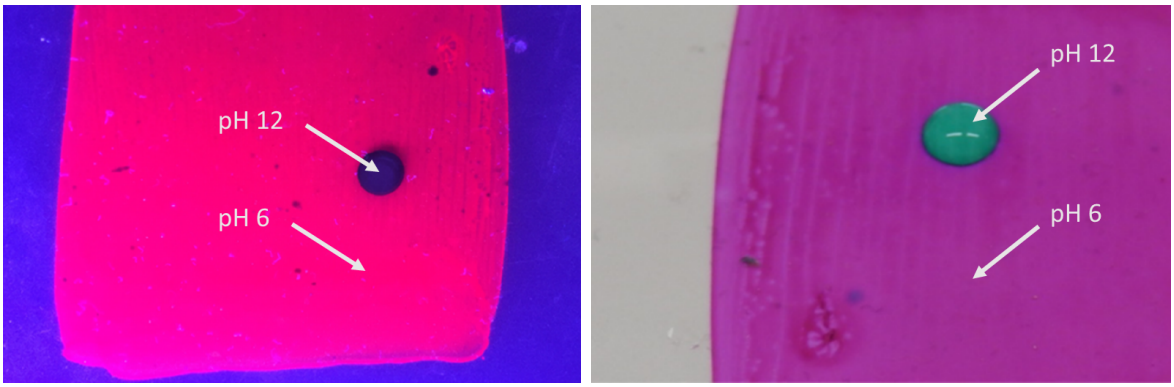

(a) UV light (b) Day light

Figure 4.16: Images of pH sensor layers based on Per-(PhIm). Protonated (pink and purple) and deprotonated (blue and green) form of indicator dye; drop: aqueous base, sensor environment: air. Excitation light source: UV-lamp $\lambda_{Ex} \sim 365\,nm$

pH Measurements

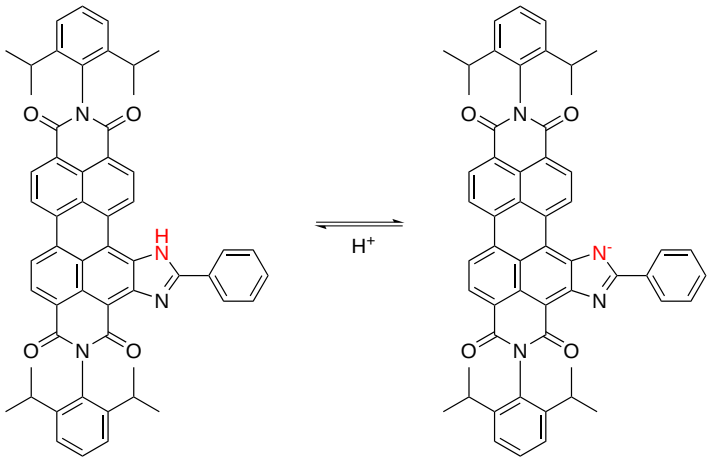

Figure 4.17: Schematic protonation/deprotonation of synthesised perylene bisimide dyes

Observations during the synthesis of laterally extended perylene bisimide dyes permitted the assumption concerning pH dependence of the dyes. The -NH group of the introduced phenylim-

idazol functionalisation could be deprotonated under basic conditions as shown in figure 4.17. Absorption spectra of dissolved Per-(PhIm) (THF) in a mixture of THF/EtOH/Buffer/NaCl 3:2:2:3 (V/V) were recorded to estimate the pK_a range of the new PBI dyes. Ionic strength (150 mM) was controlled with NaCl. For all further pH measurements sensor layers were used (dye entrapped in hydrogel D4 onto a dust-free PET support). Absorption/fluorescence spectra were recorded in buffer solutions with certain ionic strength of 150 mM. For absorption spectra usually 75 μm and for emission spectra 25 μm thick wet films were prepared.

Per − (PhIm)

In figure 4.18 the absorption spectra show a reversible deprotonation reaction at pH > 8. The protonated species of Per-(PhIm) showed absorption maximum at 589 nm and 545 nm. Absorption decrease at higher pH values. In contrast λ_{max} of the deprotonated species could be obtained at 673 nm, which increases at higher pH. This enables colorimetric pH measurements at different wavelengths. Isosbestic points could be observed at 428 nm, 483 nm, 502 nm and 608 nm.

The high pK_a value of 10.63 in solution was not expected, however it could be promising for various specific applications such as pH measurements in concrete or colorimetric carbon dioxide monitoring.

As the pH sensitivity of the Per-(PhIm) dye worked in buffer solution, further experiments were performed with dyes physically entrapped in hydrogel D4 on PET supports. As expected, the pK_a of 11.28 of the Per-(PhIm) sensor foil could be obtained, caused by the polymer matrix environment. Hydrogels are gas and water permeable and allow the uptake of a certain water amount, in case of D4 about 50 %, which additionally led to swelling of the polymer. The recorded absorption spectra in solution shown in figure 4.18 (a) exhibited similar results to the spectra of sensor foils in buffer solution in figure 4.18 (c) with a slight bathochromic shift of the maxima and a higher pK_a value as mentioned before, which was caused by the polymer environment. The higher a pK_a value the easier the protonation process will be performed. Hydrogel D4 has hydrophobic parts (less polar environment) in its structure, there deprotonation is less favourable than in hydrophilic environments, which causes a higher pK_a. The characteristic absorption maximum of protonated Per-(PhIm) appeared at 595 nm, 551 nm. The maximum of the basic form could be observed at 688 nm.

Additionally to the recorded absorption spectra of sensor foils in different buffer solutions emission spectra for pH calibration were recorded as well. In the case of Per-(PhIm) excitation wavelength λ_{Ex} 510 nm was chosen, which is exactly the second isosbestic point (fig 4.18 (e)). The emission spectra showed signals at 610 nm and 672 nm, which are characteristic for the

protonated species and the signal of the basic form of Per-(PhIm) appeared at 730 nm. Curious in this case is the higher intensity of the second maxima at 672 nm compared to the spectra shown in figure 4.12 (a). That might be caused by the influence of D4 polymer matrix on the molecule. The fluorescence of the protonated species decreased by increasing of pH. The broader maximum has a slight overlapping with the deprotonated maxima at 730 nm. However, the difference between pK_a' of 10.77 by emission the pK_a 11.28 by absorption, can be explained by Förster resonance energy transfer (FRET). Certainly, dye concentrations are much higher in hydrogel than in solution and the closer distance between molecules enables the effect of energy transfer from the acidic to the basic form of the dye. Nevertheless, considering the hydrophobic and hydrophilic regions of the polyurethane hydrogel D4, which permit different localisation patterns of the perylene molecules, could also have effects on the pK_a discrepancy [74].

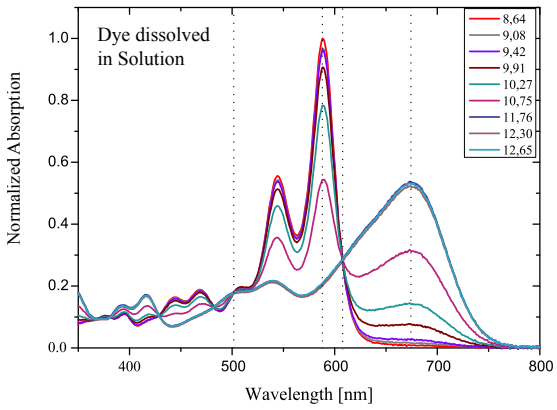

(a) Absorption spectra of dissolved Per-(PhIm) in 2.5 ml THF/EtOH/Buffer/NaCl solutions, pH 8.64-12.65 at RT

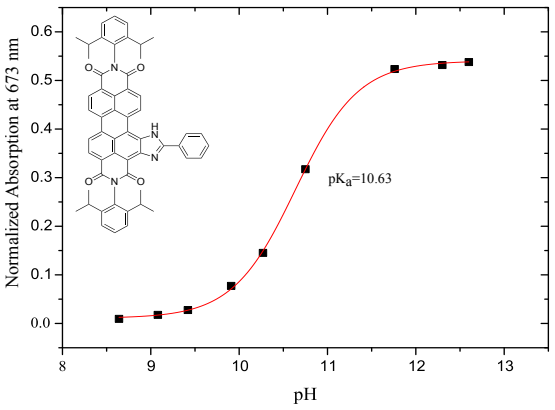

(b) Corresponding pK_a plot, respectively a sigmoidal Boltzmann fit

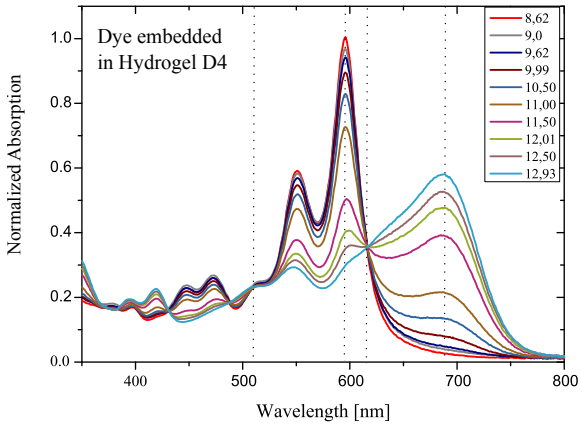

(c) Absorption spectra of pH sensor in buffer solutions, pH 8.62-12.93 at RT

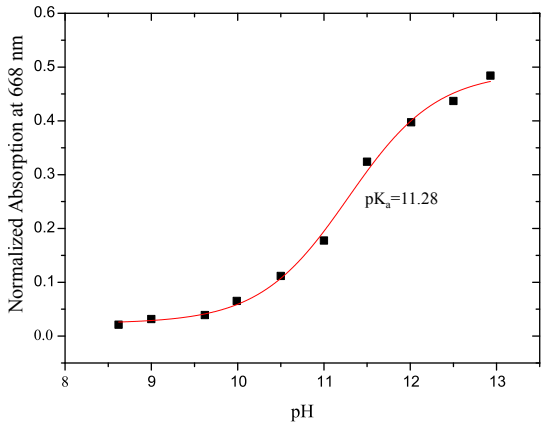

(d) Corresponding pK_a plot, respectively a sigmoidal Boltzmann fit

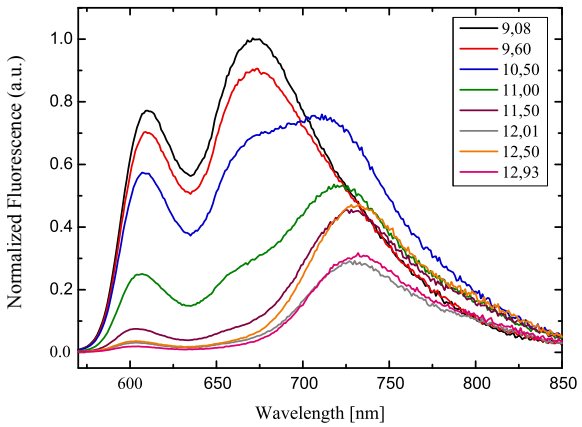

(e) Corrected emission spectra of pH sensor in buffer solutions, pH 9.08-12.93 at RT, λ_{Ex}=510 nm

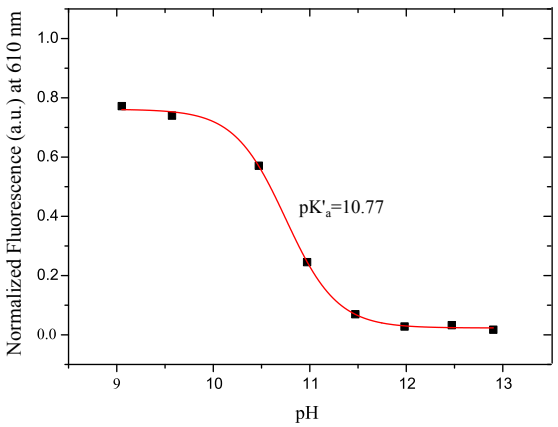

(f) Corresponding pK'_a plot, respectively a sigmoidal Boltzmann fit

Figure 4.18: Absorption and corrected emission spectra of Per-(PhIm) measured in buffer solutions and corresponding pK_a calibration curves

Per − $(PhIm)_2$

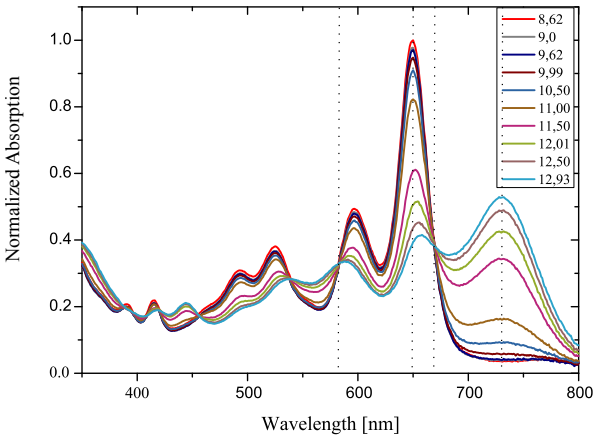

(a) Absorption spectra of pH sensor in buffer solutions, pH 8.62-12.93 at RT

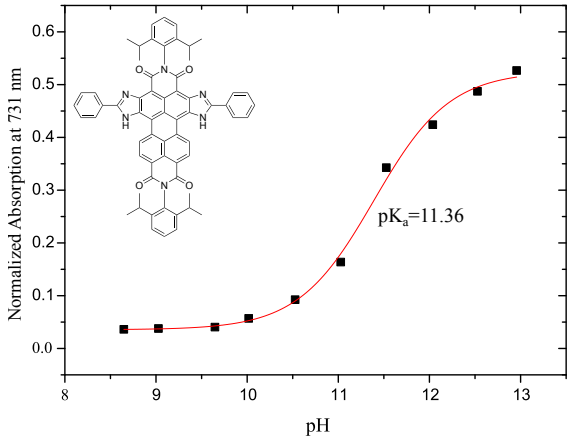

(b) Corresponding pK'_a plot, respectively a sigmoidal Boltzmann fit

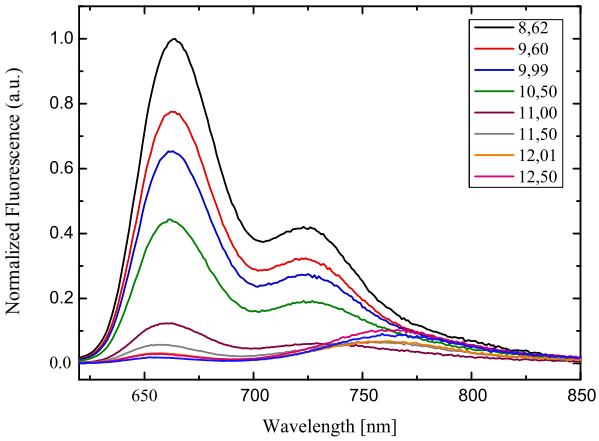

(c) Corrected emission spectra of pH sensor in buffer solutions, pH 8.62-12.50 at RT, λ_{Ex}=583 nm

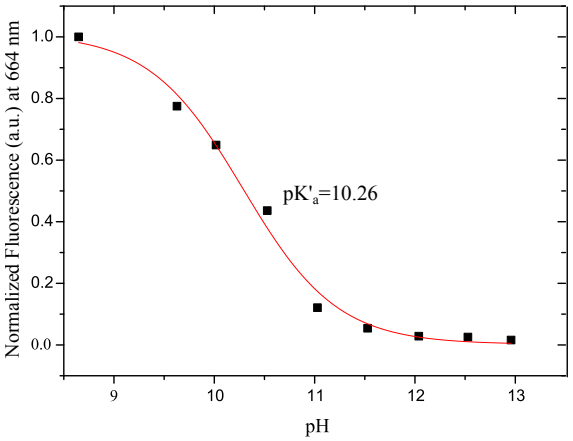

(d) Corresponding pK'_a plot, respectively a sigmoidal Boltzmann fit

Figure 4.19: Absorption and corrected emission spectra of Per−$(PhIm)_2$ embedded into hydrogel D4 measured in buffer solutions and corresponding pK'_a calibration curve

As shown before (figure 4.13, page 50), the introduction of an additional (PhIm)-group resulted in a bathochromic shift λ_{max} of about 50 nm compared to the simple mono-substituted Per-(PhIm) dye, which was caused by an enlargement of the chromophoric system. From the spectral point of view the absorption spectra of Per−$(PhIm)_2$ immobilised in hydrogel D4 possesses similar characteristics as Per-(PhIm). Absorption maximum of the acidic form obtained at 650 nm, the second characteristic band at 598 nm and the maximum of the deprotonated species at 731 nm was observed. Isosbestic points could be observed at 456 nm, 538 nm, 583 nm, and 670 nm.

Surprisingly, the pK'_a value is almost the same as of Per-(PhIm) embedded in D4, which shows formation of mono-deprotonated species, does not influence the pH properties of the dye. Although the existence of a second -NH function, which can be deprotonated, might be important for the interpretation of further carbon dioxide measurements.
Fluorescence spectra of Per$-(\mathrm{PhIm})_2$ can be seen in figure 4.19. The second isosbestic point of the absorption spectra was chosen again, as excitation wavelength (583 nm). Emission bands were obtained at 664 nm, 725 nm, which decreased due to increasing pH and the signal at 762 nm which increased at higher pH values. In comparison with the emission spectra of Per$-$(PhIm) the ratio of the signals is more alike to the characteristic emission spectrum (fig 4.12 (b)). It could be shown again, that there is no significant influence of the second phenylimidazol substitution on the pK'_a.

Per − (ClPhIm)

The relatively high pK'_a values of Per$-$(PhIm) and Per$-(\mathrm{PhIm})_2$ dyes determined the modification of the molecular structure with either different electron-donating or electron-withdrawing substituents. The introduction of chlorine atoms as electron-withdrawing group into the luminescent system was expected to cause a lower pK'_a. This fact can be used to get tunable pK'_a values for a broader field of applications. A indicator dye class with the pK'_a values tunable by introduction of electron-withdrawing/electron-donating groups is already published and in this thesis it should be adopted to perylene bisimde dyes [15, 74].

In figure 4.20 the absorption spectra of non-covalently entrapped Per$-$(ClPhIm) in hydrogel D4 matrix is shown. Absorption was rather similar to spectra of Per$-$(PhIm), Per$-(\mathrm{PhIm})_2$. Two characteristic maxima of the acidic form were determined at 596 nm and 551 nm, furthermore the maximum of the deprotonated species of the dye was obtained at 683 nm. Isosbestic points are observed at wavelengths of 429, 487, 528 as well as 616 nm. Surprisingly the introduction of the chlorine did not influence the spectral properties strongly, the maxima obtained nearly at same wavelengths as those of Per-(PhIm). However, the pK_a 10.73 of Per$-$(ClPhIm) bearing -Cl in p-position of the phenylimidazol group derived from absorption was lower than those of unchlorinated dyes (fig. 4.18, 4.19) because of the influence of the introduction of a halogen atom as weak electron withdrawing group.

The fluorescence spectra and corresponding pK'_a plot in figure 4.20 showed maxima at wavelengths of 612 nm , 663 nm appendant to the protonated species, which decreased at higher pH values and another maximum at 720 nm, belonging to the deprotonated form of the molecule. The apparent pK'_a value (pK'_a 9.40) derived from fluorescence data is about 1.3 pH units

lower than the one obtained from absorption. This can be explained by the overlapping of protonated emission spectra and deprotonated absorption spectra and high concentration, therefore close molecules entrapped into hydrogel which enable Förster resonance energy transfer.

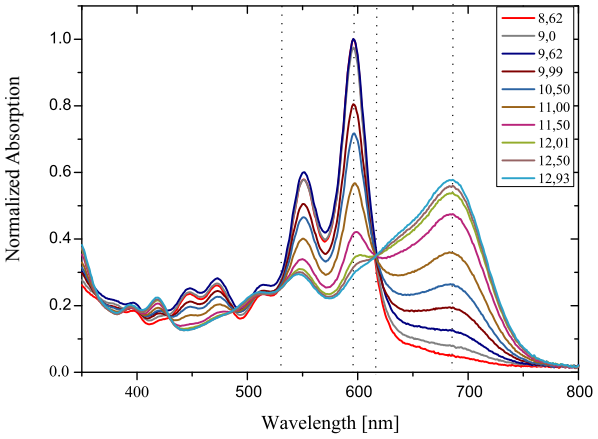

(a) Absorption spectra of pH sensor in buffer solutions, pH 8.62-12.93 at RT

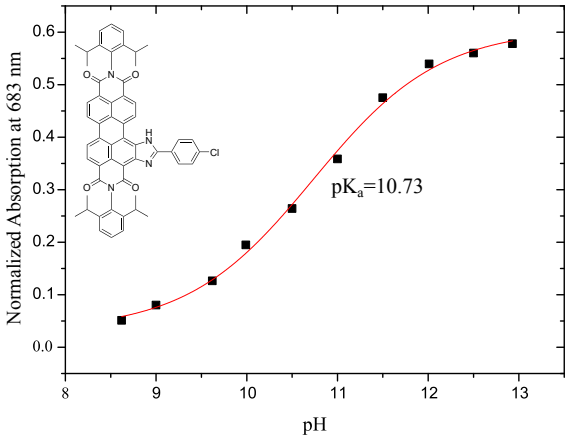

(b) Corresponding pK_a plot, respectively a sigmoidal Boltzmann fit

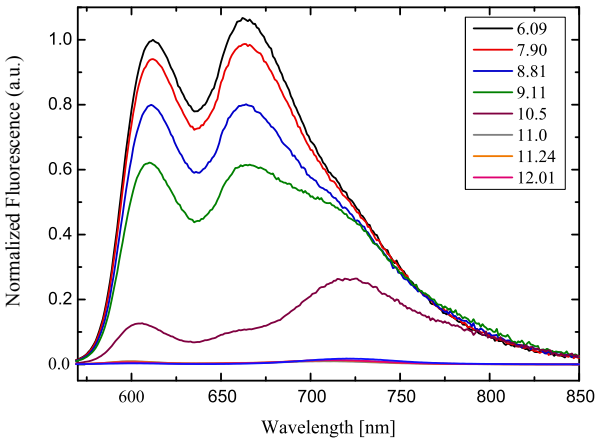

(c) Corrected emission spectra of pH sensor in buffer solutions, pH 6.09-12.01 at RT, λ_{Ex}=528 nm

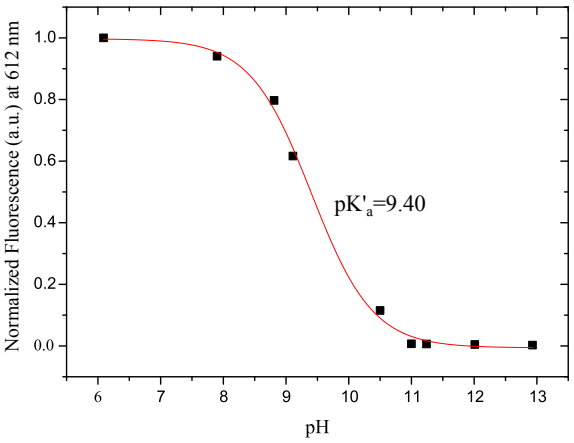

(d) Corresponding pK'_a plot, respectively a sigmoidal Boltzmann fit

Figure 4.20: Absorption and corrected emission spectra of Per−(ClPhIm) embedded into hydrogel D4 measured in buffer solutions and corresponding pK'_a calibration curve

Per − (Cl_2PhIm)

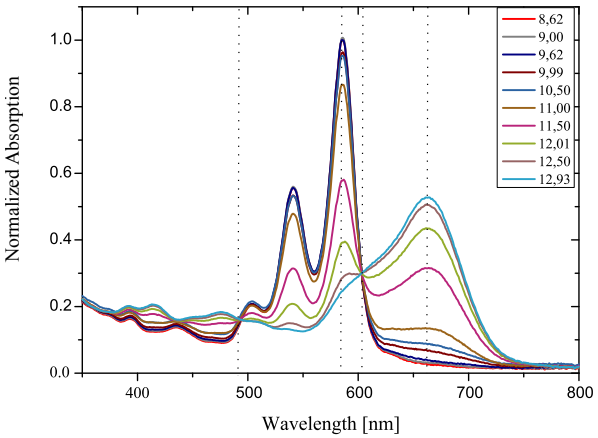

(a) Absorption spectra of pH sensor in buffer solutions, pH 8.62-12.93 at RT

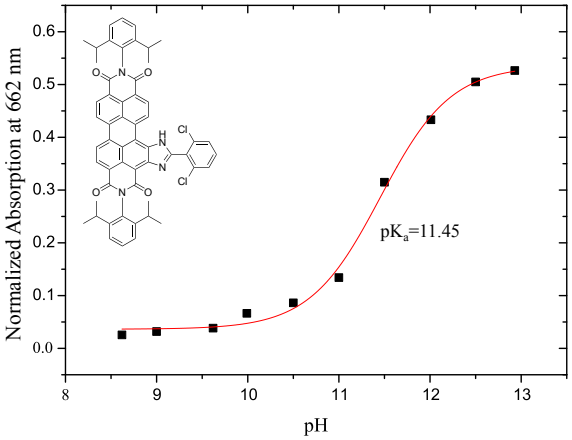

(b) Corresponding pK_a plot, respectively a sigmoidal Boltzmann fit

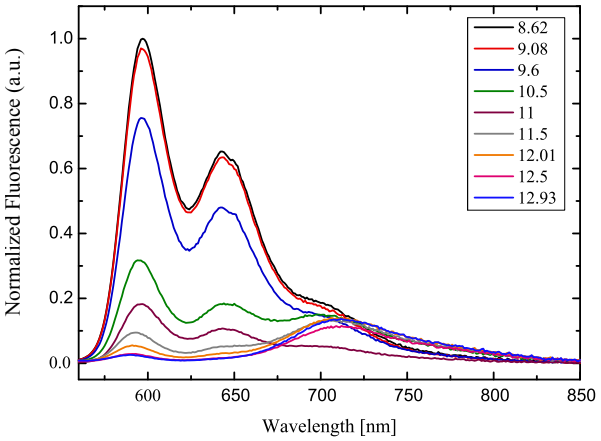

(c) Corrected emission spectra of pH sensor in buffer solutions, pH 8.62-12.93 at RT, λ_{Ex}=493 nm

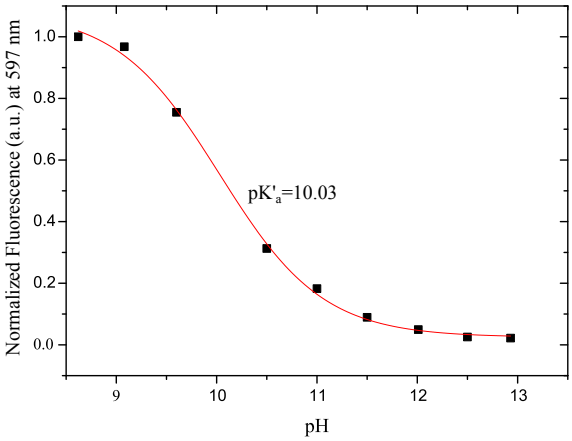

(d) Corresponding pK'_a plot, respectively a sigmoidal Boltzmann fit

Figure 4.21: Absorption and corrected emission spectra of Per−(Cl_2PhIm) embedded into hydrogel D4 measured in buffer solutions and corresponding pK'_a calibration curve

As mentioned before, the introduction of electron-withdrawing groups such as -Cl should facilitate the modification of the pK_a value of pH indicator dyes. Per-(ClPhIm) showed a slight decrease of the pK'_a in absorption spectra as well as in fluorescence spectra. This promising effect led to further investigations of introducing two chlorine atoms at the phenylimidazol group instead of one. The main difference in structural behaviour is that the halogen substituents are at the ortho position.

As shown in figure 4.21 absorption maxima of the protonated species could be observed at 586 nm, 541 nm and at 662 nm, belonging to the deprotonated form respectively. Finally just two isosbestic points were determined at 494 nm and 603 nm. Unexpectedly the pK_a value determined from the absorption spectra was calculated to be in the similar region as Per−(PhIm) and Per−$(PhIm)_2$. Additionally the fluorescence spectra (fig. 4.21(c)) showed two signals of the acidic form (597 nm, 664 nm). There the emission intensity increased at lower pH. The third signal (707 nm), the same as mentioned before for the other dyes, increased due to higher pH values.

According to the absorption spectra the apparent pK'_a derived from emission spectra (10.03) did not follow the estimation of the strong influence of the two -Cl substituents to tune the pK'_a. It should be mentioned that the sterical properties (o-positions of -Cl) may have more influence on the hindrance of the deprotonation reaction than the electronical behaviour has.

The results of the pH calibration measurements of sensor layers are concluded in table 4.4:

Table 4.4: pK'_a values and photophysical properties of four PBI dyes physically entrapped into hydrogel D4

Dye	λ_{Abs}^{max} prot. [nm]	λ_{Abs}^{max} deprot. [nm]	pK'_a Abs	λ_{Em} prot. [nm]	λ_{Em}^{max} deprot. [nm]	pK'_a Em
Per-(PhIm)	595	688	11.28	610, 672	730	10.77
Per-$(PhIm)_2$	650	731	11.36	664, 725	762	10.26
Per-(ClPhIm)	596	683	10.73	612, 663	720	9.40
Per-(Cl_2PhIm)	586	662	11.45	597, 664	707	10.03

Leaching out of a Matrix

Long term measurements as well as applications used under extreme conditions such as high pressure, high salinity or permanent contact with analyte require constant signal/noise ratio of sensors. Similar to good photostability properties the entrapment of indicator dyes into a polymer matrix are of particular interest. In this thesis the non-covalent physical immobilisation of dyes into polyurethane hydrogels in knife coated sensitive layers was focus of the investigations. Neither for protonated nor for deprotonated forms of the dyes leaching was observed. As can be seen in figure 4.22 and table 4.5. Absorption spectra were recorded regularly over 24 hours, while continuous washing with buffer in a home made flow-through cell. In the end maximum absorption intensity decreased around 6-7%. In the remaining cases the detected decrement was lower than 1.3%.

Table 4.5: Effective loss of dye after 24 hours of different perylene dyes

Dye	ΔAbs_{max} acidic [%]	ΔAbs_{max} basic [%]
Per-(PhIm)	0.08	6.9
Per-$(PhIm)_2$	6.0	1.3
Per-(ClPhIm)	0.6	0.7
Per-(Cl_2PhIm)	0.2	1.1

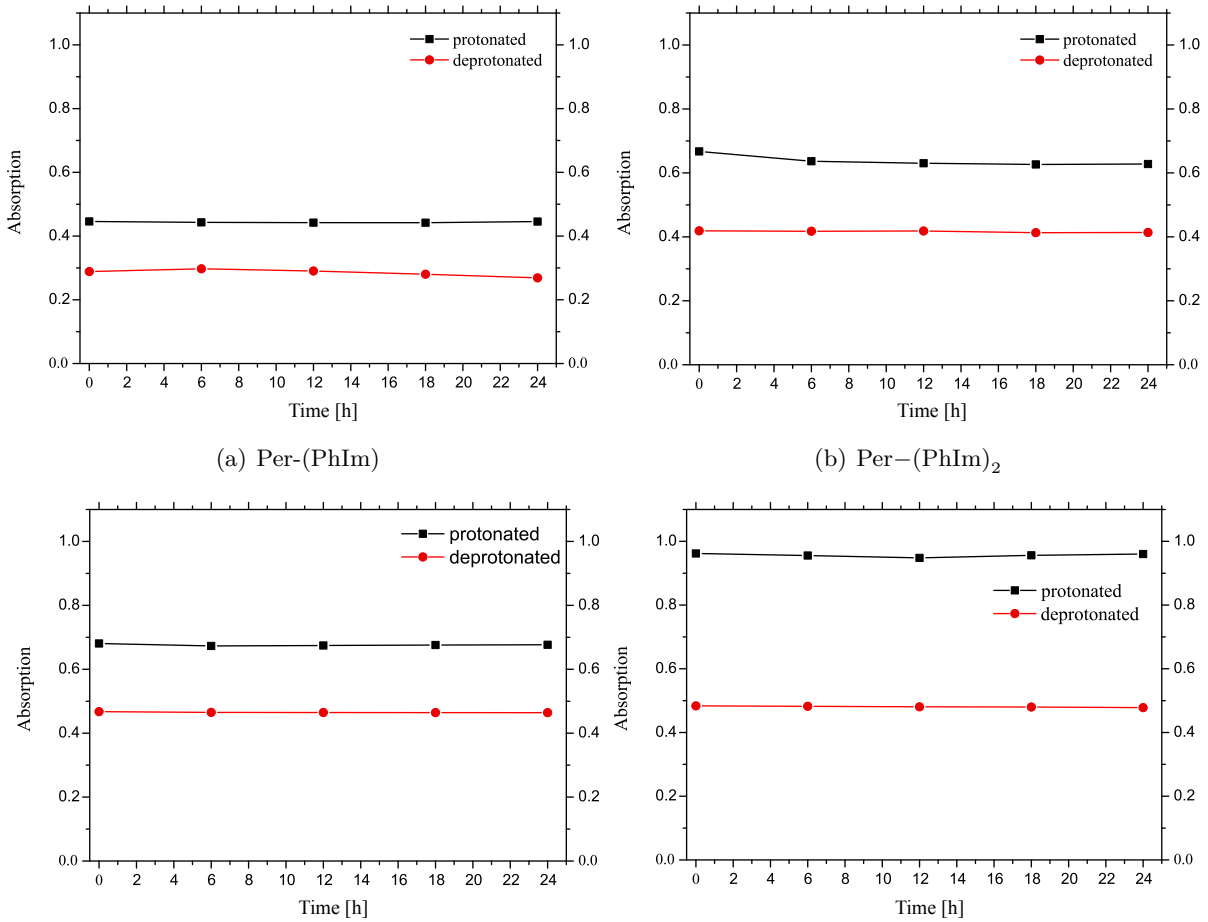

(a) Per-(PhIm)

(b) Per$-(PhIm)_2$

(c) Per$-$(ClPhIm)

(d) Per$-(Cl_2PhIm)$

Figure 4.22: Maximum absorption of pH sensitive dyes embedded into hydrogel D4 measured in a flow-through-cell over 24 hours

4.3.2 pH Sensing with Nanoparticles

PS/PVP Nanoparticles

Due to the high determined pK_a values in solution as well as in hydrogel D4 polymer matrix, alternatively incorporation of Per-(PhIm) dye into nanoparticles was performed to investigate the influence of different polymeric environments. The slightly negatively charged particles required a counterion for stabilisation of the embedded indicator dye. The ions were provided by quaternary ammonium salts (TOACl, TOAOH, TOATPB). Per-(PhIm) immobilization staining into the poly(vinylpyrrolidone)-shell of PS/PVP particles was accomplished by using EtOH/water mixture. The preparation of the beads was done by reported procedures [39].

PS/PVP with additional tetraoctylammonium chloride (TOACl)

Fluorescence spectra are shown in figure 4.23. Compared with emission spectra of Per-(PhIm) sensor layer (fig 4.18, p 57) the same intensity maxima could be observed. The apparent pK'_a value was obtained at pK'_a 8.19, a decrease of $\sim$ 2.6 pH units due to the hydrogel D4 matrix.

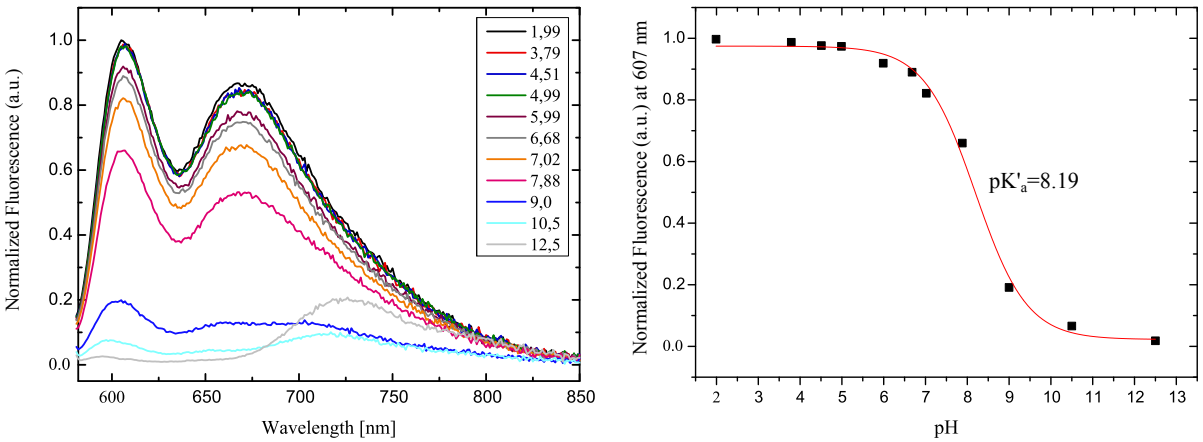

(a) Corrected emission spectra of pH sensitive PS/PVP nano beads solution, pH 1.98-12.50 at RT, λ_{Ex}=570 nm

(b) Corresponding pK'_a plot, respectively a sigmoidal Boltzmann fit

Figure 4.23: Corrected emission spectra of Per−(PhIm) incorporated into PS/PVP shell with additional TOACl measured in buffer solutions and corresponding pK'_a calibration curve

PS/PVP with additional tetraoctylammonium hydroxide (TOAOH)

In contrast to the emission spectra (fig 4.23), shown above, the emission band at 680 nm showed a higher intensity signal, than the band at shorter wavelength. Also a shift of the band from

680 nm at low pH values to 730 nm at high pH values could be observed (fig 4.24). The pK'_a plot of the recorded emission spectra showed a surprisingly high degradation of more than 5.5 pH units compared with the sensor layer consisted of hydrogel D4 (fig 4.18, p 57) to pK'_a 5.24. However, the anion of the ammonia salt OH^- and its strongly basic behaviour has a massive influence on the pK'_a value of the nano beads.

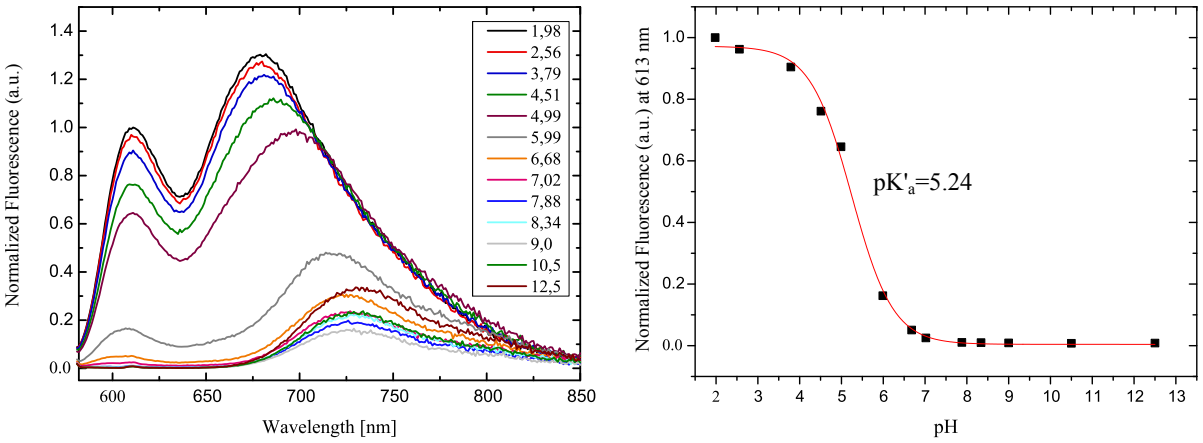

(a) Corrected emission spectra of pH sensitive PS/PVP nano beads solution, pH 1.98-12.50 at RT, λ_{Ex}=570 nm

(b) Corresponding pK'_a plot, respectively a sigmoidal Boltzmann fit

Figure 4.24: Corrected emission spectra of Per−(PhIm) incorporated into PS/PVP shell with additional TOAOH measured in buffer solutions and corresponding pK'_a calibration curve

PS/PVP with additional tetraoctylammonium tetraphenylborate (TOATPB)

Additionally to the commercially available ammonium salts, another quaternary ammonium salt was synthesised, to be used as counterion provider. The obtained pK'_a of 8.99 (fig 4.25) is similar to the TOACl-PS/PVP nano beads, what might be caused by the weak basic behaviour of these two ammonium salts.

The significant decrease of the pK'_a of PS/PVP particles with TOAOH was not expected. In general the quaternary ammonium cation should act as counterion to stabilise the deprotonated form of the dye embedded in the particles. In contrast, the anions should not affect the pK'_a that much. The beads were stored at 7 °C for a few weeks. Following fluorescence measurements showed drifts and calibration curves could not be reproduced. Furthermore, the beads and counterions might be strongly influenced by high ionic strengths, which may cause leaching of dye and TOA^+ out of the matrix.

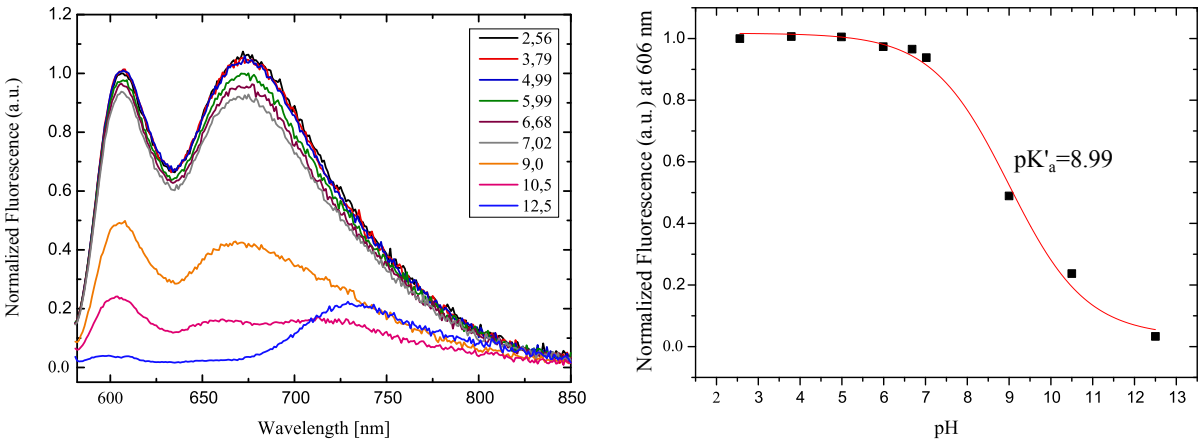

(a) Corrected emission spectra of pH sensitive PS/PVP nano beads solution, pH 2.56-12.50 at RT, λ_{Ex}=570 nm

(b) Corresponding pK'_a plot, respectively a sigmoidal Boltzmann fit

Figure 4.25: Corrected emission spectra of Per−(PhIm) incorporated into PS/PVP shell with additional TOATPB measured in buffer solutions and corresponding pK'_a calibration curve

Eudragit RL 100

Preparation of the beads was done by reported procedures [43]. Emission spectra of solutions consisted cationic Eudragit RL 100 nano beads are shown in figure 4.26. Due to the positive charge of the polymer no additional counterion is required. The pK'_a value of 9.60 could be observed. Particularly RL 100 beads can be promising since leaching of the dye is not likely.

The results of the pH calibration measurements with sensor nanoparticles are concluded in table 4.6:

Table 4.6: pK'_a values, emission properties, particle size of Per-(PhIm) embedded into nanoparticles

Dye	Concentration [% w/w]	Polymer	Counterion	λ_{Em} prot. [nm]	λ_{Em} deprot. [nm]	pK'_a Em	Size [nm]
Per-(PhIm)	0.5	PS/PVP	TOACl	607, 669	724	8.33	182
Per-(PhIm)	0.5	PS/PVP	TOAOH	613, 680	730	5.24	178
Per-(PhIm)	0.5	PS/PVP	TOATPB	606, 671	728	8.98	173
Per-(PhIm)	0.5	RL 100		596, 663	722	9.68	n.d.

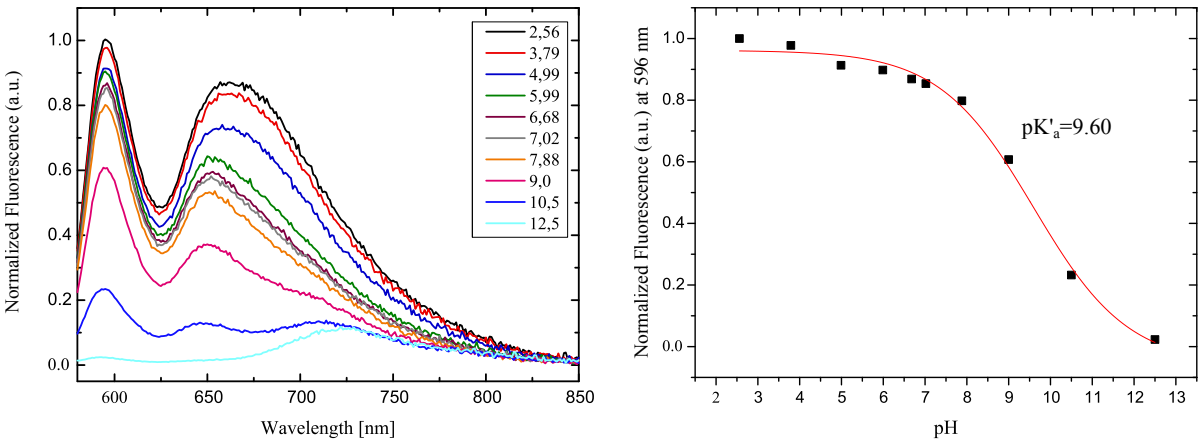

(a) Corrected emission spectra of pH sensitive RL 100 nano beads solution, pH 2.56-12.50 at RT, λ_{Ex}=570 nm

(b) Corresponding pK'_a plot, respectively a sigmoidal Boltzmann fit

Figure 4.26: Corrected emission spectra of Per−(PhIm) incorporated into RL 100 measured in buffer solutions and corresponding pK'_a calibration curve

Conclusion

The presented laterally extended perylene bisimides show characteristic absorption bands in a range from 570-780 nm for protonated/deprotonated species, which enables colorimetric measurements. Measurements in solution and of sensing films in buffer solutions, showed relatively high pK'_a values (9.40 - 11.45). Introduction of electron-withdrawing groups did not show the expected tendency of easy tunable pK'_a values, furthermore sterical hindrance should be kept in mind. The highly photostabile class of indicator dyes shows extremely bright red emission, which can be used for pH measurements. No leaching over 24 hours was observed, while measuring in a flow-through-cell. This emphasise a promising class of new pH sensitive dyes. Further applications should be designed with an addition of a reference fluorescent dye into the sensor layer to enable ratiometric pH sensing. The embedding of fluorescent Per-(PhIm) into PS/PVP and RL 100 nano beads resulted in a notable decrease of the pK'_a value (5.24 - 9.60), belonging to the polymer environment, compared to the data diverted by sensor layers. Particularly RL 100 beads can be promising since leaching of the dye is not likely.

Approximately 12 billion tons of concrete are produced annually, no other man made material is used more often. For stabilisation effects, steel is used, which corrodes under acidic conditions. Usually the pore water and moisture of concrete has an pH of 12-13, which is basic enough to form a protective layer on the steel. Due to carbonate and chloride attacks, the pH decreases to critical conditions for oxidation of steel [82, 83]. The high pK_a values of the presented perylene bisimide dyes may fit perfectly for pH monitoring in concrete based on fluorescence measurements.

4.3.3 Carbon Dioxide Measurements

For CO_2 sensitive layers, D7, a polyurethane-based hydrogel was used as polymeric matrix, which is able to swell with a water uptake of 30 %. It is a block-copolymer, which consists of hydrophobic and hydrophilic domains [38].

Determination of carbon dioxide is generally based on pH measurements. The recorded absorption/emission spectra are rather similar to those, as can be seen in chapter 4.3.1. Detection of carbon dioxide via absorption can be performed at wavelengths of the protonated/deprotonated maxima. Usually the sensor is in its deprotonated form, where an ionpair with a counter cation is built. Commonly used for carbon dioxide applications is a quaternary ammonium cation such as TOA^+, provided by the addition of TOAOH, which responsible for basic conditions. The reaction with carbon dioxide is shown below. Addition of tetraethyleneglycole (TEG) as plasticiser is essential for sensor response. First experiments were performed without TEG and no sensor response could be observed at all. The hydrogel matrix with its hydrophobic and hydrophilic patterns is one of the main differences to the commonly used *dry sensors* for carbon dioxide determination [8].

$$TOA^+Ind^- + CO_2 + H_2O \rightarrow HInd + TOA^+HCO_3^-$$

Per-(PhIm)

As shown in figure 4.27 absorption maxima could be observed at 595 nm for the protonated form and at 680 nm for the deprotonated form (ionpair with TOA^+). The isosbestic point was obtained at 616 nm. Carbon dioxide calibration was performed from 0 - 1013 hPa partial CO_2 gas pressure. The gas flow rate was kept constant by addition of N_2. At higher amounts of carbon dioxide deprotonated signal decreased, the protonated increased respectively. It should be mentioned, that at 1013 hPa pCO_2, accordingly 100 % pCO_2 gas flow, the sensor foil did not show complete protonation. However, complete protonation was induced by irreversible poisoning of the sensor with gaseous hydrochloric acid in the end of the experiment.

According to the absorption spectra, fluorescence spectra were recorded under same conditions. $\lambda_{Ex} = 510$ nm was chosen as excitation wavelength to obtain fluorescence intensity maxima at 604 nm, 655 nm (protonated species) and 720 nm as can seen in figure 4.28. The two bands at shorter wavelengths increased nearly linear, related to higher amounts of CO_2. At the end of the experiment, the state of total protonation was determined by poisoning with gaseous HCl. The relative fluorescence intensity signal of the poisoned foil compared to the signal of 1013 hPa carbon dioxide gas flow showed 3 times higher intensity (fig 4.28 (b)).

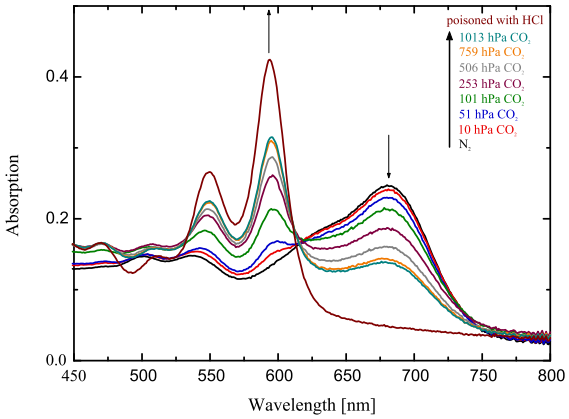

Figure 4.27: Absorption spectra at 25.6 °C, Per-(PhIm) immobilised in hydrogel D7 in carbon dioxide gas phase

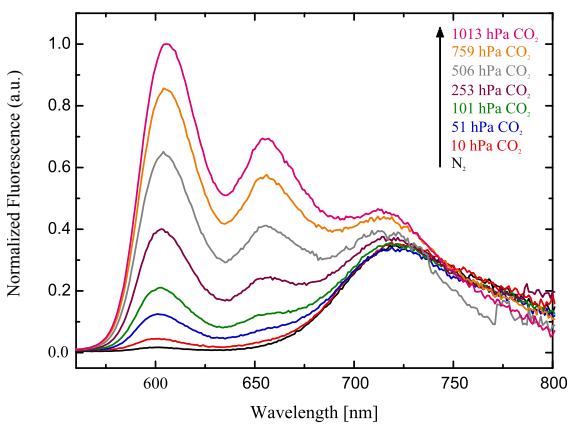

(a) Corrected emission spectra at 25 °C, $\lambda_{Ex} = 510$ nm

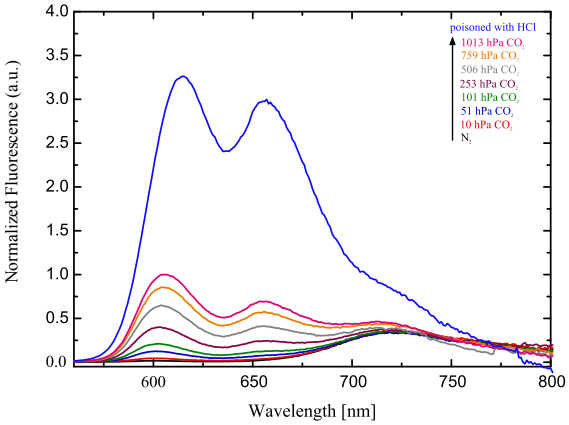

(b) Corrected emission spectra of HCl poisoned foil compared with calibration curves from (a)

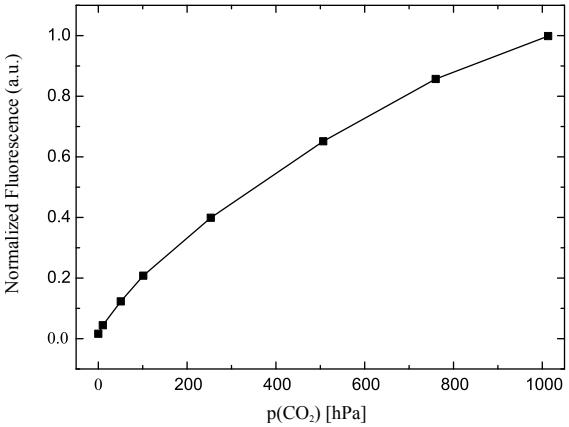

(c) Relative increase of fluorescence at 604 nm

Figure 4.28: Corrected emission spectra and calibration plot of Per-(PhIm) immobilised in hydrogel D7 in carbon dioxide gas phase

Per-$(PhIm)_2$

Due to the two protonation sites of Per-$(PhIm)_2$, an additional absorption/emission band could be obtained at longer wavelength > 750 nm (fig 4.29, fig 4.31, fig 4.33). Those signals only were observed at very low amounts of carbon dioxide (< 10 hPa). This fact enabled measurements in two different dynamic ranges (10 - 1013 hPa; 0.25 - 10 hPa pCO_2) with even one indicator dye. It should be mentioned that baseline adjusting was challenging without any presence of carbon dioxide for determinations below 5 hPa. The single appearance of the emission band at 800 nm at very low carbon dioxide partial pressures (fig 4.33) enabled high sensitivity to 1 hPa pCO_2 at least.

As can be seen in the fluorescence spectra (fig 4.31 (a), 4.33 (a)) three emission bands were obtained. The signal at 650 nm is related to the protonated form. The band at 750 nm is obtained for the mono deprotonated form (fig 4.30) and the signal at 800 nm refers to the doubly deprotonated form (fig 4.32), which only was obtained at very low pCO_2 < 0.5hPa pressures. Furthermore, dual range sensing might be potentially possible, but signals for doubly deprotonated form are ∼ 10 % of the completely protonated signal intensity.

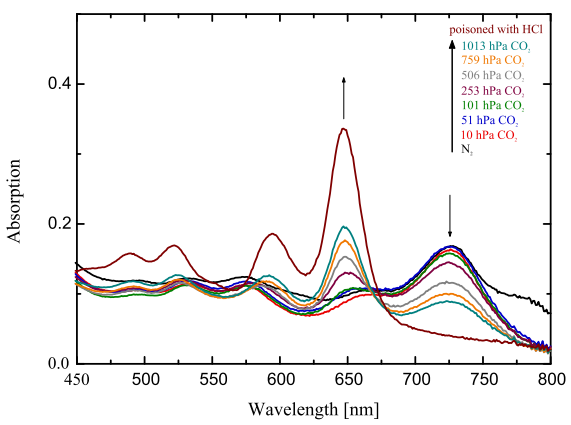

(a) Range from 0 to 1013 hPa pCO_2

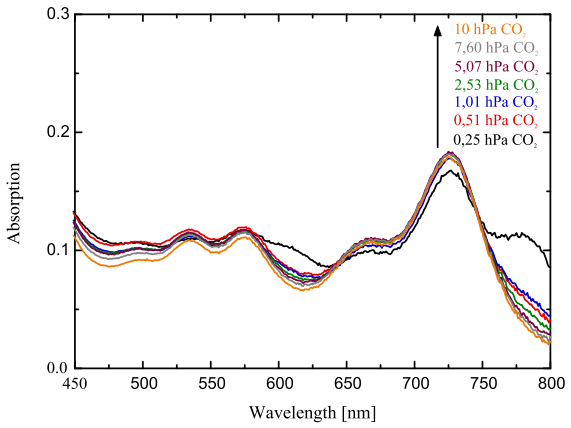

(b) Range from 0.25 to 10 hPa pCO_2

Figure 4.29: Absorption spectra at 25.6 °C of Per-$(PhIm)_2$ immobilised in hydrogel D7 in carbon dioxide gas phase

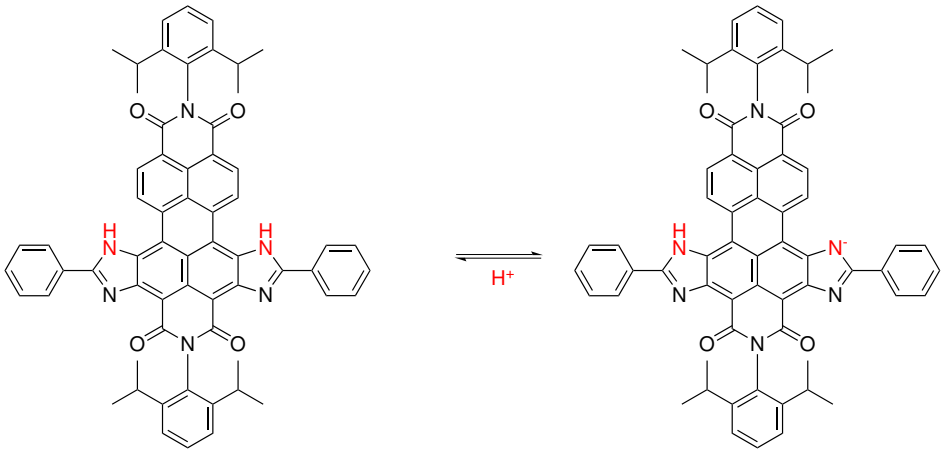

Figure 4.30: Formation of mono deprotonated species, belonging to the emission band at 750 nm

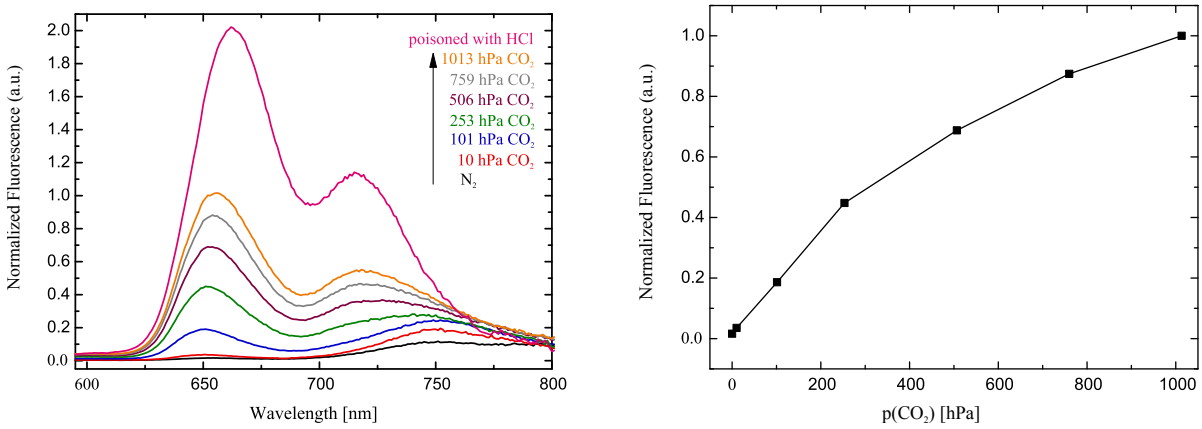

(a) Corrected emission spectra at 25 °C, $\lambda_{Ex} = 583$ nm

(b) Relative increase of fluorescence intensity at 653 nm

Figure 4.31: Corrected emission spectra and calibration plot of Per-$(PhIm)_2$ immobilised in hydrogel D7 in carbon dioxide gas phase in the range of 10 - 1013 hPa

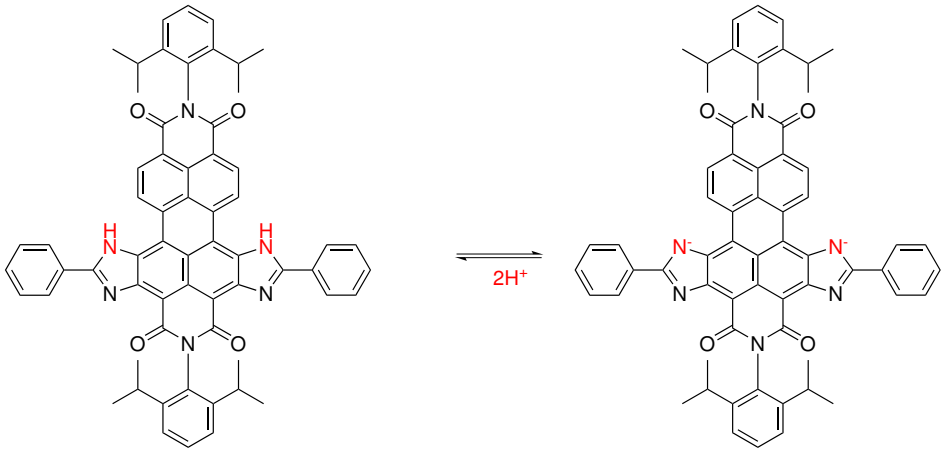

Figure 4.32: Formation of doubly deprotonated species, belonging to the emission band at 800 nm

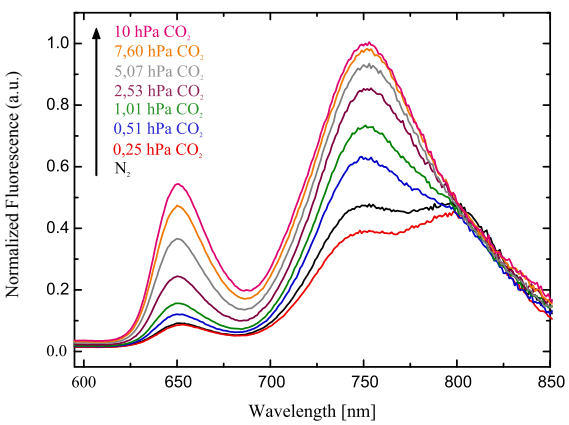

(a) Corrected emission spectra at 25 °C, $\lambda_{Ex} = 583$ nm

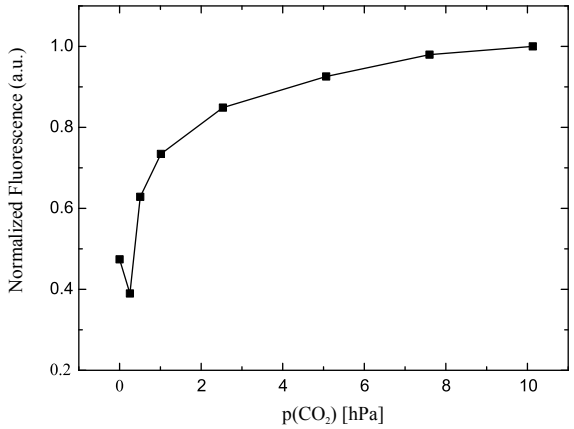

(b) Relative increase of fluorescence intensity at 752 nm

Figure 4.33: Corrected emission spectra and calibration plot of Per-$(PhIm)_2$ immobilised in hydrogel D7 in carbon dioxide gas phase in the range of 0.25 - 10 hPa

Per-(ClPhIm)

Closer studies of the performed absorption and emission spectra of Per-(ClPhIm) (fig 4.34, 4.35) showed an enormous decrease of sensitivity. The bands of the protonated species did not show higher intensity related to bands of the deprotonated state either in absorptions spectra or in emission spectra. The completely protonated form exhibited 5 times higher fluorescence intensity (fig 4.35 (c)), than the signal determined at 1013 hPa pCO_2. This large gap of protonation capability of the sensor foil induced experiments under higher pressure of gaseous carbon dioxide with this fluorescence based sensor.

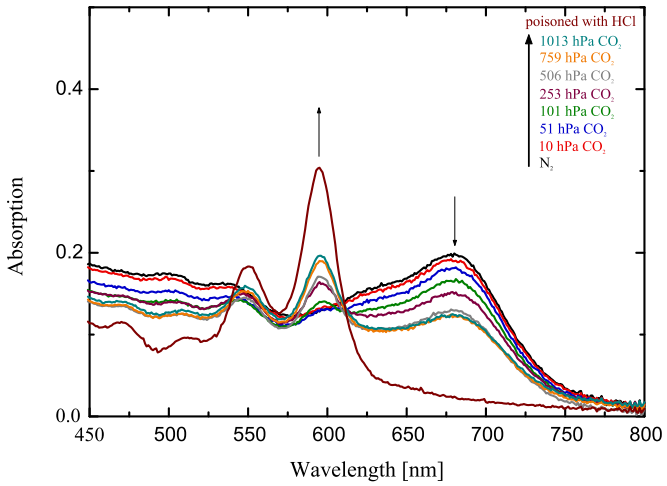

Figure 4.34: Absorption spectra at 25.6 °C of Per-(ClPhIm) immobilised in hydrogel D7 in Carbon Dioxide gas phase

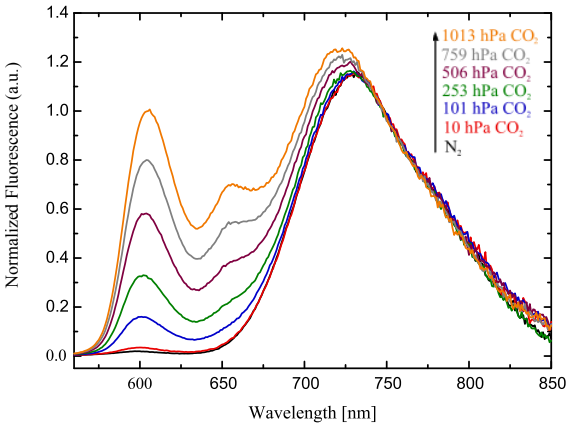

(a) Corrected emission spectra at 25 °C, $\lambda_{Ex} = 528$ nm

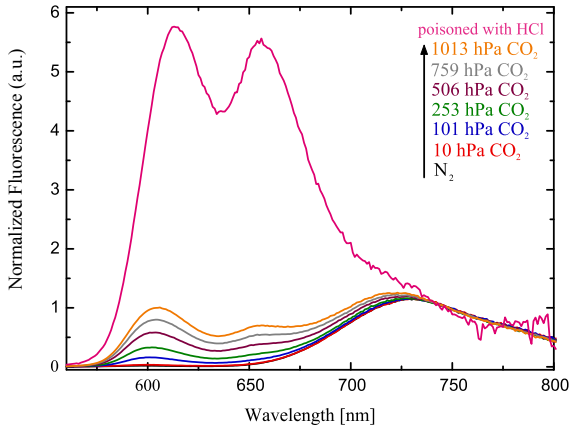

(b) Corrected emission spectra of HCl poisoned foil compared with calibration curves from (a)

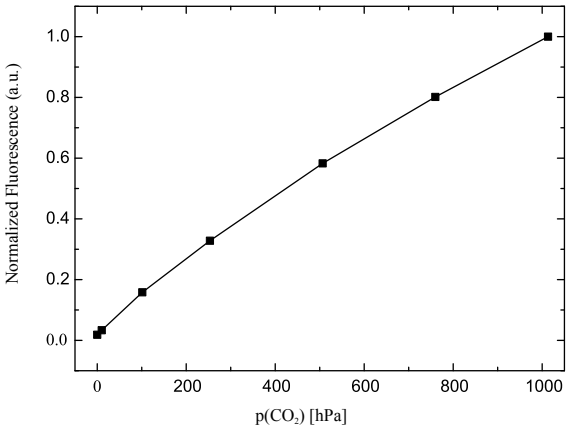

(c) Relative increase of fluorescence intensity at 605 nm

Figure 4.35: Corrected emission spectra and calibration plot of Per-(ClPhIm) immobilised in hydrogel D7 in Carbon Dioxide gas phase

Per-(Cl_2PhIm)

Contrary to minor sensitivity to carbon dioxide of Per-(ClPhIm), Per-(Cl_2PhIm) showed a quite high protonation rate at 1013 hPa pCO_2, respectively, as can be seen in absorption/emission spectra (fig 4.36, 4.37). The measurements were performed at three different temperatures to investigate the sensitivities of the sensor foil. The ratiometric comparison of the increasing signal at 595 nm to the intersection point 720 nm (fig 4.37 (d)) showed a higher sensitivity at 17 °C at lower amounts of carbon dioxide in the gaseous phase up to 101 hPa. Particularly strong effect from 17 °C to 25 °C could be determined, up to 33 °C the effect got less significant.

Surprisingly the sensitivity of Per-(Cl_2PhIm) is so much lower than of Per-(ClPhIm) since the pK_a values are similar. That could be caused by molecular properties. The sterical hindrance

of the two chlorine atoms on the (de)protonation process might have a strong influence because they are located close to the protonation site.

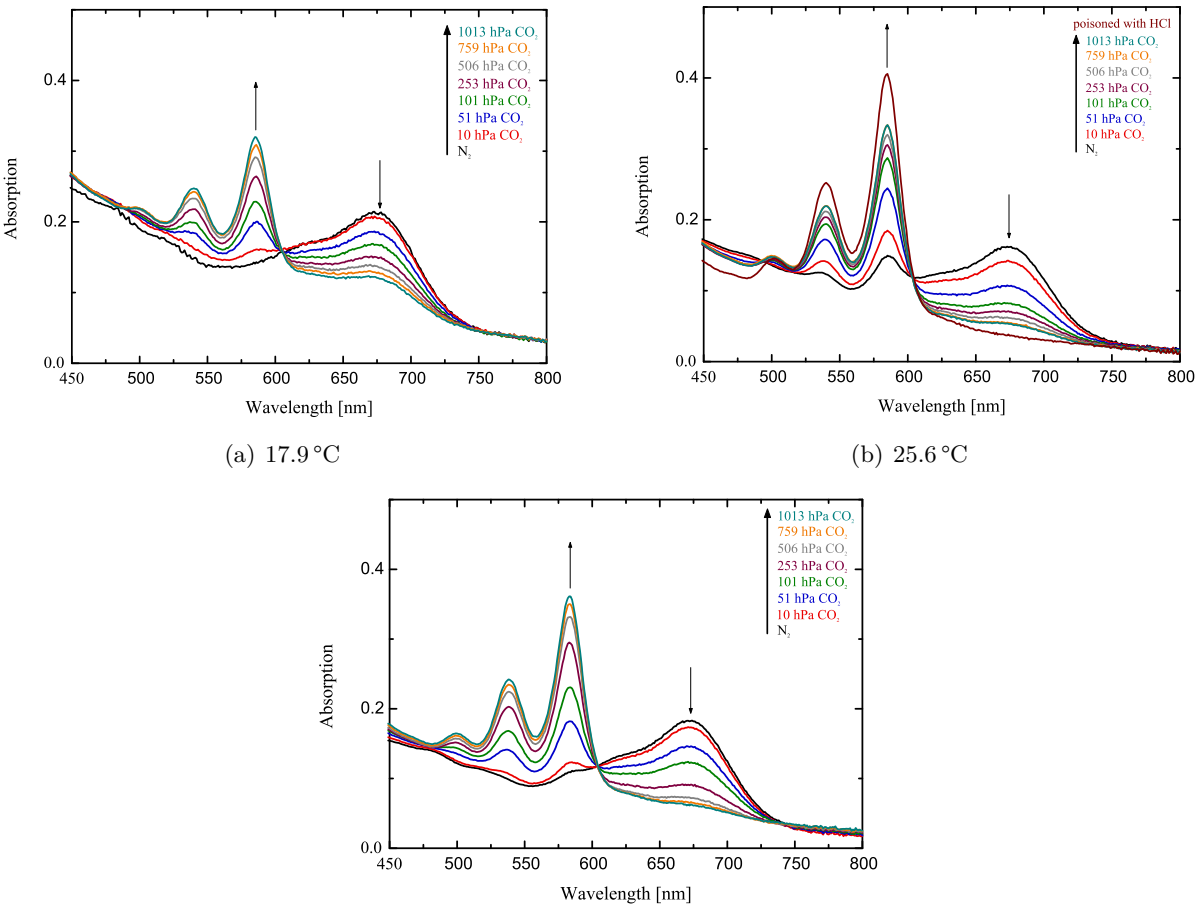

(a) 17.9 °C

(b) 25.6 °C

(c) 33.4 °C

Figure 4.36: Absorption spectra at 17.9 °C, 25.6 °C and 33.4 °C of Per−(Cl_2PhIm) immobilised in hydrogel D7 in carbon dioxide gas phase

Protonation Capability at atmospheric pressure

Accordingly to the shown spectra, absorption intensity at given pCO_2 were shown in figure 4.38. Per-(Cl_2PhIm) showed protonation rates of nearly 90 % at atmospheric pressure and almost more than 60 % at 100 hPa pCO_2, however the other 3 dyes were only protonated to 40 - 60 % at 1000 hPa, respectively. Surprisingly, Per-(ClPhIm) is the most sensitive dye, although low pK_a usually results in lower sensitivity. However, the obtained pK'_a values (tab 4.4) were all similar and such sensitivity differences were not expected. Furthermore the sterical influence of the halogen substituents at ortho-position on the easier removing of the counterion should be kept in mind.

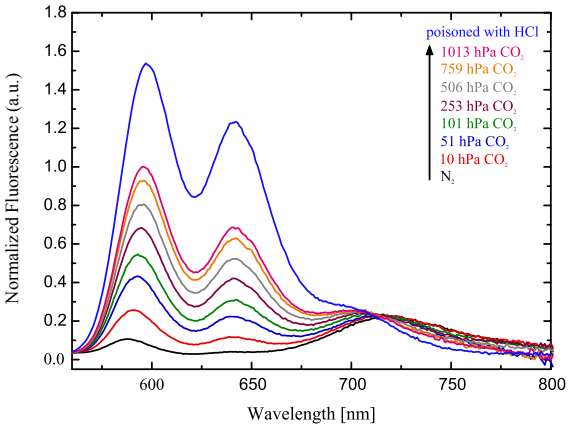

(a) Corrected emission spectra at 17 °C

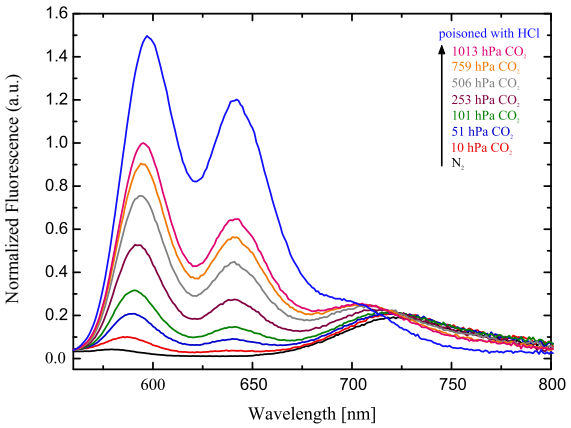

(b) Corrected emission spectra at 25 °C

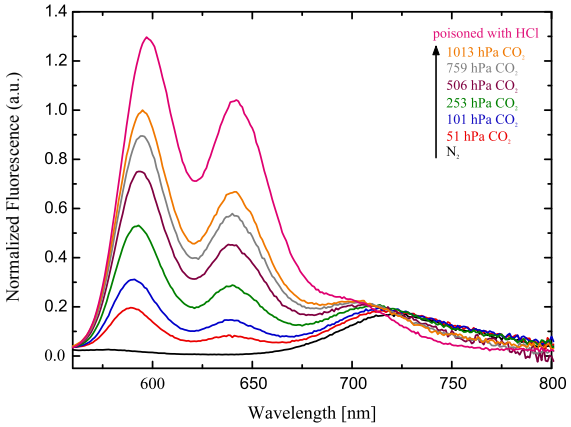

(c) Corrected emission spectra at 33 °C

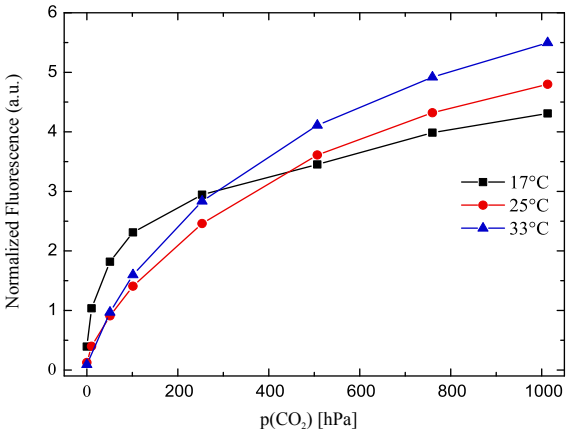

(d) Relative increase of fluorescence intensity at 595 nm

Figure 4.37: Corrected emission spectra and calibration of Per-(Cl_2PhIm) immobilised in hydrogel D7 in carbon dioxide gas phase, at different temperatures; $\lambda_{Ex} = 493\,nm$

4.3.4 Carbon Dioxide Determination under Higher Pressure

Due to the high residual protonation capability recorded with absorption of three out of four dyes shown in figure 4.38, as well as in particularly shown emission spectra (fig 4.28, 4.31, 4.35), determination of higher CO_2 pressures was achieved. At this stage of the thesis, the possibility of detection is shown, further investigations on calibration and long term experiments have to be adjusted.

Per-(ClPhIm) was chosen due to the highest protonation potential, to perform the experiment with higher pressures above ambient atmospheric pressures. The carbon dioxide sensor foil was fixed in a glass syringe with grease. The syringe was filled with gaseous CO_2 and subsequently encapsulated. The implemented carbon dioxide was compressed as can be seen in figure 4.39,

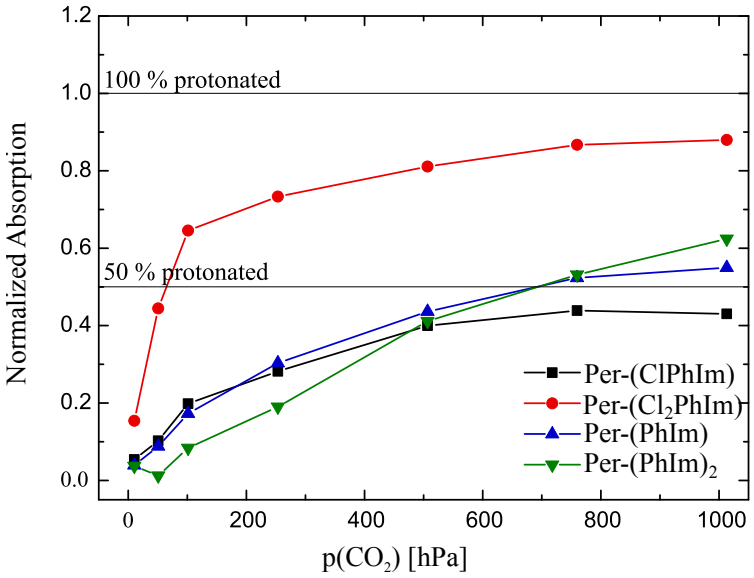

Figure 4.38: Normalized absorption maxima at 25.6 °C immobilised in hydrogel D7 in carbon dioxide gas phase

looking at the scale at the syringe. The CO_2 compression resulted in a brighter emission of the sensor foil.

4.3.5 Carbon Dioxide Determination in Drinks

Soft drinks as well as beer owe their popularity to the refreshing properties. Dissolved carbon dioxide, in form of hydrogencarbonate, better known as the bubbles, which often cause hiccup at hot summer days are main characteristics of such drinks. To generate those bubbles, the solutions had to be oversaturate with CO_2 under higher pressures. Immediately after the opening of a bottle, the pCO_2 is higher than the ambient atmospheric pressure. As mentioned before, three of four synthesised perylene dyes showed a high residual protonation capability at pressures of about 1000 hPa (fig.4.38).

The determination of different partial carbon dioxide pressures in different drinks was the aim of this experiment. A sensor foil was fixed on a optical fibre connected to a lock-in amplifier. The sensor was kept in the freshly opened bottle and the signal amplitude was recorded. At first water was measured, followed by water bubbled with gaseous CO_2, mineral water, beer and Coca-cola. The tendencies of recorded signal due to pCO_2 were shown in figure 4.40. The high noise ratio is caused by the bubbles and movements of the sensor. Some drift can be observed due to osmotic pressure or bubble accumulation. Nevertheless, a good proof of concept could be shown.

Figure 4.39: Sensor layer fixed in a 50 ml encapsulated glass syringe, filled with 100 % CO_2. Gas compression from left to right results in brighter red emission. Excitation with UV-lamp $\lambda_{Ex} \sim 365$ nm.

Conclusion

The appropriation of gas and water permeable hydrogel D7 in combination with a plasticiser and an additional hydrophobic filter membrane was investigated. In contrast to the common used *plastic type sensors* or *dry sensors* developed by Kawabata and later on by Mills et al [30, 84], the water uptake of the hydrogel of 30 % is high and the presence of the plasticiser tetraetyhleneglycole is essential for sensor response. The investigations of two dynamic range measurements with Per-$(PhIm)_2$ should be pursued.

Calibration could obtained over a wide range of pCO_2 pressures with absorption as well as with fluorescence spectroscopy. At the measurements under higher carbon dioxide pressures notable results could be obtained. Both, determination of higher gas pressure and higher pressure in solution were achieved. Further investigations in this field could be the improvement of the setup for calibration measurements, but the shown results already indicate that the sensors are promising for further applications.

4.3.6 Water Sensing

Determination of water and humidity is an important issue in numerous procedures in industry. There are a few sensing mechanisms established, e.g. holographic sensors [85], polymer coated platinum electrodes [86], fluorescence-lifetime based sensors [87] or a fluorescence based sensor, containing water sensitive dye cations [88].

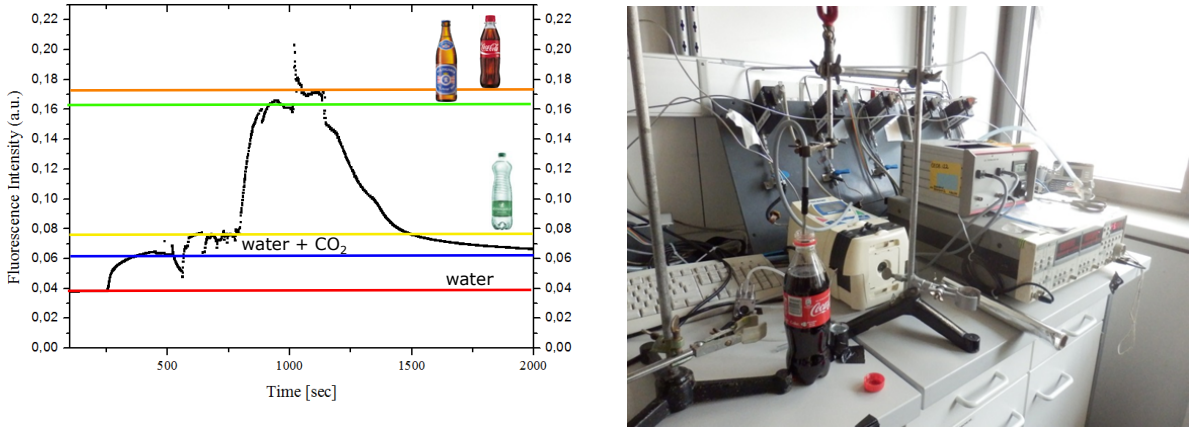

(a) Fluorescence signal intensity

(b) Setup with lock-in, optic fibers and sensor foil

Figure 4.40: Determination of different amounts of carbon dioxide dissolved in drinks

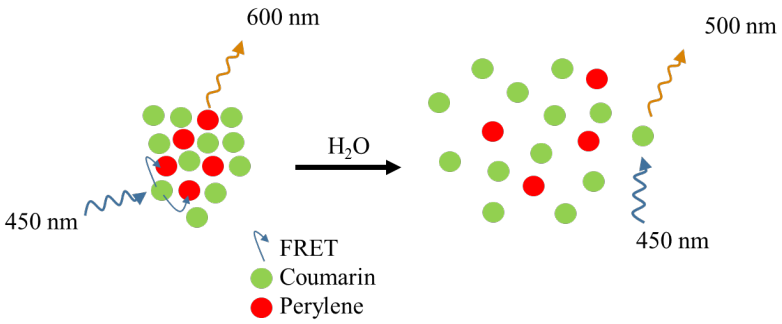

Figure 4.41: Schematic illustration of energy transfer process between close molecules in dry sensor and insufficient distance of the molecules in wet water swollen sensor

The substitution of the pH sensitive group of Per-(ClPhIm) resulted in a extremely bright red emitting fluorescence indicator dye Per-(ClPhIm)-*t*-ButylPh with outstanding photophysical properties (tab 4.1) without analyte sensitive group. In combination with a coumarin dye, which neither bears an analyte sensitive group and appropriate spectral properties Förster resonance energy transfer can be enabled, due to optimal distance and sufficient concentration, schematically shown in figure 4.41. The emission spectrum of the coumarin dye overlaps with the absorption spectrum of Per-(ClPhIm)-*t*-ButylPh, as can be seen in figure 4.42.

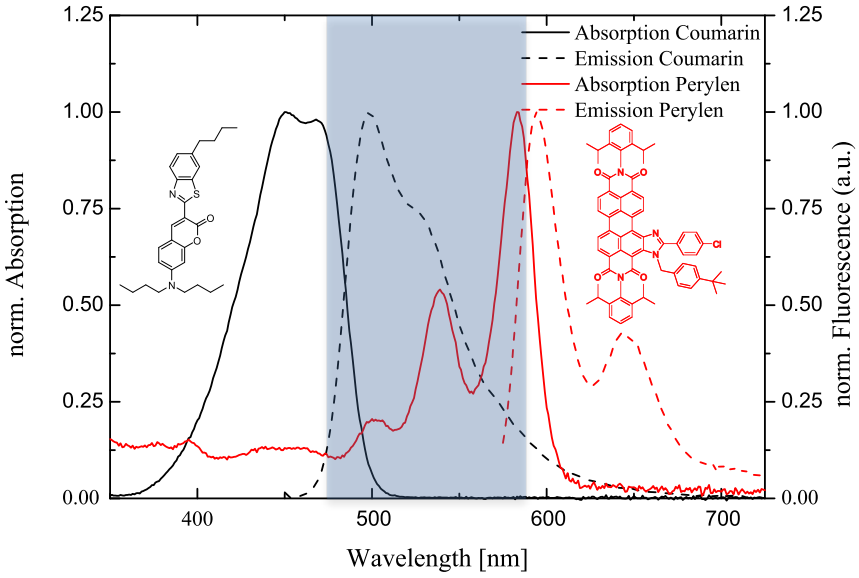

Figure 4.42: Absorption and emission spectra of coumarin dye and Per-(ClPhIm)-*t*-ButylPh dye

Certain amounts of Per-(ClPhIm)-*t*-ButylPh and coumarin were dissolved in THF and added to a stock-solution of hydrogel D4. Additionally to the involved dyes TiO_2 was added to the cocktail to enhance backscattering of the light which leads to increased signal intensities. Hydrogel D4 is able to undergo a wateruptake of 50 %, resulting in swelling of the polymer. This swelling effect causes an increase of the distance between the embedded dye molecules due to a decrease of the FRET capability.

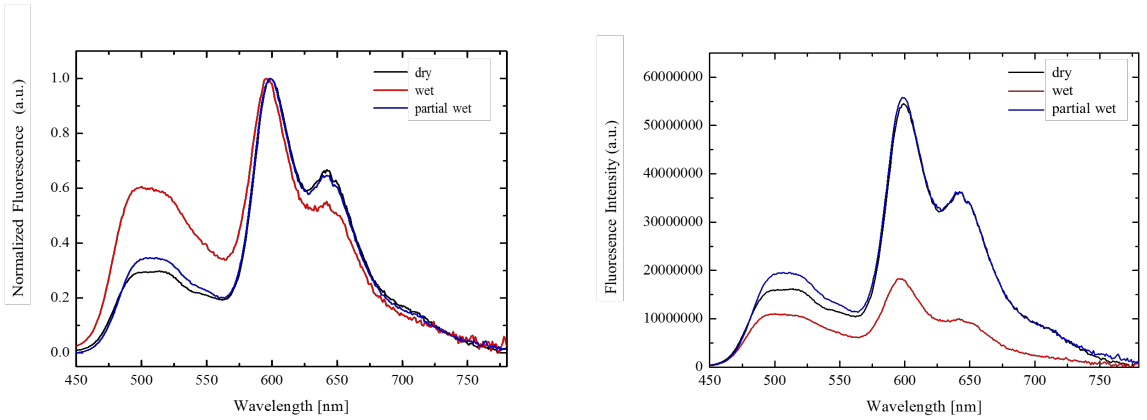

(a) Corrected normalized emission spectra of water sensor

(b) Corrected emission spectra of water sensor

Figure 4.43: Corrected emission spectra of sensor dry, wet and partial wet $\lambda_{Ex} = 440\,nm$

The presented sensor based on Förster resonance energy transfer is an alternative sensor concept. Sensor activation is not necessary. Cross-sensitivity effects to analyts (e.g. H^+) should not be determined due to the absence of analyte sensitive groups bearing the chromophoric system of the dyes, but ionic strength can affect the swelling. Emission spectra of the sensor layer were recorded λ_{Ex} 440 nm (absorption range of coumarin). The sensor foil was fixed in a cuvette and measured with and without water presence (fig 4.43).

As can be seen in table 4.7 the relative fluorescence intensity of coumarin increased, during the water presence, because the distance and concentration was not sufficient to enable FRET.

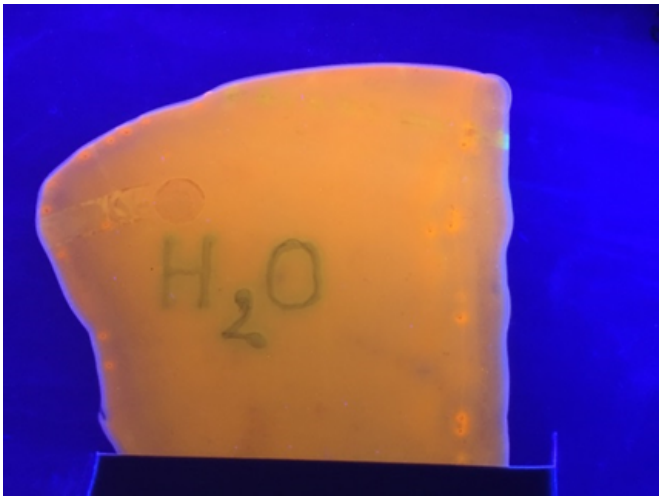

Figure 4.44: Image of sensor: Letters written with water (green) and dry sensor layer (orange), Excitation light source: UV-lamp $\lambda_{Ex} \sim 365$ nm

Table 4.7: Fluorescence intensity ratio of coumarin band and perylene band

water presence	norm. Fluorescence intensity	
	Coumarin (500 nm)	Perylen (600 nm)
dry	0.29	1
wet	0.60	1
partial wet	0.35	1

Conclusion

The produced water sensor showed remarkable results with attendance of liquid water. The swelling of the polymer material influenced the location of the included dyes that much, that differences of the transferred energy by FRET could be recorded with fluorescence spectroscopy. Further investigations on applications should be focused on measurements of water saturated N_2 gas flows.

5 Conclusion

In this thesis, a new class of core-functionalized perylene bisimide indicator dyes for optical chemosensors was developed. The introduction of phenyl-imidazol groups in the bay-region of a commercial available fluorescent dye resulted in a pH sensitivity in high pK_a ranges. Due to the outstanding photophysical properties of the dyes, applications for pH measurements with optical sensor layers, dye implementation in nanoparticles as well as carbon dioxide measurements in different pressure ranges were investigated.

The already known synthesis was not time consuming due to an one-step reaction. However, the perception that the basic form of the molecule has a different absorbance than the protonated species enable further investigations in the field of pH sensitive perylene dyes. This fact led to following experiments with benzonitrile derivates, to tune the pK_a of obtained PBI dyes by introducing electron-withdrawing groups. Nevertheless, the expected pK_a tendency of the new four dyes could not be observed, which might be caused by the sterical influence of the electron-withdrawing groups. Absorption and emission based pH measurements were performed with indicator dyes physically entrapped into a polyurethane-based hydrogel D4 with obtained pK_a values of (9.40 - 11.45). The pK_a values of nanoparticles could be observed in a range of 5.24 - 9.60 depending on polymer type and counterions.

The relatively high pK_a values were also suitable for optical carbon dioxide measurements. The pH indicator dyes were embedded into a polyurethane-based hydrogel matrix in combination with a plasticiser and a quaternary ammonium counterion. The produced sensors showed different dynamic ranges. In the case of $\mathrm{Per-(PhIm)_2}$ dual range sensing (0.25 - 10 hPa and 10 - 1013 hPa) would be potentially possible, because of two protonation sites. On the other hand, Per-(ClPhIm) showed a high protonation capability for CO_2 pressures above atmospheric conditions.

At last, but not least a non pH sensitive fluorescent dye could be synthesised by alkylation of the protonation site, which was used for a FRET based water sensor. Two suitable dyes were embedded into a water swellable hydrogel matrix. Water presence resulted in swelling of the polymer matrix, which caused a greater distance between the dye molecules and a decrease of the transferred energy. This could be measured by fluorescence spectroscopy.

6 References

[1] Bernard Valeur and Wiley InterScience (Online service). *Molecular fluorescence principles and applications*. English. New York: Wiley-VCH, 2001.

[2] Joseph R. Lakowicz. *Principles of fluorescence spectroscopy*. 3rd ed. New York: Springer, 2006.

[3] T. W. J. Gadella, ed. *FRET and FLIM techniques*. 1st ed. Laboratory techniques in biochemistry and molecular biology v. 33. Amsterdam ; Boston: Elsevier, 2009.

[4] Gerhard Neurauter, Ingo Klimant, and Otto S. Wolfbeis. "Microsecond lifetime-based optical carbon dioxide sensor using luminescence resonance energy transfer". en. In: *Analytica Chimica Acta* 382.1-2 (Feb. 1999), pp. 67–75.

[5] Susanne Schutting, Sergey M. Borisov, and Ingo Klimant. "Diketo-Pyrrolo-Pyrrole Dyes as New Colorimetric and Fluorescent pH Indicators for Optical Carbon Dioxide Sensors". en. In: *Analytical Chemistry* 85.6 (Mar. 2013), pp. 3271–3279.

[6] Peter Gründler. *Chemische Sensoren: Eine Einführung für Naturwissenschaftler und Ingenieure*. de. Springer-Verlag, July 2006.

[7] Ramaier Narayanaswamy and Otto S. Wolfbeis. *Optical Sensors: Industrial, Environmental and Diagnostic Applications*. en. Springer Science & Business Media, Jan. 2004.

[8] Francesco Baldini and North Atlantic Treaty Organization, eds. *Optical chemical sensors*. NATO science series vol. 224. Dordrecht: Springer, 2006.

[9] Sergey M. Borisov and Otto S. Wolfbeis. "Optical Biosensors". en. In: *Chemical Reviews* 108.2 (Feb. 2008), pp. 423–461.

[10] Otto S. Wolfbeis. "Materials for fluorescence-based optical chemical sensors". en. In: *Journal of Materials Chemistry* 15.27-28 (2005), p. 2657.

[11] Christine. Munkholm et al. "Polymer Modification of Fiber Optic Chemical Sensors as a Method of Enhancing Fluorescence Signal for pH Measurement". en. In: *Analytical Chemistry* 58.7 (June 1986), pp. 1427–1430.

[12] Nils H. Janzen et al. "Evaluation of fluorimetric pH sensors for bioprocess monitoring at low pH". en. In: *Bioprocess and Biosystems Engineering* 38.9 (May 2015), pp. 1685–1692.

[13] Xu-dong Wang et al. "A water-sprayable, thermogelating and biocompatible polymer host for use in fluorescent chemical sensing and imaging of oxygen, pH values and temperature". In: *Sensors and Actuators B: Chemical* 221 (Dec. 2015), pp. 37–44.

[14] Lin Yuan, Weiying Lin, and Yanming Feng. “A rational approach to tuning the pKa values of rhodamines for living cell fluorescence imaging”. en. In: *Organic & Biomolecular Chemistry* 9.6 (2011), p. 1723.

[15] Susanne Schutting et al. “NIR optical carbon dioxide sensors based on highly photostable dihydroxy-aza-BODIPY dyes”. en. In: *J. Mater. Chem. C* 3.21 (2015), pp. 5474–5483.

[16] Daniel Aigner et al. “Enhancing Photoinduced Electron Transfer Efficiency of Fluorescent pH-Probes with Halogenated Phenols”. en. In: *Analytical Chemistry* 86.18 (Sept. 2014), pp. 9293–9300.

[17] L.M. Daffy et al. “Arenedicarboximide building blocks for fluorescent photoinduced electron transfer pH sensors applicable with different media and communication wavelengths”. English. In: *Chemistry - A European Journal* 4.9 (1998), pp. 1810–1815.

[18] Richard A. Bissell et al. “Fluorescent PET (photoinduced electron transfer) sensors with targeting/anchoring modules as molecular versions of submarine periscopes for mapping membrane-bounded protons”. en. In: *Journal of the Chemical Society, Chemical Communications* 4 (1994), p. 405.

[19] Daniel Aigner et al. “New fluorescent pH sensors based on covalently linkable PET rhodamines”. en. In: *Talanta* 99 (Sept. 2012), pp. 194–201.

[20] D. Aigner et al. “pH-sensitive perylene bisimide probes for live cell fluorescence lifetime imaging”. en. In: *J. Mater. Chem. B* 2.39 (Aug. 2014), pp. 6792–6801.

[21] Daniel Aigner, Sergey M. Borisov, and Ingo Klimant. “New fluorescent perylene bisimide indicators—a platform for broadband pH optodes”. en. In: *Analytical and Bioanalytical Chemistry* 400.8 (June 2011), pp. 2475–2485.

[22] D. Willoughby, Roger C. Thomas, and Christof J. Schwiening. “Comparison of simultaneous pH measurements made with 8-hydroxypyrene-1,3,6-trisulphonic acid (HPTS) and pH-sensitive microelectrodes in snail neurones”. en. In: *Pflügers Archiv* 436.4 (July 1998), pp. 615–622.

[23] E. Pastoriza-Munoz, R.M. Harrington, and M.L. Graber. “Parathyroid hormone decreases HCO3 reabsorption in the rat proximal tubule by stimulating phosphatidylinositol metabolism and inhibiting base exit”. English. In: *Journal of Clinical Investigation* 89.5 (1992), pp. 1485–1495.

[24] Monique M. Martin and Lars Lindqvist. “The pH dependence of fluorescein fluorescence”. In: *Journal of Luminescence* 10.6 (July 1975), pp. 381–390.

[25] James E. Whitaker, Richard P. Haugland, and Franklyn G. Prendergast. “Spectral and photophysical studies of benzo[c]xanthene dyes: Dual emission pH sensors”. In: *Analytical Biochemistry* 194.2 (May 1991), pp. 330–344.

[26] John W. Severinghaus and A. Freeman Bradley. “Electrodes for Blood pO2 and pCO2 Determination”. en. In: *Journal of Applied Physiology* 13.3 (Nov. 1958), pp. 515–520.

[27] Mahesh Uttamlal and David R. Walt. “A Fiber-Optic Carbon Dioxide Sensor for Fermentation Monitoring”. en. In: *Nature Biotechnology* 13.6 (June 1995), pp. 597–601.

[28] Otto S. Wolfbeis et al. “Fiber-optic fluorosensor for oxygen and carbon dioxide”. In: *Analytical Chemistry* 60.19 (Oct. 1988), pp. 2028–2030.

[29] C Munkholm. “A fiber-optic sensor for CO2 measurement”. In: *Talanta* 35.2 (Feb. 1988), pp. 109–112.

[30] Andrew. Mills, Qing. Chang, and Neil. McMurray. “Equilibrium studies on colorimetric plastic film sensors for carbon dioxide”. en. In: *Analytical Chemistry* 64.13 (July 1992), pp. 1383–1389.

[31] Andrew Mills, Anne Lepre, and Lorraine Wild. “Breath-by-breath measurement of carbon dioxide using a plastic film optical sensor”. en. In: *Sensors and Actuators B: Chemical* 39.1-3 (Mar. 1997), pp. 419–425.

[32] Naoki Nakamura and Yutaka Amao. “Optical sensor for carbon dioxide combining colorimetric change of a pH indicator and a reference luminescent dye”. In: *Analytical and Bioanalytical Chemistry* 376.5 (July 2003), pp. 642–646.

[33] I.M. Pérez de Vargas-Sansalvador et al. “Phosphorescent sensing of carbon dioxide based on secondary inner-filter quenching”. en. In: *Analytica Chimica Acta* 655.1-2 (Nov. 2009), pp. 66–74.

[34] Susanne Schutting et al. “New highly fluorescent pH indicator for ratiometric RGB imaging of pCO $_2$”. In: *Methods and Applications in Fluorescence* 2.2 (Apr. 2014), p. 024001.

[35] Merima Čajlaković, Alessandro Bizzarri, and Volker Ribitsch. “Luminescence lifetime-based carbon dioxide optical sensor for clinical applications”. en. In: *Analytica Chimica Acta* 573-574 (July 2006), pp. 57–64.

[36] C. Guillaume, P. Chalier, and N. Gontard. “Modified atmosphere packaging using environmentally compatible and active food packaging materials”. en. In: *Environmentally Compatible Food Packaging*. Elsevier, 2008, pp. 396–418.

[37] Junji Watanabe and Mitsuru Akashi. “Novel Biomineralization for Hydrogels: Electrophoresis Approach Accelerates Hydroxyapatite Formation in Hydrogels”. en. In: *Biomacromolecules* 7.11 (Nov. 2006), pp. 3008–3011.

[38] Bernhard M. Weidgans et al. “Fluorescent pH sensors with negligible sensitivity to ionic strength”. en. In: *The Analyst* 129.7 (2004), p. 645.

[39] Sergey M. Borisov, Torsten Mayr, and Ingo Klimant. “Poly(styrene- *block* -vinylpyrrolidone) Beads as a Versatile Material for Simple Fabrication of Optical Nanosensors”. en. In: *Analytical Chemistry* 80.3 (Feb. 2008), pp. 573–582.

[40] Sergey M. Borisov, Danielle L. Herrod, and Ingo Klimant. “Fluorescent poly(styrene-block-vinylpyrrolidone) nanobeads for optical sensing of pH”. en. In: *Sensors and Actuators B: Chemical* 139.1 (May 2009), pp. 52–58.

[41] S. M. Borisov, G. Nuss, and I. Klimant. “Red Light-Excitable Oxygen Sensing Materials Based on Platinum(II) and Palladium(II) Benzoporphyrins”. In: *Analytical Chemistry* 80.24 (Dec. 2008), pp. 9435–9442.

[42] Lorenz H. Fischer et al. “Dual sensing of pO2 and temperature using a water-based and sprayable fluorescent paint”. en. In: *The Analyst* 135.6 (2010), p. 1224.

[43] Andreas Fercher et al. “Intracellular O $_2$ Sensing Probe Based on Cell-Penetrating Phosphorescent Nanoparticles”. en. In: *ACS Nano* 5.7 (July 2011), pp. 5499–5508.

[44] Sergey M. Borisov et al. “Precipitation as a simple and versatile method for preparation of optical nanochemosensors”. en. In: *Talanta* 79.5 (Oct. 2009), pp. 1322–1330.

[45] Alina V. Kondrashina et al. “A Phosphorescent Nanoparticle-Based Probe for Sensing and Imaging of (Intra)Cellular Oxygen in Multiple Detection Modalities”. en. In: *Advanced Functional Materials* 22.23 (Dec. 2012), pp. 4931–4939.

[46] Swarnali Das, Preeti K. Suresh, and Rohitas Desmukh. “Design of Eudragit RL 100 nanoparticles by nanoprecipitation method for ocular drug delivery”. In: *Nanomedicine: Nanotechnology, Biology and Medicine* 6.2 (Apr. 2010), pp. 318–323.

[47] Daniel Aigner et al. “Fluorescent materials for pH sensing and imaging based on novel 1,4-diketopyrrolo-[3,4-c]pyrrole dyes”. en. In: *Journal of Materials Chemistry C* 1.36 (2013), p. 5685.

[48] Christopher Kohl et al. “Towards Highly Fluorescent and Water-Soluble Perylene Dyes”. en. In: *Chemistry - A European Journal* 10.21 (Nov. 2004), pp. 5297–5310.

[49] Heinz Langhals, Rami Ismael, and Oktay Yürük. “Persistent Fluorescence of Perylene Dyes by Steric Inhibition of Aggregation”. en. In: *Tetrahedron* 56.30 (July 2000), pp. 5435–5441.

[50] G Seybold. “New perylene and violanthrone dyestuffs for fluorescent collectors”. In: *Dyes and Pigments* 11.4 (1989), pp. 303–317.

[51] Andreas Rademacher, Suse Märkle, and Heinz Langhals. “Lösliche Perylen-Fluoreszenzfarbstoffe mit hoher Photostabilität”. de. In: *Chemische Berichte* 115.8 (Aug. 1982), pp. 2927–2934.

[52] Heinz Langhals, Jan Karolin, and Lennart B-Å. Johansson. “Spectroscopic properties of new and convenient standards for measuring fluorescence quantum yields”. In: *Journal of the Chemical Society, Faraday Transactions* 94.19 (1998), pp. 2919–2922.

[53] G Schnurpfeil. “Syntheses of uncharged, positively and negatively charged 3,4,9,10-perylene-bis(dicarboximides)”. en. In: *Dyes and Pigments* 27.4 (1995), pp. 339–350.

[54] Jianqiang Qu et al. “Ionic Perylenetetracarboxdiimides: Highly Fluorescent and Water-Soluble Dyes for Biolabeling”. en. In: *Angewandte Chemie* 116.12 (Mar. 2004), pp. 1554–1557.

[55] Daniela Baumstark and Hans-Achim Wagenknecht. “Perylene Bisimide Dimers as Fluorescent “Glue” for DNA and for Base-Mismatch Detection”. en. In: *Angewandte Chemie International Edition* 47.14 (Mar. 2008), pp. 2612–2614.

[56] Yuri Avlasevich, Chen Li, and Klaus Müllen. “Synthesis and applications of core-enlarged perylene dyes”. en. In: *Journal of Materials Chemistry* 20.19 (2010), p. 3814.

[57] Daniel Aigner et al. “Novel near infra-red fluorescent pH sensors based on 1-aminoperylene bisimides covalently grafted onto poly(acryloylmorpholine)”. en. In: *Chemical Communications* 49.21 (2013), p. 2139.

[58] Tien-Lung Chiu et al. “Low reflection and photo-sensitive organic light-emitting device with perylene diimide and double-metal structure”. en. In: *Thin Solid Films* 517.13 (May 2009), pp. 3712–3716.

[59] Roland Stolarski and Krzysztof J. Fiksinski. “Fluorescent perylene dyes for liquid crystal displays”. en. In: *Dyes and Pigments* 24.4 (Jan. 1994), pp. 295–303.

[60] A. J. Breeze et al. “Polymer—perylene diimide heterojunction solar cells”. en. In: *Applied Physics Letters* 81.16 (2002), p. 3085.

[61] Jianqiang Qu et al. “Dendronized Perylene Diimide Emitters: Synthesis, Luminescence, and Electron and Energy Transfer Studies”. en. In: *Macromolecules* 37.22 (Nov. 2004), pp. 8297–8306.

[62] Tomas Edvinsson et al. “Intramolecular Charge-Transfer Tuning of Perylenes: Spectroscopic Features and Performance in Dye-Sensitized Solar Cells”. en. In: *The Journal of Physical Chemistry C* 111.42 (Oct. 2007), pp. 15137–15140.

[63] Heinz Langhals and Wolfgang Jona. “Intense Dyes through Chromophore–Chromophore Interactions: Bi- and Trichromophoric Perylene-3,4:9,10-bis(dicarboximide)s”. en. In: *Angewandte Chemie International Edition* 37.7 (Apr. 1998), pp. 952–955.

[64] Christophe Ego et al. “Attaching Perylene Dyes to Polyfluorene: Three Simple, Efficient Methods for Facile Color Tuning of Light-Emitting Polymers”. en. In: *Journal of the American Chemical Society* 125.2 (Jan. 2003), pp. 437–443.

[65] Heinz Langhals, Andreas J. Esterbauer, and Simon Kinzel. “Red shining silica: macroscopic pigments and nanoparticles by silylation”. en. In: *New Journal of Chemistry* 33.9 (2009), p. 1829.

[66] Kremer Pigmente. *Product discription for Lumogen red F300*. 2015.

[67] Glenn A. Crosby and James N. Demas. “Measurement of photoluminescence quantum yields. Review”. en. In: *The Journal of Physical Chemistry* 75.8 (Apr. 1971), pp. 991–1024.

[68] David Türp et al. “Synthesis of Nanometer-Sized, Rigid, and Hydrophobic Anions”. en. In: *Angewandte Chemie International Edition* 50.21 (May 2011), pp. 4962–4965.

[69] Heinz Langhals, Gertrud Schönmann, and Kurt Polborn. “Anthracene Carboxyimides and Their Dimers”. en. In: *Chemistry - A European Journal* 14.17 (June 2008), pp. 5290–5303.

[70] Heinz Langhals and Simon Kinzel. “Laterally Extended Naphthalene Tetracarboxylic Bisimides”. en. In: *The Journal of Organic Chemistry* 75.22 (Nov. 2010), pp. 7781–7784.

[71] W. Phillips Winter. “AN INVESTIGATION OF SODAMIDE AND OF CERTAIN OF ITS REACTION-PRODUCTS. [1]”. en. In: *Journal of the American Chemical Society* 26.11 (Nov. 1904), pp. 1484–1512.

[72] Simon Kinzel. *Dissertation, Perylenfarbstoffe mit lateraler heterocyclischer Ringerweiterung, Ludwig-Maximilians-Universität München,* 2010.

[73] Reinhard Brückner. *Reaktionsmechanismen: organische Reaktionen, Stereochemie, moderne Synthesemethoden.* ger. 3. Aufl., aktualisiert und überarb., 2. korrigierter Nachdr. Berlin: Spektrum Akad. Verl, 2009.

[74] Tijana Jokic et al. “Highly Photostable Near-Infrared Fluorescent pH Indicators and Sensors Based on BF $_2$ -Chelated Tetraarylazadipyrromethene Dyes”. en. In: *Analytical Chemistry* 84.15 (Aug. 2012), pp. 6723–6730.

[75] Noël Boens, Volker Leen, and Wim Dehaen. “Fluorescent indicators based on BODIPY”. en. In: *Chem. Soc. Rev.* 41.3 (2012), pp. 1130–1172.

[76] Claudia R. Schröder, Bernhard M. Weidgans, and Ingo Klimant. “pH Fluorosensors for use in marine systems”. en. In: *The Analyst* 130.6 (2005), p. 907.

[77] Mariana Beija, Carlos A. M. Afonso, and José M. G. Martinho. “Synthesis and applications of Rhodamine derivatives as fluorescent probes”. en. In: *Chemical Society Reviews* 38.8 (2009), p. 2410.

[78] S. J. Strickler and Robert A. Berg. “Relationship between Absorption Intensity and Fluorescence Lifetime of Molecules”. en. In: *The Journal of Chemical Physics* 37.4 (1962), p. 814.

[79] Lennart B.-Å. Johansson and Heinz Langhals. “Spectroscopic studies of fluorescent perylene dyes”. en. In: *Spectrochimica Acta Part A: Molecular Spectroscopy* 47.7 (Jan. 1991), pp. 857–861.

[80] Gilbert O. Fruhwirth and Albin Hermetter. “Seeds and oil of the Styrian oil pumpkin: Components and biological activities”. en. In: *European Journal of Lipid Science and Technology* 109.11 (Nov. 2007), pp. 1128–1140.

[81] Tobias Abel et al. “Fast responsive, optical trace level ammonia sensor for environmental monitoring”. en. In: *Chemistry Central Journal* 6.1 (2012), p. 124.

[82] John P Broomfield. *Corrosion of steel in concrete understanding, investigation and repair.* English. London [etc.]: E & FN Spon [etc.] : [Online:] Taylor & Francis, 1997.

[83] Christoph Dauberschmidt and Michael Raupach. “Untersuchungen zu den Korrosionsmechanismen von Stahlfasern in chloridhaltigem Beton”. PhD thesis. Aachen, Techn. Hochsch., Diss., 2006, 2006.

[84] Yuji Kawabata et al. “Fiber-optic sensor for carbon dioxide with a ph indicator dispersed in a poly(ethylene glycol) membrane”. en. In: *Analytica Chimica Acta* 219 (Jan. 1989), pp. 223–229.

[85] Jeff Blyth et al. “Holographic Sensor for Water in Solvents”. en. In: *Analytical Chemistry* 68.7 (Jan. 1996), pp. 1089–1094.

[86] Amy E. Clough. “Measuring the water content of synthetic lubricants with polymer-coated sensors”. en. In: *Analytica Chimica Acta* 315.1-2 (Oct. 1995), pp. 15–26.

[87] Qing Chang et al. “A fluorescence lifetime-based solid sensor for water”. en. In: *Analytica Chimica Acta* 350.1-2 (Sept. 1997), pp. 97–104.

[88] Francisco Galindo et al. “Water/humidity and ammonia sensor, based on a polymer hydrogel matrix containing a fluorescent flavylium compound”. en. In: *Journal of Materials Chemistry* 15.27-28 (2005), p. 2840.

7 List of Figures

8 List of Tables

9 Appendix

9.1 NMR and MALDI-TOF spectra

9.1.1 Per-(PhIm)

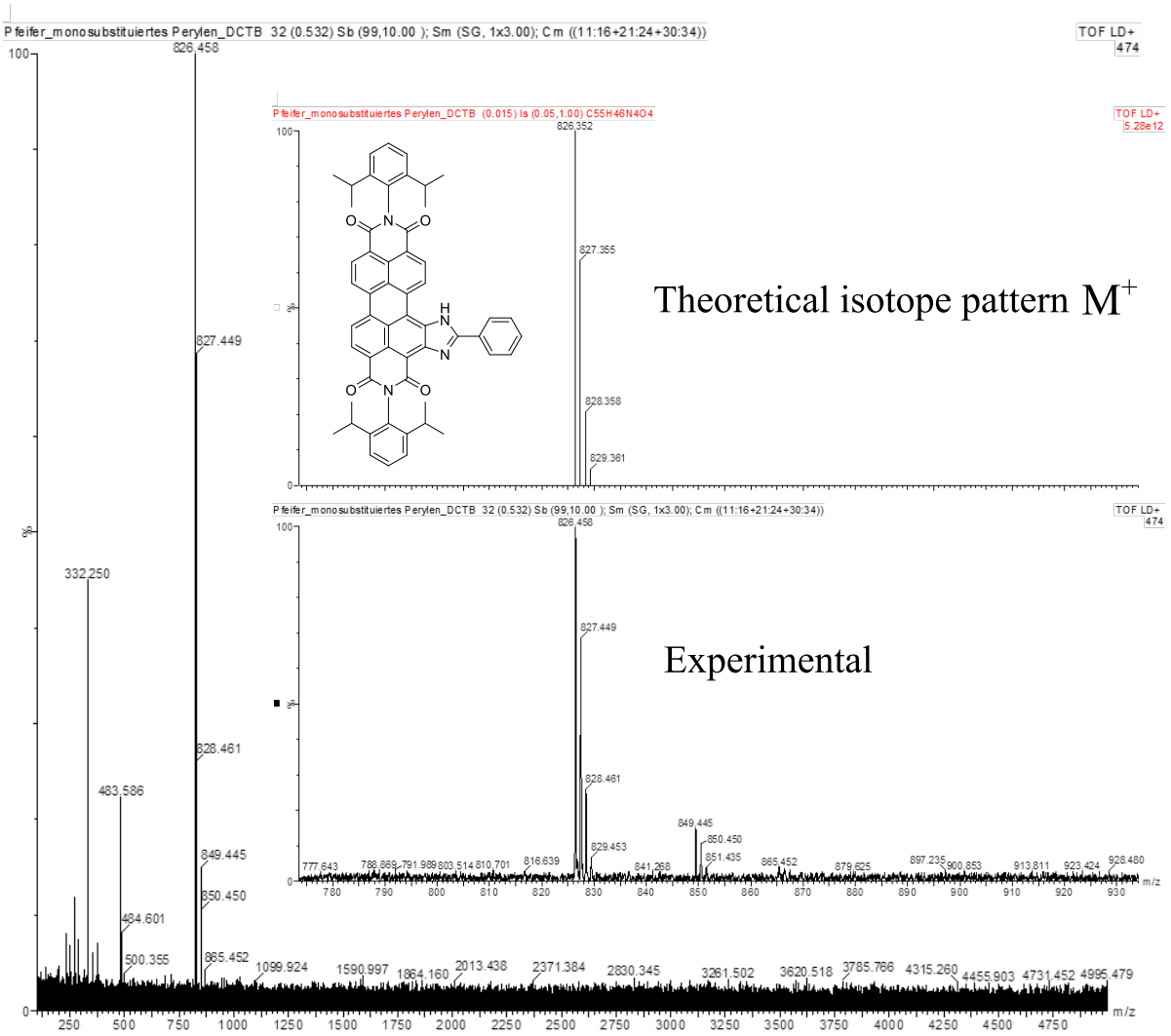

Figure 9.1: MALDI-TOF spectra of Per-(PhIm), found: M^+: 826.458, MNa^+: 849.445 [m/z]

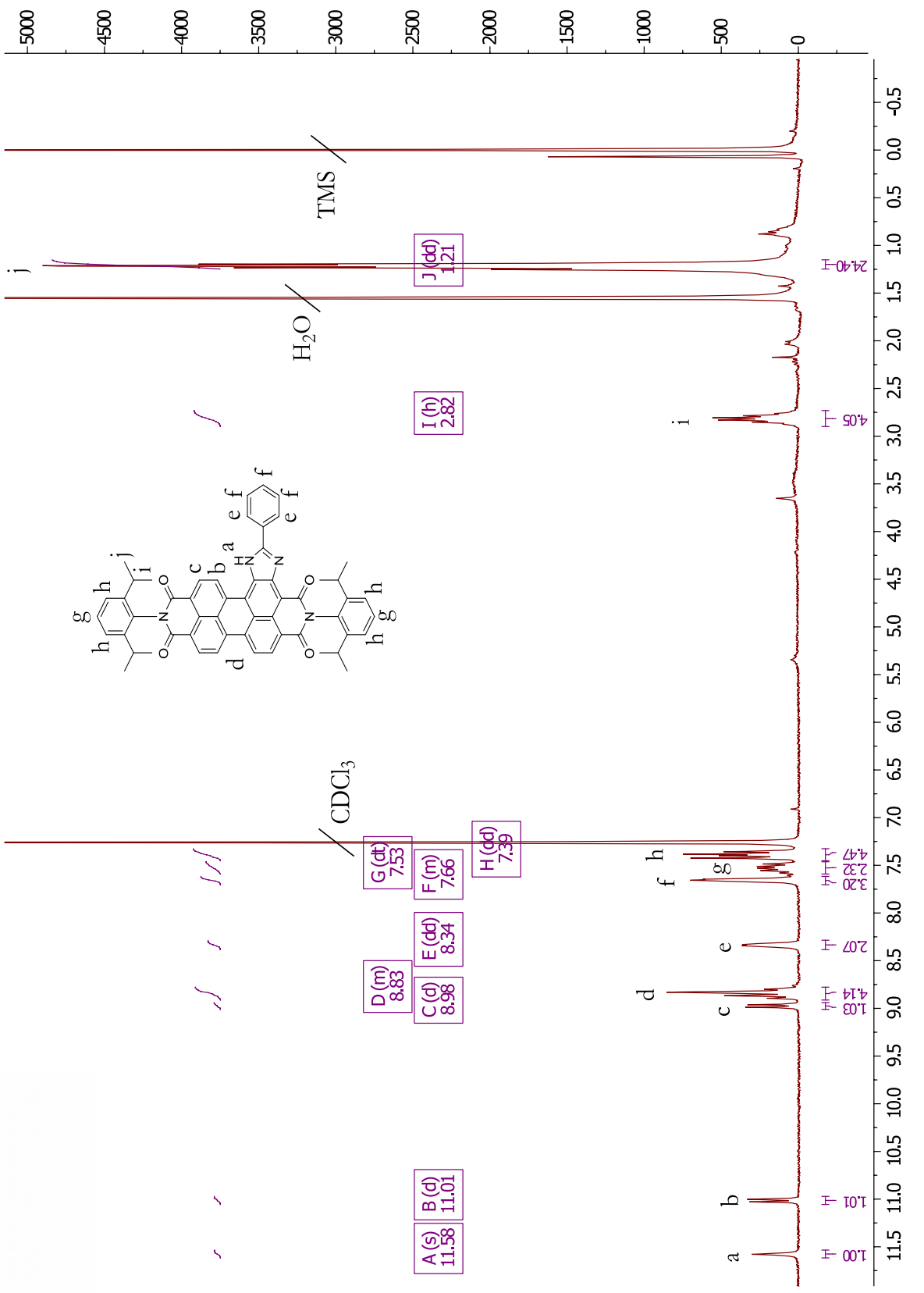
TMS
H2O
CDCl3
A (s) 11.58
B (d) 11.01
C (d) 8.98
D (m) 8.83
E (dd) 8.34
F (m) 7.66
G (dt) 7.53
H (dd) 7.39
I (h) 2.82
J (dd) 1.21
1.00
1.01
4.14
2.07
3.20
2.32
4.47
4.05
24.40

9.1.2 Per-$(PhIm)_2$

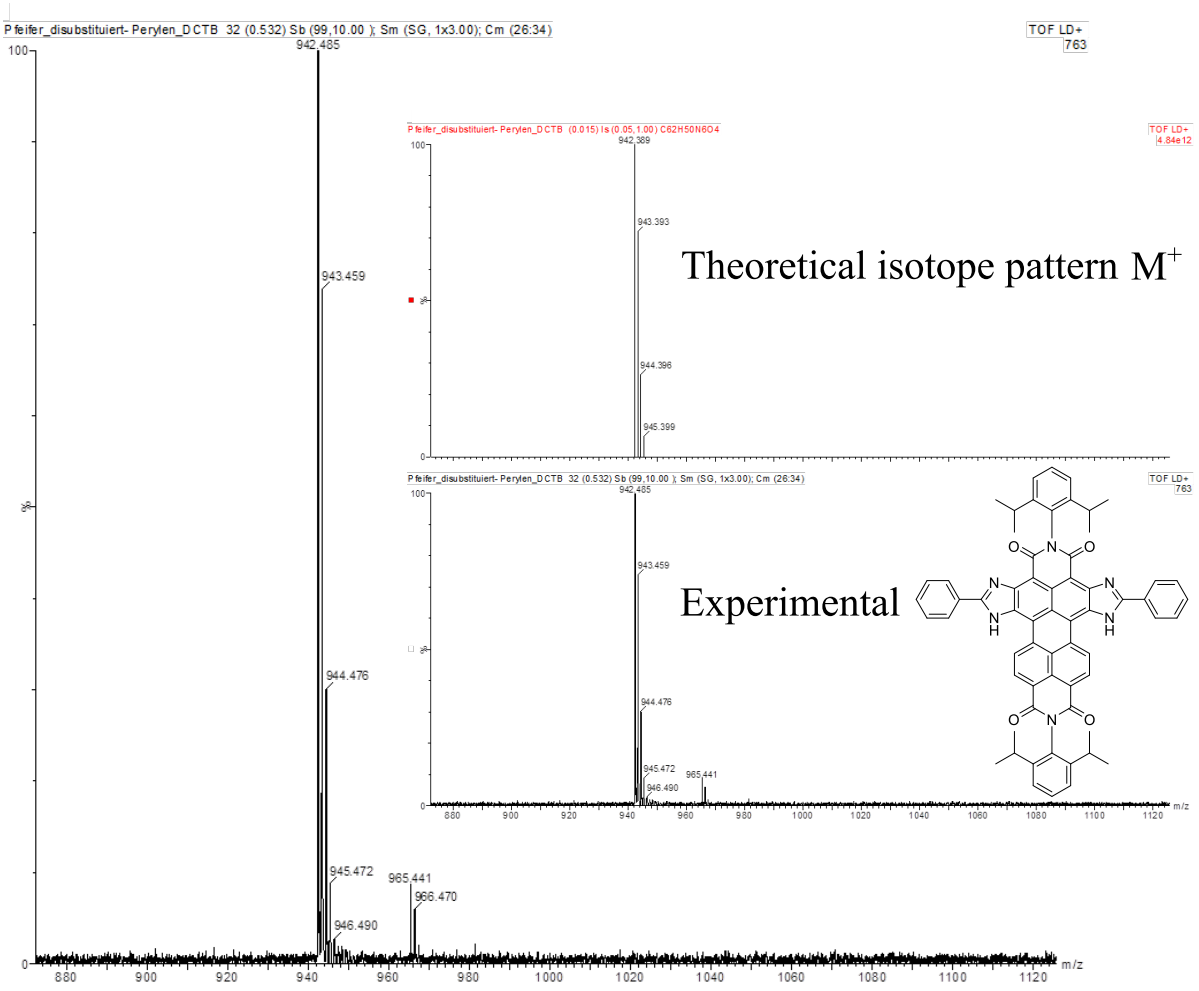

Figure 9.2: MALDI-TOF spectra of Per-$(PhIm)_2$, found: M^+: 942.485, MNa^+: 965.441 [m/z]

9.1.3 Per-$(PhIm)_3$

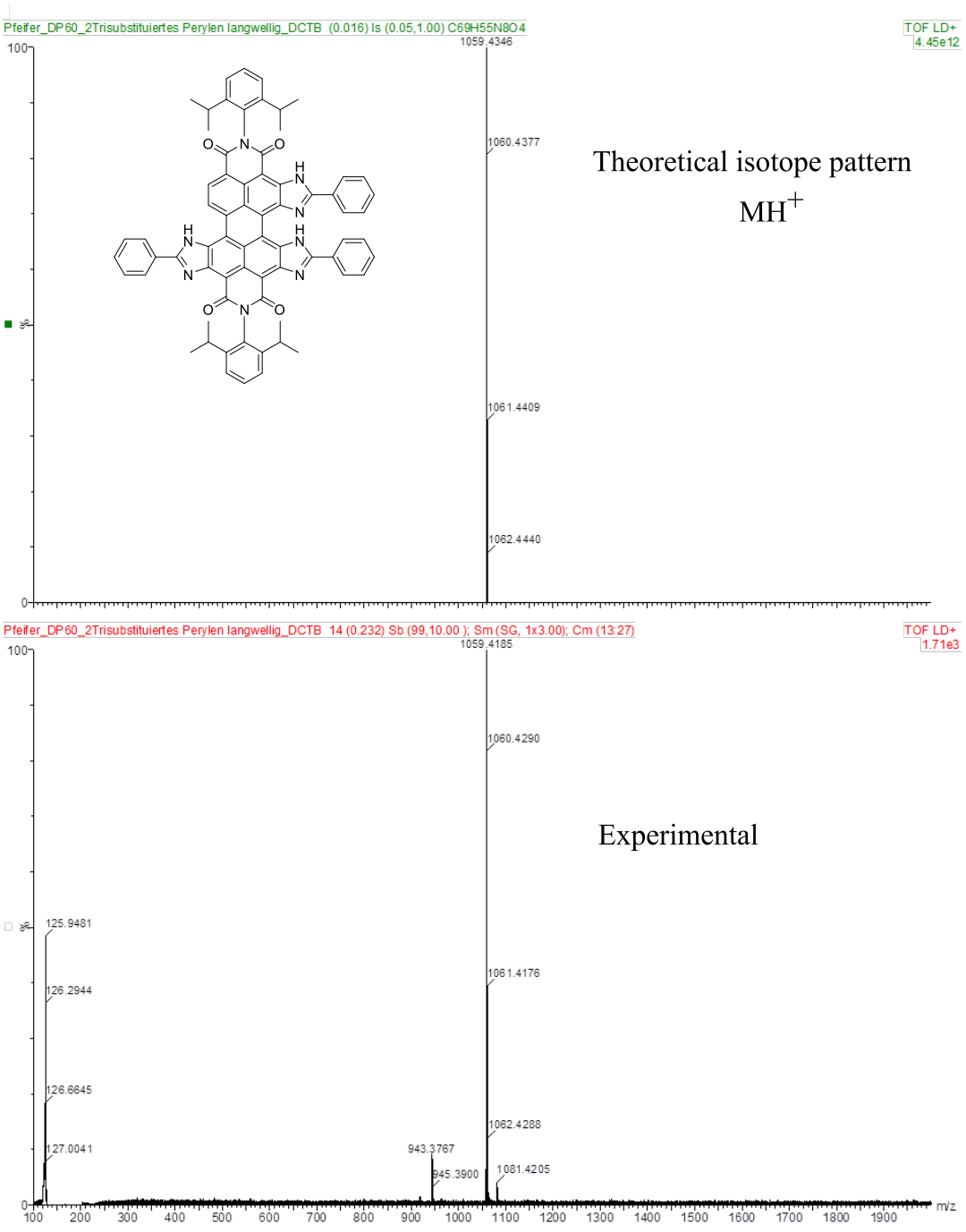

Figure 9.3: MALDI-TOF spectra of Per-$(PhIm)_3$, found: MH^+: 1059.4185, $Per-(PhIm)_2H^+$: 943.3767 [m/z]

9.1.4 Per-(ClPhIm)

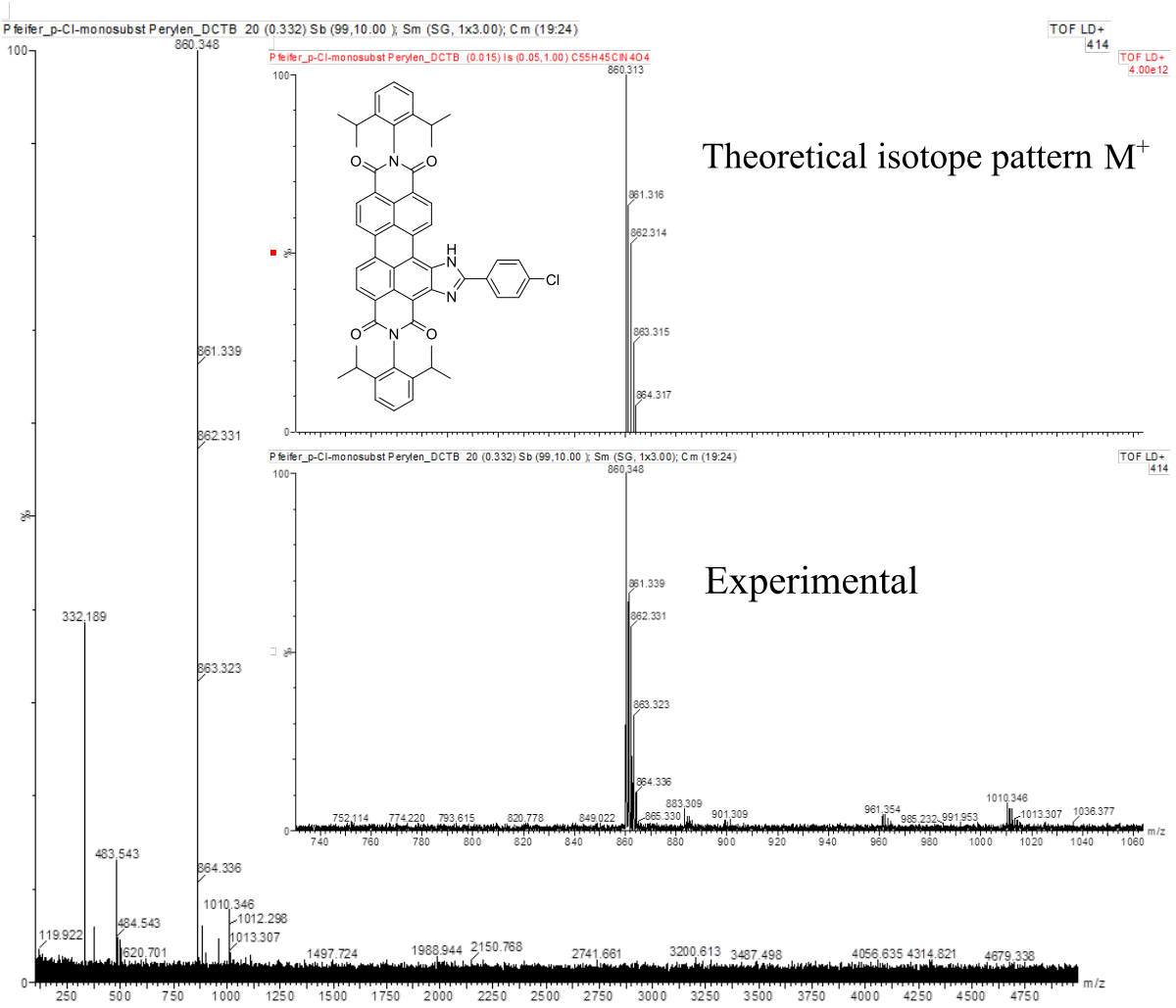

Figure 9.4: MALDI-TOF spectra of Per-(ClPhIm), found: M^+: 860.348 [m/z]

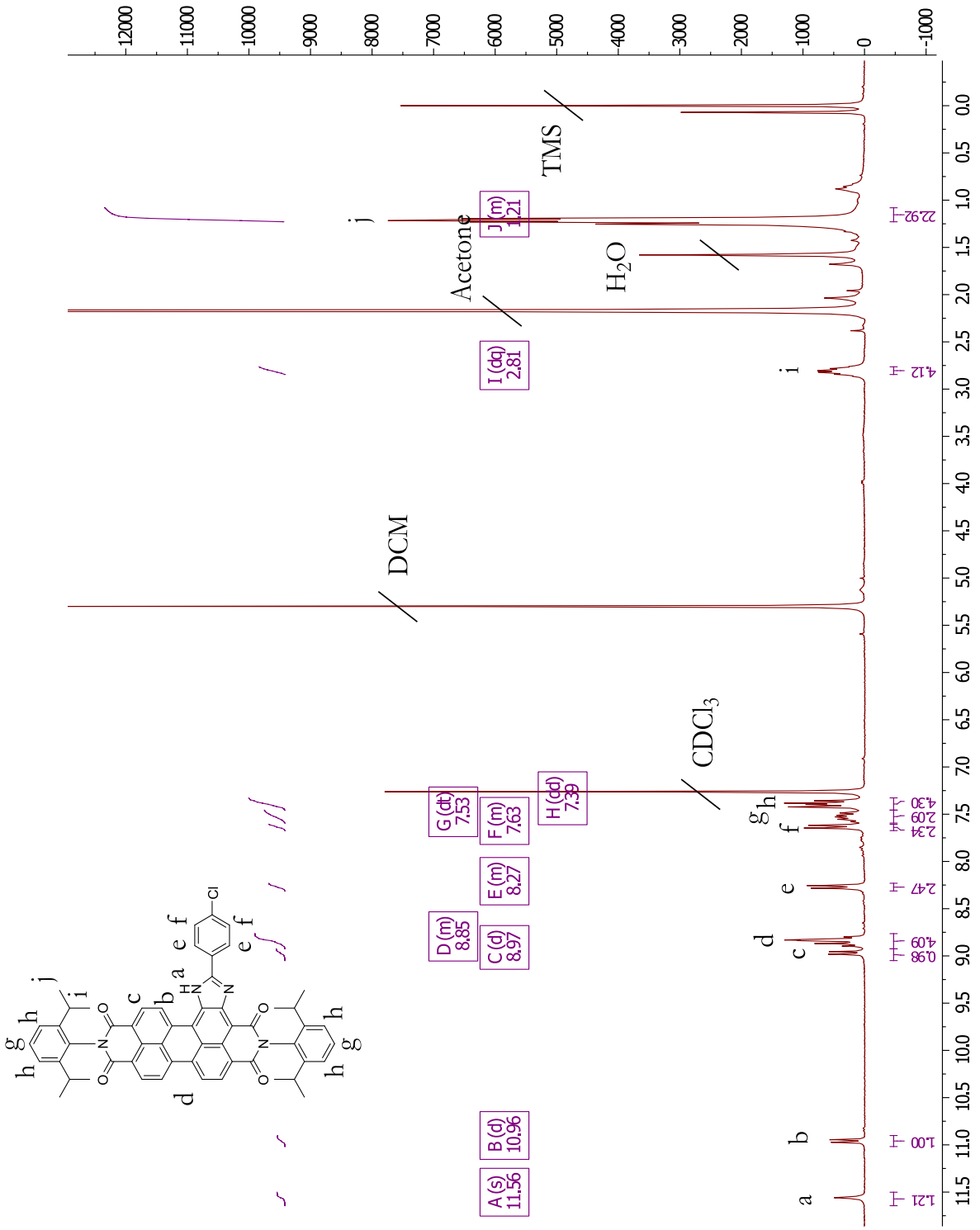
A (s) 11.56
B (d) 10.96
C (d) 8.97
D (m) 8.85
E (m) 8.27
F (m) 7.63
G (dt) 7.53
H (dd) 7.39
I (dq) 2.81
J (m) 1.21
DCM
Acetone
TMS
H_2O
$CDCl_3$
1.21
1.00
0.98
4.09
2.47
2.34
2.09
4.30
4.12
22.92

9.1.5 Per-(Cl_2PhIm)

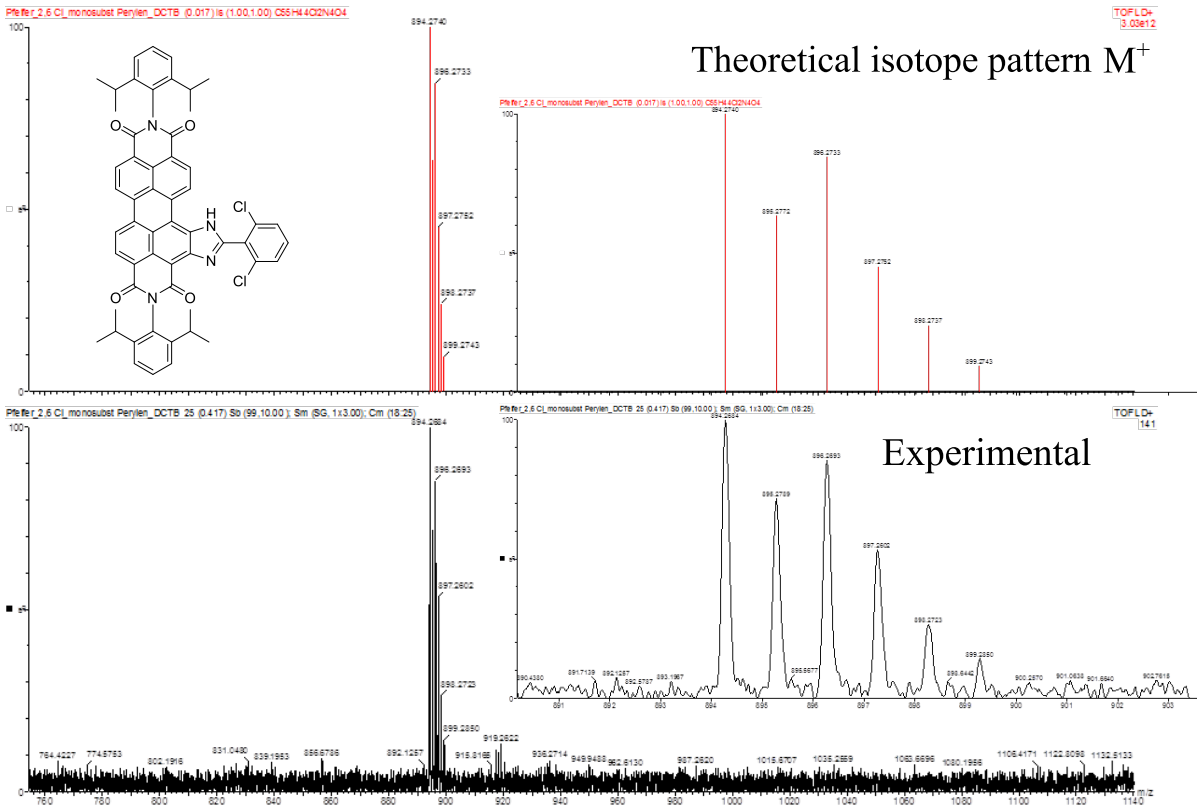

Figure 9.5: MALDI-TOF spectra of Per-(Cl_2PhIm), found: M^+: 894.2684 [m/z]

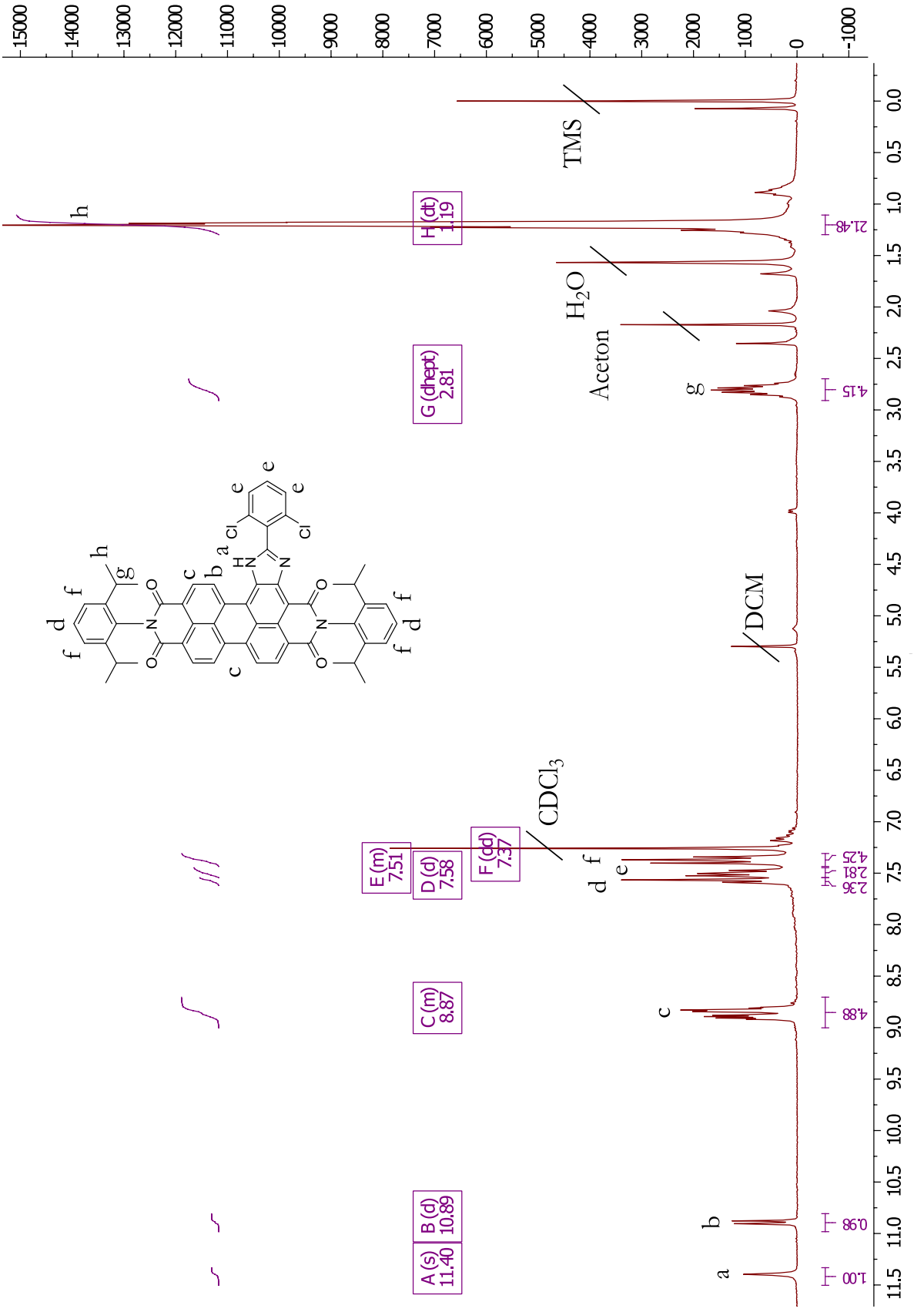
A (s) 11.40
B (d) 10.89
C (m) 8.87
D (d) 7.58
E (m) 7.51
F (dd) 7.37
G (dhept) 2.81
H (dt) 1.19
TMS
H2O
Aceton
DCM
CDCl3
1.00
0.98
4.88
2.36
2.81
4.25
4.15
21.48

9.1.6 Per-(ClPhIm)-*t*-ButylPh

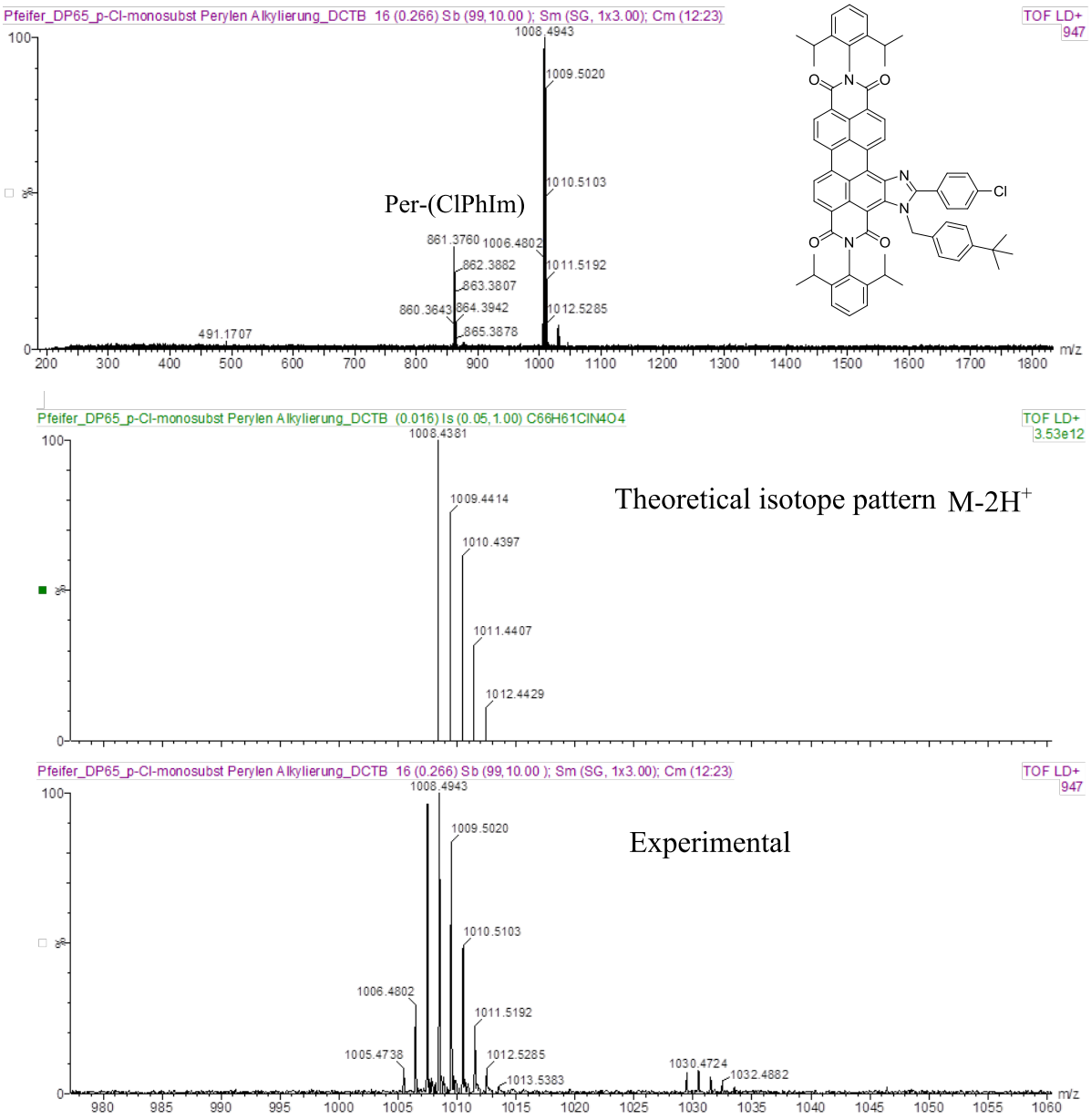

Figure 9.6: MALDI-TOF spectra of Per-(ClPhIm)-*t*-ButylPh, found: $M2H^+$: 1008.4943 [m/z]

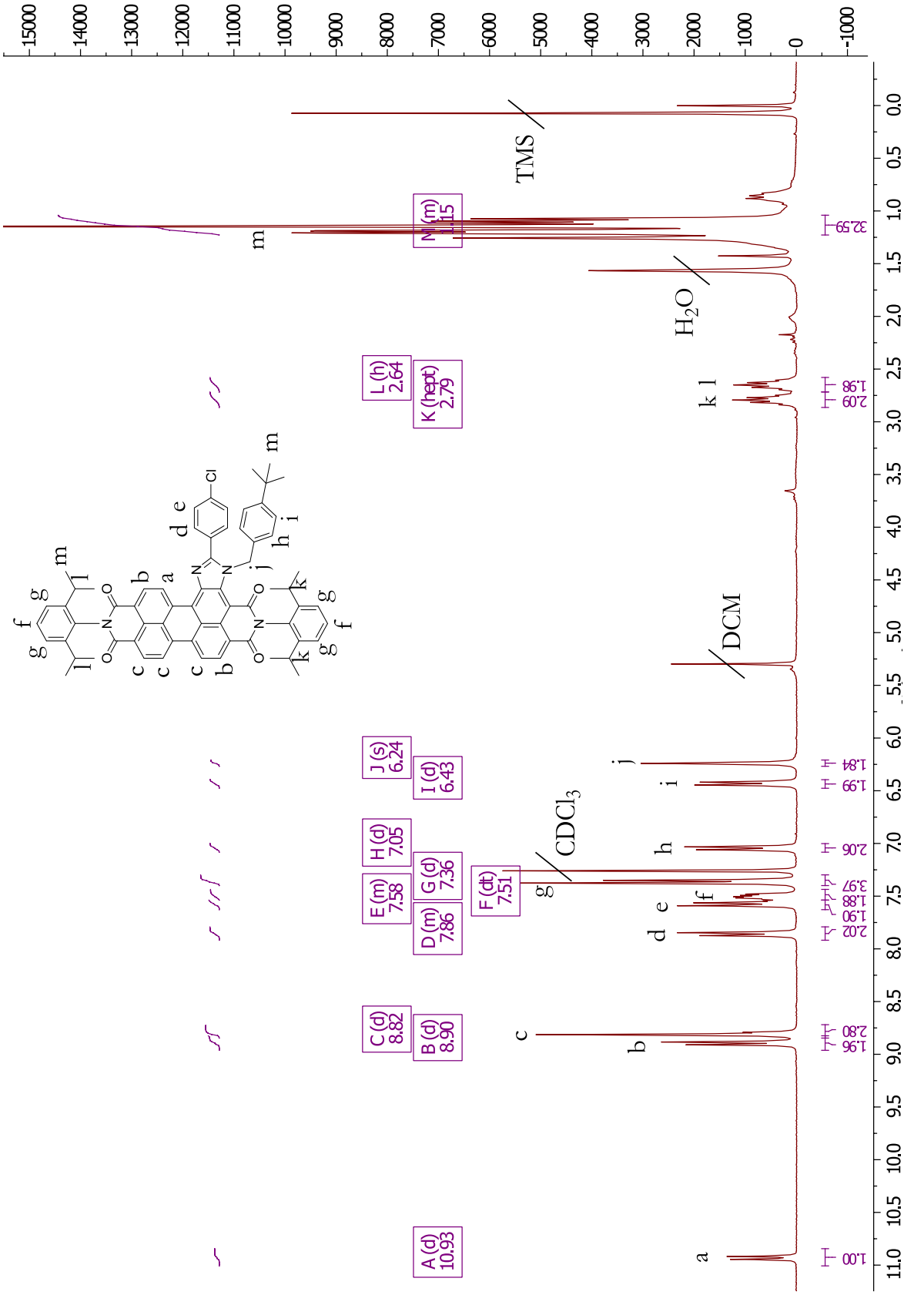
A (d) 10.93
B (d) 8.90
C (d) 8.82
D (m) 7.86
E (m) 7.58
F (dt) 7.51
G (d) 7.36
H (d) 7.05
I (d) 6.43
J (s) 6.24
K (heptet) 2.79
L (h) 2.64
M (m) 1.15
TMS
H_2O
DCM
$CDCl_3$
Cl

9.1.7 TOATPB

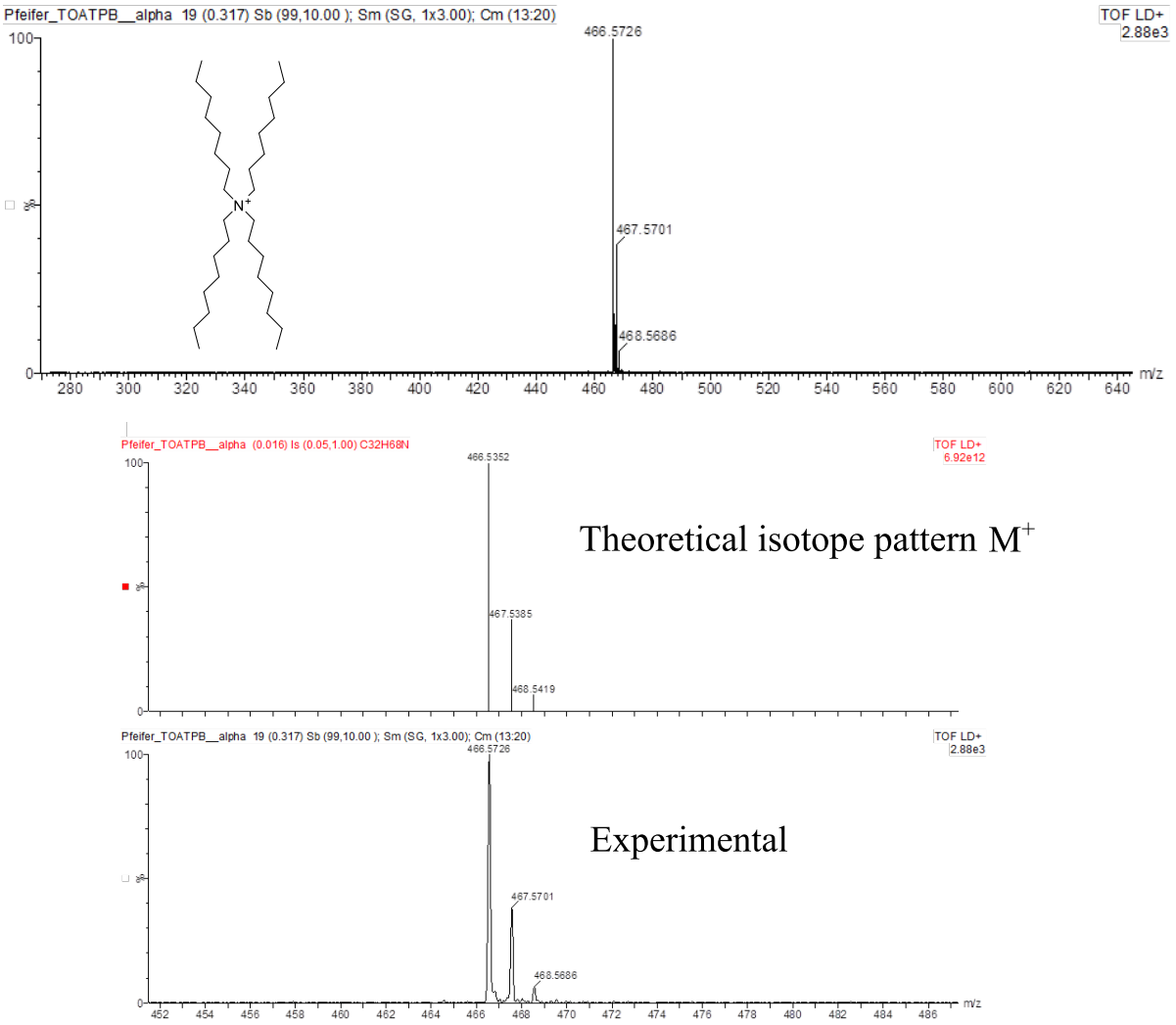

Figure 9.7: MALDI-TOF spectra of TOA^+, found: M^+: 466.5726 [m/z]

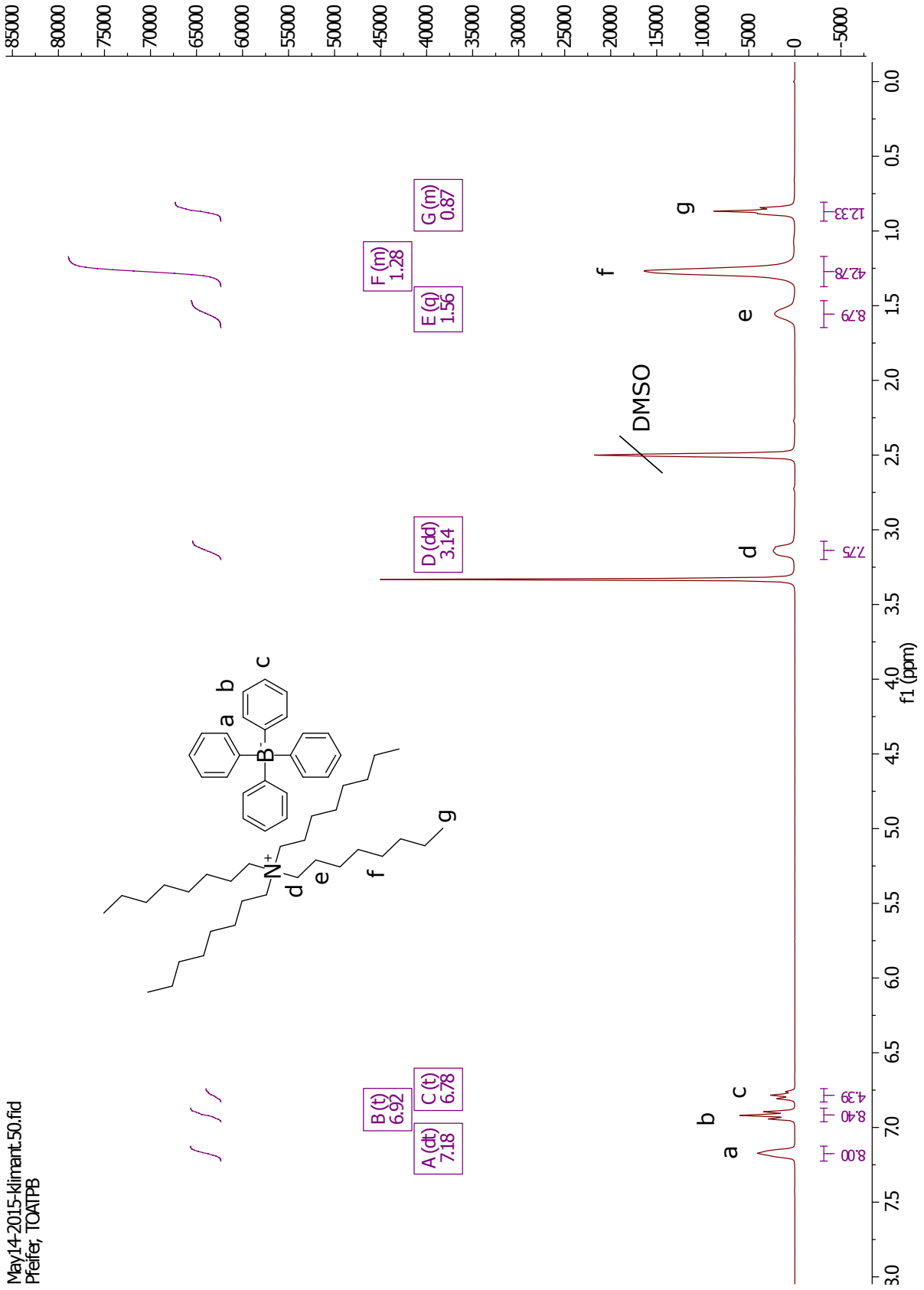
May14-2015-klimant.50.fid
Pfeifer, TOATPB
A (dt) 7.18
B (t) 6.92
C (t) 6.78
D (dd) 3.14
E (q) 1.56
F (m) 1.28
G (m) 0.87
DMSO
a
b
c
d
e
f
g
8.00
8.40
4.39
7.75
8.79
42.78
12.33
f1 (ppm)

9.1.8 Per-(PhIm)-N(EtHex)$_2$

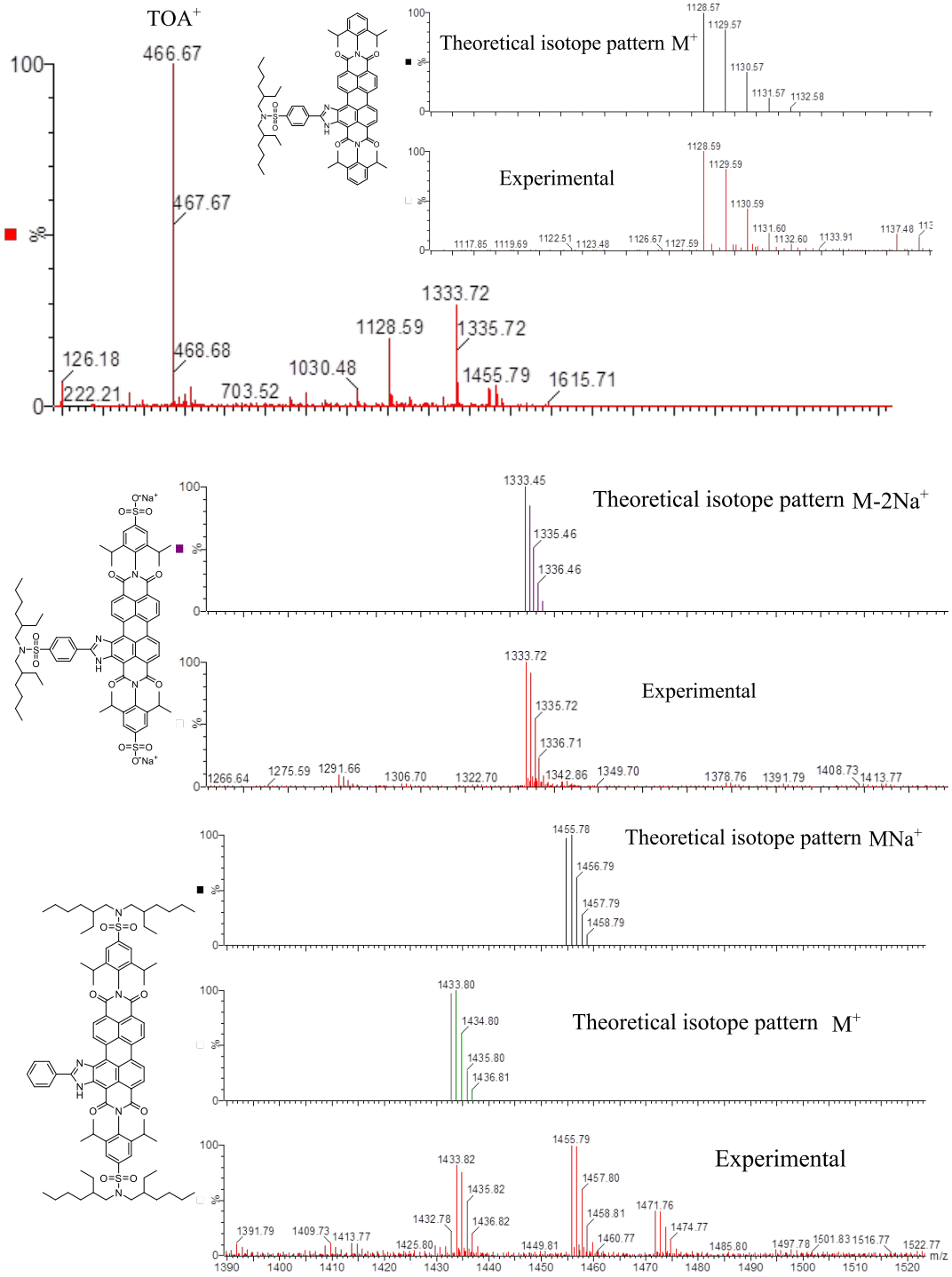

Figure 9.8: MALDI-TOF spectra of Per-(PhIm)-N(EtHex)$_2$, found: M^+: 1128.59, $M2Na^+$: 1333.72, M^+: 1433.80, MNa^+: 1455.78, TOA^+ contamination: 466.67 [m/z]

9.2 Lifetimes

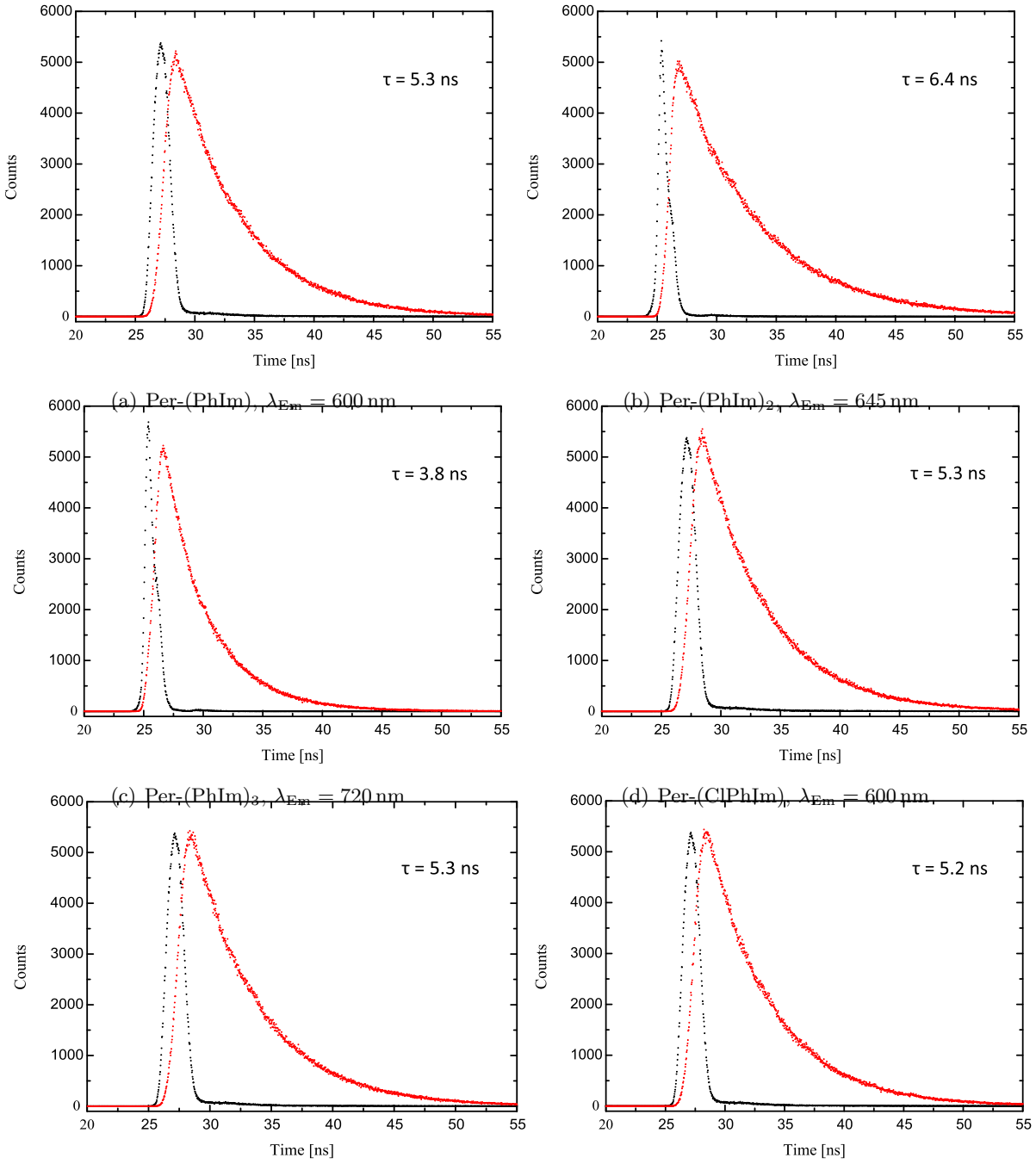

(a) Per-(PhIm), $\lambda_{Em} = 600\,nm$

(b) Per-$(PhIm)_2$, $\lambda_{Em} = 645\,nm$

(c) Per-$(PhIm)_3$, $\lambda_{Em} = 720\,nm$

(d) Per-(ClPhIm), $\lambda_{Em} = 600\,nm$

(e) Per$-(Cl_2PhIm)$, $\lambda_{Em} = 600\,nm$

(f) Per-(ClPhIm)-*t*-ButylPh, $\lambda_{Em} = 600\,nm$

Figure 9.9: Mono-exponential decay curves of new perylene bisimide dyes (red), prompt measurement (black)

9.3 List of Chemicals

Chemical	Supplier
1-Iodobutan	ABCR
2,6-Dichlorobenzonitrile	Sigma-Aldrich
2-Ethylhexylbromide	ABCR
4-Chlorobenzonitrile	TCI
4-tert-Butylbenzyl bromide	Sigma-Aldrich
Acetic acid 99%	VWR
Aceton	Brenntag
Benzonitril	Sigma-Aldrich
CAPS	Roth
Chloroform	VWR
Chlorosolfonic acid	Sigma-Aldrich
Cyclohexan	VWR
Dichloromethane	Fisher Chemical
Ethylacetate	VWR
HCl 37%	VWR
K_2CO_3	Roth
KOH	Roth
Lumogen Orange	Kremer Pigmente
Lumogen Red	Kremer Pigmente
Methanol	VWR
MOPS	Roth
N,N-Diisopropylethylamine	TCI
N,N-Dimethylformamide anhydrous	Sigma-Aldrich
Na_2SO_4	Roth
NaCl	Roth
$NaNH_2$ 95%	Sigma-Aldrich
$NaNH_2$ 99%	Acros
NaOH	Roth
Silica Gel	Acros
Tetrahydrofuran	VWR
Toluene	VWR
Triethylamine	Roth
Trifluoroacetic acid	Roth
$CDCl_3$	Euriso-top

Chemical	Supplier
DMSO-d6	Euriso-top
2-Bromoethylmethacrylate	Sigma-Aldrich
Tetraoctylammonium-chloride	Sigma-Aldrich
Tetraoctylammonium-hydroxide (20% solution in MeOH)	Sigma-Aldrich
Hydrogel D4	HydroMed
Hydrogel D7	HydroMed
FHUP hydrophobic membrane	Millipore Merck

9.4 Abbreviations

CH	Cyclohexane
DCM	Dichloromethane
EtAc	Ethylacetate
EtOH	Ethanol
FRET	Förster Resonance Energy Transfer
HOMO	Highest Occupied Molecule Orbital
hPa	hecto Pascal
LED	Light Emitting Diode
LUMO	Lowest Unoccupied Molecule Orbital
MeOH	Methanol
n.d.	not determined
N_2	Nitrogen (gaseous)
PBI	Perylene Bisimide
PS/PVP	Polystyrene-polyvinylpyrrolidone
RT	Room Temperature
TEA	Triethylamine
THF	Tetrahydrofuran
TOACl	Tetraoctylammonium-chloride
TOAOH	Tetraoctylammonium-hydroxide
TOATPB	Tetraoctylammonium-tetraphenylborate
UV-Vis	Ultraviolet-Visible
ε	Molar absorption coefficient
ϕ_F	Quantum yield